ELSEVIER

Review and assessment of turbulence models for hypersonic flows

Christopher J. Roy[a],*, Frederick G. Blottner[b]

[a]*Aerospace Engineering Department, Auburn University, 211 Aerospace Engineering Building, Auburn, AL 36849-5338, USA*
[b]*Consultant, Sandia National Laboratories, Albuquerque, NM, USA*

Abstract

Accurate aerodynamic prediction is critical for the design and optimization of hypersonic vehicles. Turbulence modeling remains a major source of uncertainty in the computational prediction of aerodynamic forces and heating for these systems. The first goal of this article is to update the previous comprehensive review of hypersonic shock/turbulent boundary-layer interaction experiments published in 1991 by Settles and Dodson (Hypersonic shock/boundary-layer interaction database. NASA CR 177577, 1991). In their review, Settles and Dodson developed a methodology for assessing experiments appropriate for turbulence model validation and critically surveyed the existing hypersonic experiments. We limit the scope of our current effort by considering only two-dimensional (2D)/axisymmetric flows in the hypersonic flow regime where calorically perfect gas models are appropriate. We extend the prior database of recommended hypersonic experiments (on four 2D and two 3D shock–interaction geometries) by adding three new geometries. The first two geometries, the flat plate/cylinder and the sharp cone, are canonical, zero-pressure gradient flows which are amenable to theory-based correlations, and these correlations are discussed in detail. The third geometry added is the 2D shock impinging on a turbulent flat plate boundary layer. The current 2D hypersonic database for shock–interaction flows thus consists of nine experiments on five different geometries. The second goal of this study is to review and assess the validation usage of various turbulence models on the existing experimental database. Here we limit the scope to one- and two-equation turbulence models where integration to the wall is used (i.e., we omit studies involving wall functions). A methodology for validating turbulence models is given, followed by an extensive evaluation of the turbulence models on the current hypersonic experimental database. A total of 18 one- and two-equation turbulence models are reviewed, and results of turbulence model assessments for the six models that have been extensively applied to the hypersonic validation database are compiled and presented in graphical form. While some of the turbulence models do provide reasonable predictions for the surface pressure, the predictions for surface heat flux are generally poor, and often in error by a factor of four or more. In the vast majority of the turbulence model validation studies we review, the authors fail to adequately address the numerical accuracy of the simulations (i.e., discretization and iterative error) and the sensitivies of the model predictions to freestream turbulence quantities or near-wall y^+ mesh spacing. We recommend new hypersonic experiments be conducted which (1) measure not only surface quantities but also mean and fluctuating quantities in the interaction region and (2) provide careful estimates of both random experimental uncertainties and correlated bias errors for the measured quantities and freestream conditions. For the turbulence models, we recommend that a wide-range of turbulence models (including newer models) be re-examined on the current hypersonic experimental database, including the more recent experiments. Any future turbulence model validation efforts should carefully assess the numerical accuracy and model sensitivities. In addition, model corrections (e.g., compressibility corrections) should be carefully examined for their

*Corresponding author. Tel.: +1 334 844 5187; fax: +1 334 844 6803.
E-mail address: cjroy@eng.auburn.edu (C.J. Roy).

effects on a standard, low-speed validation database. Finally, as new experiments or direct numerical simulation data become available with information on mean and fluctuating quantities, they should be used to improve the turbulence models and thus increase their predictive capability.

Contents

1. Introduction

1.1. Background

Turbulence plays a key role in determining the aerodynamic forces and heating for hypersonic vehicles. However, experimental data for turbulence model validation are difficult to obtain. There are very few flight tests in the open literature, and these tests generally provide only small amounts of data, usually with large experimental uncertainties. There are many more ground-based wind tunnel tests on simplified geometries in hypersonic flow. These ground tests generally provide much more data than the flight tests, and usually with smaller experimental uncertainties. However, due to the extremely high velocities found in hypersonic flow, the hypersonic ground tests generally do not match the same high total enthalpy and low freestream turbulence levels typical of hypersonic flight. The validation of turbulence models with wind tunnel data thus generally involves significant extrapolation to flight enthalpies. Because of these difficulties in obtaining validation data for turbulent, hypersonic flows, designers are forced to rely heavily on computational fluid dynamics and the associated models for turbulence, chemistry, ablation, etc.

The current effort builds on the reviews by Settles and Dodson [1–4] conducted in the early 1990s. Differences between the Settles and Dodson reviews and the current work are that the current effort:

1. has a different scope since only hypersonic flows are considered,
2. includes new experimental data since 1994,
3. addresses the steps required for validating turbulence models, and
4. takes the additional step of reviewing and assessing turbulence models as applied to the existing hypersonic experimental database.

The current article can be considered both as an update to the Settles and Dodson work, as well as an extension which includes the steps of validating the turbulence models. Finally, we soften the Settles and Dodson requirement that the upstream boundary layer be fully characterized by the experiment in cases where the predictive capabilities of the turbulence model are judged to be sufficiently good, i.e., flat plates or cylinders with natural transition.

1.2. Scope

The validation of turbulence models should necessarily include a wide range of flows. However, the extremely wide range of turbulent flows and available experimental data are enormous, so we are forced to limit the scope of this article. Prediction of the more basic turbulent flows needs to be improved

Nomenclature

a	speed of sound, m/s
A	incompressible transformation function
B	incompressible transformation function
c_p	specific heat at constant pressure, J/(kg K)
C_f	skin-friction coefficient
C_μ	turbulence modeling constant
f	general solution variable
F	compressible to incompressible transformation function
F_s	safety factor in the GCI
G	Mangler transformation function
h_c	heat transfer coefficient, W/(m² K)
H	total enthalpy, J/kg
k	turbulent kinetic energy, m²/s²
l	turbulent length scale, m
L	reference length, m
m	incompressible transformation function, flat plate to sharp cone scaling exponent
M	Mach number
p	order of accuracy of the numerical method, pressure, N/m²
Pr	Prandtl number
q	square root of turbulent kinetic energy, m/s, heat flux, W/m²
q_w	wall heat flux, W/m²
r	grid refinement factor, recovery factor
R	specific gas constant, J/(kg K)
R_{af}	Reynolds analogy factor
R_n	nose radius, m
Re	Reynolds number
S_f	flat plate to sharp cone scaling factor
St	Stanton number
t	time, s
T	temperature, K
T^*	dimensionless total temperature
Tu	turbulence intensity
u	x-component of velocity, m/s
u^+	wall-tangent component of velocity in turbulence coordinates
u_τ	turbulence friction velocity ($u_\tau = (\tau_w/\rho_w)^{1/2}$), m/s
v	y-component of velocity, m/s
V	total fluid velocity, m/s
x	spatial coordinate (usually main flow direction), m
X	axial distance from the leading edge, m
y	spatial coordinate (usually wall-normal direction), m
y^+	wall-normal mesh spacing in turbulence coordinates ($y^+ = u_\tau y/v$)

Greek letters

α	incompressible transformation function
β	turbulence modeling constant, incompressible transformation function
γ	ratio of specific heats
δ	boundary-layer thickness, m
Δy	height of first cell off the wall, m
ε	specific dissipation rate, m²/s³
κ	Karman constant (typically $\kappa = 0.41$)
ρ	density, kg/m³
μ	absolute molecular viscosity, kg/(m s)
μ_T	turbulent eddy viscosity, kg/(m s)
v	kinematic molecular viscosity, m²/s
θ	momentum thickness, m
τ	shear stress, N/m²
ω	turbulence frequency, 1/s
ζ	enstrophy, 1/s²

Subscripts

∞	freestream quantity
aw	adiabatic wall value
e	boundary-layer edge property
inc	incompressible value
k	grid level (1 = finest grid)
0	total (stagnation) conditions
RE	Richardson extrapolated quantity
T	turbulence quantity
w	wall value

Superscript

$*$	incompressible value
$\bar{f}$	denotes Reynolds-average of f
$\tilde{f}$	denotes Favre-average of f

Acronyms

DNS	direct numerical simulation
ERCOFTAC	European Research Community on Flow, Turbulence and Combustion
GCI	Roache's grid convergence index
NASA	National Aeronautics and Space Administration
RANS	Reynolds-averaged Navier–Stokes
RMS	root mean square

and validated before the more complex flows are investigated. Furthermore, while we have endeavored to include all appropriate experimental and computational studies, it is inevitable that some qualified studies will be overlooked. We apologize in advance for such omissions.

Herein we consider only two-dimensional (2D)/axisymmetric hypersonic flows, where the freestream Mach number is limited to values greater than or equal to approximately five. In addition, only wall-bounded flows are considered, thus eliminating flows such as hypersonic mixing layers and jets. While there are ongoing research efforts in advanced turbulence models such as Reynolds stress models and large Eddy simulation (LES), the most complex models currently employed in design studies (where a large number of parametric cases must be considered) are one- and two-equation turbulence models. We therefore limit the current study to these models. We also limit this study to models where integration of the governing equations to the wall is performed, thereby eliminating the use of wall functions. This choice was primarily driven by the fact that a majority of the cases of interest for hypersonic flows include shock-boundary-layer interactions, where the assumptions inherent in the use of wall functions are difficult to justify. We further limit our scope to cases where the transition from laminar to turbulent flow occurs naturally, and where this transition location is specified in the experimental description. The focus here is not on the prediction of transition, which itself is a difficult challenge for hypersonic flows. Finally, the effects of surface roughness, ablation, chemical reactions, real gases, and body rotation are all neglected as the existing experimental database does not yet adequately address these phenomena.

In most cases, turbulence models are expected to be valid for a wide range of problems and not "tuned" for a very limited class of turbulent flows (this latter approach more closely resembles model calibration or parameter fitting than a true prediction). Therefore, the testing of a turbulence model for high speed flows should include the evaluation of the model for all speeds and various flow geometries to determine its limitations. Here we limit our study to include only those models which have a well-established validation history over a wide range of flow conditions including low-speed flows. We therefore will not discuss efforts where the researchers propose model improvements, but do not address the effects of these model improve-

ments on the prior model validation heritage. We strongly recommend that future high-speed turbulence modelers test their compressible flow model improvements on a standard set of incompressible flows as well, or at least give arguments as to why their corrections will not impact low-speed flows. See Marvin and Huang [5] for a recommended set of external aerodynamics test cases in the subsonic through supersonic regime.

1.3. Molecular transport for hypersonic flows

Due to the difficulties of reproducing high enthalpy environments in ground-based facilities, experimental freestream static temperatures are often quite low, sometimes on the order of 50 K or below. In addition, the most common test gases are air, nitrogen, and helium. For these reasons, appropriate molecular models for viscosity and thermal conductivity should be used. See Appendix D for recommended low temperature molecular transport models for both air and nitrogen.

1.4. Turbulence

1.4.1. Physics

The Navier–Stokes equations contain all of the physics necessary to simulate turbulent flows. However, due to the wide range of length and time scales associated with simulating turbulence at Reynolds numbers typical of flight vehicles, this direct simulation approach for turbulence is well beyond the capabilities even of today's fastest computers. Engineers are thus forced to rely on turbulence models, which account for the effects of the turbulence rather than simulate it directly. The simplest turbulence modeling approach is Reynolds-Averaged Navier–Stokes (RANS), where all of the turbulent length and time scales are modeled via temporal filtering of the Navier–Stokes equations. For compressible flows, density-weighted (or Favre) averaging is used. See Wilcox [6] for details of the Reynolds and Favre averaging procedures.

1.4.2. Compressibility effects

Typically turbulence models have been developed for incompressible flows and then extended without much change to compressible flows. This approach in many cases is not adequate. For complex turbulent flows, Coakley et al. [7] have recommended corrections to apply to the two-equation $k-\varepsilon$ and $k-\omega$ turbulent eddy viscosity models. In addition, Aupoix

and Viala [8] have proposed corrections to the $k-\varepsilon$ model for compressible flows. The authors have used flat plate flows and mixing layers to assess the compressible corrections introduced. Significant efforts to assess turbulence models for compressible flows have occurred at NASA Ames Research Center. The results of these investigations have been published by Horstman [9], Horstman [10], Coakley and Huang [11], Huang and Coakley [12], Coakley et al. [7], Bardina et al. [13], and Bardina et al. [14]. See A.1 for additional discussion of the compressibility effects for hypersonic flows.

2. Turbulence model validation methodology

The turbulence model validation methodology presented herein is influenced heavily by the work of Marvin [15] and Marvin and Huang [5]. The proposed validation framework [16] includes guidelines for documentation, model sensitivities, and model validation. In addition, it is recommended that a significant effort be made to estimate the numerical accuracy of the simulations as part of the validation procedure. Listed below are six criteria for assessing the models. The first three criteria (2.1–2.3) focus on the thorough documentation of the model evaluation efforts. Details of the flow case and the models used must be given in enough detail so that the results are reproducible by other researchers. The last three criteria (2.4–2.6) list the specific standards for evaluating the models. The turbulence models should be evaluated by first establishing the numerical accuracy of the simulations, then by examining model sensitivities, and then finally by validation comparisons to experimental data.

2.1. Cases examined

Details of (or references to) the specific flow problem examined should be given including flow-field geometry and relevant physics (ideal gas versus equilibrium thermochemistry, transport properties, etc.). All required boundary conditions should be listed including inflow and outflow conditions, wall boundary conditions for temperature, incoming boundary-layer thickness, freestream turbulence intensities, a measure of the freestream turbulence dissipation rate, etc. One of the difficulties encountered in the specification of computational boundary conditions is that the level of information required may not be fully characterized in the

experiment. For example, a large number of otherwise excellent hypersonic validation data sets fail to report the thickness of the turbulent boundary-layer upstream of the interaction region; this information is especially important when the boundary layer is tripped to force transition to turbulence. It should be clearly stated whether the flow is fully turbulent or transitional. Finally, the data available for model validation should be given (feature location, surface quantities, turbulent field profiles, etc.).

2.2. Turbulence models examined

It should be clearly stated which form of the turbulence model is employed. It is strongly recommended that the standard model constants be used so as to build on prior turbulence model validation efforts. Where applicable, the form of the low Reynolds number wall damping functions used should be stated. The treatment of the near-wall regions should also be listed (i.e., integration to the wall versus wall functions).

2.3. Model implementation issues

The form of the governing equations should be given. For example, different results may be found when employing the full Navier–Stokes, thin-layer Navier–Stokes, parabolized Navier–Stokes, viscous shock layer equations, or boundary-layer equations. The boundary conditions employed in the simulation, including both flow properties and turbulence quantities, should be specified. Finally, any limiting of the turbulence quantities should be discussed. For example, limiting of the ratio of production to dissipation of turbulent kinetic energy to some ratio (e.g., $P/\rho\varepsilon \leqslant 5$) is often used. In addition, realizeability constraints on the turbulence variables and/or normal turbulent stresses [17] should also be discussed.

2.4. Efforts to establish numerical accuracy

The numerical accuracy of the simulations is an important factor to consider when comparing to experimental data; for example, if the numerical accuracy of pressure distributions is estimated to be $\pm20\%$, then agreement with experimental data within 5% does not mean the model is accurate within 5%. The first step towards determining the accuracy of the simulations is code verification, i.e.,

building confidence that the code is solving the governing equations correctly. Code verification can be performed by comparison of the code results to exact solutions to the governing equations, highly accurate numerical benchmark solutions, or by the method of manufactured solutions [18–21]. Once one has confidence that the code is verified, then the accuracy of the individual solutions must be verified. Solution accuracy includes assessing the errors due to incomplete iterative convergence [16], temporal convergence for unsteady problems, and grid convergence [18,21]. Methods for estimating the grid convergence errors based on systematic grid refinement [22] tend to be the most reliable and are applicable to any type of discretization including finite-difference, finite-volume, and finite-element. Grid convergence error estimates for hypersonic flows are complicated by the presence of shock waves, which tend to reduce the spatial order of accuracy to first order on sufficiently refined meshes [23,24], regardless of the nominal order of the spatial discretization scheme.

2.4.1. Grid convergence

Discretization error is defined as the difference between the exact solution to the discrete equations and the exact solution to the original partial differential equations. Discretization error can be estimated by performing computations on two or more meshes. The Richardson extrapolation procedure [18] can be used to obtain an estimate of the exact solution from the relation

$$f_{RE} = f_1 + \frac{f_1 - f_2}{3}, \tag{1}$$

where 1 denotes the fine mesh and 2 the coarse mesh. This relation assumes that the numerical scheme is second-order, that both mesh levels are in the asymptotic grid convergence range, and that a mesh refinement factor of two (i.e., grid doubling) is used. A more general expression for the Richardson extrapolated value is given by

$$f_{RE} = f_1 + \frac{f_1 - f_2}{r^p - 1}, \tag{2}$$

where r is the grid refinement factor and p is the order of accuracy (either formal or observed). The formal order of accuracy can be found from a truncation error analysis of the discretization method. If solutions are available on three meshes,

then the observed order of accuracy can be calculated from

$$p = \frac{\ln[(f_3 - f_2)/(f_2 - f_1)]}{\ln(r)}, \tag{3}$$

where 2 now denotes the medium mesh and 3 the coarse mesh. Here it is assumed that the refinement factor between the coarse and medium mesh is equal to that between the medium and fine mesh.

The accuracy of the solutions can be estimated using the exact solution approximated by f_{RE} which gives the discretization error as

$$\% \text{ Error of } f_k = 100\% \times \frac{f_k - f_{RE}}{f_{RE}}, \tag{4}$$

where $k = 1, 2$, etc. is the mesh level. Since it is equally possible that the true exact solution is above or below this estimate, it is generally recommended that some factor of safety be included in the error estimate. Roache [22] combines the concept of a factor of safety along with absolute values to produce an error band rather than an error estimate. The resulting error (or numerical uncertainty) estimate is referred to as the Grid Convergence Index, or GCI. The GCI thus produces an error (or uncertainty) band around the fine mesh solution and is given by

$$GCI = \frac{F_s}{r^p - 1} \left| \frac{f_2 - f_1}{f_1} \right|. \tag{5}$$

When solutions from only two meshes are available, Roache recommends a factor of safety of three. For three meshes where the observed order of accuracy agrees with the formal order of accuracy, a much less conservative value of $F_s = 1.25$ is suggested by Roache.

2.4.2. Iterative convergence

When iterative or relaxation methods are employed, an additional error source arises due to incomplete iterative convergence. The numerical error due to incomplete iterative convergence is usually assessed by evaluating norms of the residuals, where the residual is defined by substituting the current numerical solution into the discretized governing equations. For steady-state flows, the residual is calculated with the steady-state terms only, even if the temporal terms are included to speed up the convergence process. The residuals will approach zero as the steady-state solution is reached and the current solution satisfies the discretized form of the steady equations. These

residuals can generally be driven to zero within machine round-off tolerance; however, this extreme level of iterative convergence is generally not necessary. Many studies (e.g., [16,20]) suggest that for computational fluid dynamics simulations, the residual reduction levels correlate quite well with the actual iterative error in the flow properties.

2.5. Turbulence model sensitivities

Model sensitivity studies should be performed to determine practical guidelines for model use. A systematic study of the effects of the freestream turbulence levels on the numerical predictions should be performed. The normal spacing at the wall (y^+) should also be varied in order to test model robustness and accuracy for both integration to the wall and wall functions. In addition to establishing the solution accuracy, a mesh refinement study can also be used to determine a given turbulence model's sensitivity to the mesh density.

The sensitivity to the freestream turbulence levels can manifest in two forms: changes in the location of transition from laminar to turbulent flow and changes in the eddy viscosity levels in the turbulent region. The former may actually be a desirable characteristic when bypass transition is being modeled, while the latter is generally undesirable. Experimental evidence [25,26] suggests that surface properties (e.g., shear stress) in the fully-developed turbulent region are generally not affected by freestream turbulence intensity, at least in the case of low-speed flows.

2.6. Turbulence model validation results

Model validation results should be presented in a quantitative manner rather than qualitatively. For example, the percent difference between the predictions (with demonstrated numerical accuracy) and experiment should be plotted or explicitly stated. Whenever possible, experimental error bounds should be given for all measurements used for validation. These error bounds should include contributions from instrument uncertainty, experimental run-to-run uncertainty, physical model alignment uncertainty, flowfield non-uniformities, etc. Bias errors are generally difficult to quantify, so if possible, multiple measurement techniques should be employed and, furthermore, tests in multiple facilities should be performed. Techniques are available for converting some experimental bias errors into random uncertainties [27].

3. Turbulence validation database for 2D/ axisymmetric hypersonic flows

3.1. Overview

The validation of turbulence models must rely on real-world observations, i.e., experimental data, to establish model accuracy. The experimental data have been mainly obtained from wind tunnels, where detailed measurements can be performed, rather than in flight. There is a long history of high speed turbulent wind tunnel flow experiments. Compilation of experimental data for compressible turbulent boundary layers up to approximately 1980 is given in AGARD reports by Fernholz and Finley [28–30]. For high speed compressible turbulence, an experimental database has been developed by Settles and Dodson [1–4] for two- and three-dimensional shock-wave boundary-layer interaction flows, attached boundary layers, and free shear flows. The hypersonic portions of these databases are described below along with other more limited reviews. In addition, a discussion is provided on the role of both correlations and direct numerical simulation (DNS) data in turbulence model validation.

3.2. Previous experimental databases

3.2.1. AGARD experimental review

There has been a significant effort by Fernholz and Finley [28–30] to document available experimental data for compressible turbulent flow up to about 1980. A total of 77 experiments are reviewed with 59 given in Ref. [28] and 18 given in Ref. [29]. A further compilation of compressible boundary-layer data is given in Ref. [30]. The number of hypersonic experiments is limited. In addition, these reports do not provide a clear recommendation for a limited list of experiments that should be used for validation of turbulence models.

3.2.2. Experimental reviews by Settles and Dodson

A very careful assessment of validation experiments for compressible turbulent flow was performed by Settles and Dodson in the early 1990s [1–4]. They developed a list of eight *necessary criteria* for validation experiments which is given below (in abbreviated form) in the order in which they were applied.

1. *Baseline applicability*: Supersonic or hypersonic turbulent flow with shock wave/boundary layer interaction.

2. *Simplicity*: Experimental geometries sufficiently simple that they may be readily modeled by CFD methods.
3. *Specific applicability*: Must provide useful experimental data for testing turbulence models.
4. *Well-defined experimental boundary conditions*: Sufficient boundary condition data must be supplied to allow CFD solutions to be performed without any assumptions.
5. *Well-defined experimental error bounds*: Must provide an analysis of the accuracy and repeatability of the data.
6. *Consistency criterion*: All data must be self-consistent (i.e., different measurements cannot be contradictory).
7. *Adequate documentation of data*: Data must be available in *tabulated form* and capable of being put into machine-readable form.
8. *Adequate spatial resolution of data*: Sufficient data must be presented such that key features of the flow are clearly resolved.

In addition to the above necessary criteria, the following *desirable criteria* were also used in the evaluation of the experiments:

1. *Turbulent data*: Turbulent properties (Reynolds stress, etc.) of the flow field are given.
2. *Realistic test conditions*: Flow conditions and boundary conditions typical of actual hypersonic flight.
3. *Non-intrusive instrumentation*: Preference is given to non-intrusive experimental data.
4. *Redundant measurements*: Preference is given to experiments in which redundant data are taken.
5. *Flow structure and physics*: Preference is given to those experiments that reveal flow structure and physical mechanisms.

The initial study [1] examined 105 experimental studies of shock wave interactions with turbulent boundary layers at Mach 3 or higher. There are five experiments at hypersonic conditions that were considered as acceptable while seven experiments at supersonic conditions that were considered as acceptable. The second study [2] examined 39 experiments of attached boundary layers with pressure gradients and 45 supersonic turbulent mixing layer experiments. The authors recommended nine experiments as acceptable for attached boundary layers with pressure gradients and three experiments as acceptable for supersonic turbulent

mixing layers. The last report [3] has reviewed seven additional experiments and has corrections to three of the previously reviewed experiments. A summary of the supersonic and hypersonic shock/boundary-layer interaction experiments has been published in Ref. [4].

None of the references to the acceptable supersonic experiments are included in the list of references of this review, but are available in Ref. [4]. For hypersonic flow conditions, seven experiments on six flow geometries are classified as acceptable for validation of turbulence models. The data for all of the acceptable experiments are tabulated in the Settles and Dodson reports and available in electronic format. The Settles and Dodson flow geometries have been numbered with the first four being 2D or axisymmetric and the next four being 3D experiments. Additional flow geometries or flow problems will be discussed in this paper, with a total of seven geometries being recommended for turbulence model validation. The Settles and Dodson flow geometries numbers are as follows:

(1) *Two-dimensional compression corner*. For a freestream Mach number of 9, the wall pressure and heat flux have been determined in the experiment of Coleman and Stollery [31].
(2) *Cylinder with conical flare*. For a freestream Mach number of 7, the wall pressure and heat flux have been measured and flow field surveys have been made in the experiment of Kussoy and Horstman [32].
(3) *Cone with conical flare*. For a freestream Mach number of 11 and 13, the wall pressure and heat flux have been measured in the experiments of Holden et al. [33] and Holden [34].
(4) *Axisymmetric impinging shock*. For a freestream Mach number of 7, the wall pressure, skin friction and heat flux have been measured and flow field surveys have been made in the experiment of Kussoy and Horstman [35].
(5) *Flat plate with two fins* (*crossing shocks*). For a freestream Mach number of 8.3, the wall pressure and heat flux have been measured, and surveys in the flow field have been made in the experiment of Kussoy and Horstman [36].
(6) *Flat plate with 3D fin*. For a freestream Mach number of 6, the wall pressure and heat flux have been measured in the experiment of Law [37]. For a freestream Mach number of 8.2, the wall pressure and heat flux have been measured

and surveys in the flow field have been made in the experiment of Kussoy and Horstman [38,39]. For hypersonic flow at Mach 4.9, the Rodi and Dolling experiments [40] are also acceptable.

(7) *Cylinder with skewed flare*. For hypersonic flow, Settles and Dodson have no available experiments.

(8) *Three-dimensional compression corner with sweep*. For hypersonic flow, Settles and Dodson have no available experiments.

3.2.3. ERCOFTAC database

A comprehensive database of European work is being developed on the web [41] and has the name European Research Community on Flow, Turbulence and Combustion (ERCOFTAC). A complete review of this database has not yet been performed, but most of the databases are presently very limited as this effort is in the early stages of development.

3.2.4. Holden database

A review of the hypersonic experiments that have been performed at Calspan has been made by Holden and Moselle and reported in Ref. [42]. There are numerous experiments that have been performed that are of interest:

(1) Sharp and blunted cones at Mach 11 with laminar, transitional and turbulent flow have been investigated. This work is documented by Holden [43].
(2) Flow over a cone/flare model at Mach 11–16 has been investigated. Earlier experiments on this flow geometry is one of the Settles and Dodson acceptable experiments. This work is documented by Holden [44].
(3) Two-dimensional compression corner [42].
(4) Flat plate with 3D fin [34,42].
(5) Flat plate [42,45,46].
(6) Two-dimensional impinging shock [42,47,48].

3.2.5. Other limited reviews

It has been nearly 15 years since a comprehensive review has been performed on the new experiments in hypersonic flow. There have been several limited reviews of hypersonic experiments at the California Institute of Technology by Hornung [49] and hypersonic flow research in Europe by Groenig and Olivier [50].

3.3. Theory-based correlations

Theory-based correlations exist for two of the simpler geometries discussed herein: the flat plate and the sharp cone. In some respects, theory-based correlations can be considered superior to any single experimental data set since they mitigate the experimental bias errors that vary from facility to facility as well as bias errors associated with a given measurement technique.

3.3.1. Correlations for the flat plate

The turbulence properties of interest are the wall skin friction, heat transfer, and profiles of velocity and temperature across the boundary layer. While a summary of the flat plate correlations is presented here, a detailed discussion can be found in Appendix B.

Correlation of skin-friction data: The basic approach which transform the experimental compressible local skin friction and momentum thickness Reynolds number to incompressible values for a flat plate is the Van Driest II theory [51]. Squire [52] estimates that the accuracy of the Van Driest II correlation is within $\pm 3\%$ for the flat plate. Based on the sometimes erratic agreement between experiments and the correlation (e.g., see [53,45]), we feel that this error estimate is somewhat optimistic and should be increased to at least $\pm 5\%$ for hypersonic flows.

Correlation of heat transfer: Reynolds' analogy is used to predict the wall heat flux, which is expressed as the compressible Stanton number $St = q_{\mathrm{w}}/[\rho_{\mathrm{e}}u_{\mathrm{e}}(H_{\mathrm{w}} - H_{\mathrm{aw}})]$. Reynolds' analogy is written in terms of the compressible local skin friction $2St/C_{\mathrm{f}} = R_{\mathrm{af}}$, where R_{af} is the Reynolds analogy factor. Experiments indicate that $0.9 < R_{\mathrm{af}} < 1.3$. While there are insufficient reliable experimental data to establish the Reynolds analogy factor, for hypersonic flows a reasonable choice at present appears to be $R_{\mathrm{af}} \cong 1$. Additional work is needed to establish the appropriate value for the Reynolds analogy factor for hypersonic flow.

Mean velocity profiles: In the log-law region, similarity of the Favre-averaged velocity $\tilde{u}$ can be obtained with the Van Driest velocity transformation (see Appendix B). Huang et al. [54] have also obtained the transformed velocity from the wall to the edge of the boundary by taking into account the viscous sublayer and by including a wake function. This procedure gives the skin friction, velocity, and temperature profiles as a function of the Reynolds

number. It has been developed as a seven step procedure with iteration of the solution until converged (see Appendix B for details).

Mean temperature profiles: The general form of the mean temperature across the zero-pressure gradient turbulent compressible boundary layer as a function of the mean turbulent velocity and turbulent kinetic energy is

$$T = T_w - \alpha \tilde{u} - \beta \tilde{u}^2 - \gamma_T k. \tag{6}$$

Huang, Bradshaw, and Coakley (HBC) [54] have developed the temperature equation by neglecting the convective terms in the momentum and energy equations. Their analysis (see Appendix B) yields the following relations for the variables in Eq. (6):

$$\alpha = (Pr_T/c_p)(q_w/\tau_w), \quad \beta = Pr_T/2c_p,$$

$$\gamma_T = Pr_T/c_p. \tag{7}$$

3.3.2. Correlations for the sharp cone

One of the problems with the sharp cone is the lack of a theoretical correlation of the experimental data to use as a benchmark solution. For laminar flow, the skin friction and heat transfer for a flat plate are multiplied by $\sqrt{3}$ to obtain the cone values. There does not appear to be a well established approach to transform the turbulent flat plate results to the cone. Van Driest [55] has suggested an approximate approach that has been developed further in the book by White [56] using the von Karman momentum integral relation (see Appendix C for more details). The flat plate skin friction and wall heat flux are multiplied by a scale factor G that gives the *Cone Rule* as follows:

$$(C_f)_{cone} = G(C_f)_{plate}, \quad (q_w)_{cone} = G(q_w)_{plate}, \tag{8}$$

where $G = \sqrt{3} = 1.732$ for laminar flow and $G \approx 1.13$ for turbulent flow.

A correlation of the heat transfer on axisymmetric flight vehicles with flat plate relations has been investigated by Zoby and Sullivan [57] and an additional correlation including ground data has been investigated by Zoby and Graves [58]. The former includes six references for experimental data on sharp cones where the Mach number varies from 2.0 to 4.2. An assessment of the theoretical correlations for sharp cones was given in Roy and Blottner [59].

3.4. Direct numerical simulation database

The numerical solution of the unsteady Navier–Stokes equations with refined grids as formulated in the DNS and LES methods has the potential of providing an accurate numerical simulation database with limited or no turbulence modeling assumptions. However, the increased fidelity of these approaches requires additional temporal and spatial information for the specification of the initial and boundary conditions. As computer speed and memory size have increased, the accuracy and capabilities of these computational fluid dynamic approaches have increased and will increase in the future. Next a brief indication is given of the turbulent flat plate and sharp cone flow problems that are being solved with the DNS and LES methods.

Martin [60]: Martin [60] has started to develop a DNS database of hypersonic turbulent boundary-layer flows over a flat plate. She provides a review of previous DNS solutions that have been obtained for high speed compressible flows. The list includes a review of other work as well as her previous papers with coworkers. Martin has obtained DNS solutions for perfect gas and reacting air flows over a flat plate. Martin presented DNS solutions for perfect gas flow with the gas viscosity modeled with a power law dependence on temperature. The simulations use freestream conditions corresponding to an altitude of 20 km and the Mach number varies from 3 to 8. The wall temperature is specified to be nearly the adiabatic temperature. At Mach 8, the wall temperature is 2713 K and would result in significant dissociation of the oxygen in air. The perfect gas model is not adequate to simulate these physical flow conditions. From the simulation solutions obtained, the mean flow velocity across the boundary layer has been determined, then transformed with the Van Driest transformation to incompressible form, and presented in figures for the cases simulated. No information is presented on the wall skin friction and heat transfer. This work is important as it is starting to provide useful DNS solutions at hypersonic flow conditions. However, there is a need to extend this work by obtaining simulations with a gas model that are more appropriate for flight conditions or modify the flow to wind tunnel conditions.

Yan et al. [61]: Yan et al. [61] have obtained LES solutions with the Monotonically Integrated LES (MILES) technique for flat plate flow at Mach

number 2.88 and 4. Both adiabatic and isothermal wall boundary conditions are used. The authors have provided a list of researchers that have studied compressible LES with no work performed at hypersonic flow conditions. The authors' velocity profile predictions are compared to the law of the wall analysis and experimental data of Zheltovodov at Mach 2.9 and 3.74, although the computations are at a lower Reynolds number than the experiment. LES temperature profiles are also compared to experimental data. The comparisons for velocity and temperature at Mach 2.9 are good but the comparison at Mach 4 is poor. The interesting results of this investigation are concerned with heat transfer and Reynolds analogy. The authors indicate that Reynolds analogy factor is $R_{af} = 2St/C_f = 1/Pr_{tm} = 1.124$ where the mean Prandtl number $Pr_{tm} = 0.89$. At Mach 4, the LES solution gives $R_{af} = 1.23$ while the experimental value is $R_{af} = 1.12$. The Reynolds analogy factors differ by 10%. The simulations obtained in this article indicate the potential of the LES technique to help validate turbulence models; however, the subgrid scale model required in LES can affect the results and therefore is a limitation of this approach.

Pruett and Chang [62]: The Pruett and Chang [62] investigations are concerned with DNS of hypersonic boundary-layer flows on sharp cones and cone-flare models. The initial work in 1995 is an approximate simulation of the geometry and flow conditions in the wind tunnel experiment of Stetson et al. [63]. A 7° half-angle cone in a Mach 8 flow is simulated. The inviscid flow at the edge of the boundary layer is specified, and the wall temperature is specified as the laminar adiabatic wall temperature, which is given as 611 K. The freestream properties are estimated from the Sims tables [142], which give the total temperature as 733 K, static temperature as 53 K, and the unit Reynolds number as 3.407×10^6/m. Pruett and Chang [64] in 1998 published an investigation of DNS of hypersonic boundary-layer flow on a flared cone. The DNS solution is for the quiet (low freestream turbulence) wind tunnel experiment of Lachowicz et al. [65], where the freestream turbulence has been reduced significantly. The axial length of the cone-flare model is 0.51 m and the sharp cone axial length is 0.254 m. The freestream flow conditions for the simulation are specified as Mach number 8, static temperature 55 K, total temperature 450 K, and unit Reynolds number 8.85×10^6/m. In both of the above DNS the air viscosity is determined with

Sutherland viscosity law, and a perfect gas model is used. Although the Pruett and Chang DNS computations do not provide useful information on fully developed turbulent flow on the conical part of the models, the numerical simulations indicate the future potential for providing valuable data for validation of compressible turbulence models.

Comments on DNS database: For flows without chemical reactions and for typical flight conditions, the wall temperature needs to be sufficiently low. The maximum gas temperature occurs in the boundary layer due to viscous dissipation and can be sufficiently high to produce vibrational excitation. Complete simulation without chemical reactions requires a vibrational non-equilibrium model. The solutions from the complete model can be bounded by using perfect gas and thermally perfect gas models, which makes DNS solutions with these models valuable. The gas models need a more appropriate viscosity model than Sutherland viscosity law. For hypersonic wind tunnel conditions, the stagnation temperature is sufficiently high to have vibrational excitation while the freestream temperature in the test section is low. The model requirements are the same as for flight conditions as vibrational non-equilibrium effects can be important. Keyes viscosity model should be used due to the low gas temperatures. The desired database should include a matrix of accurate solutions which depend on Mach number, boundary-layer momentum thickness Reynolds number, and wall temperature. A series of solutions should be obtained with only one of the variables varying and with the other two variables held constant. These solutions would provide a database that can be used to validate the Van Driest transformation approach to correlate compressible turbulent skin friction and heat transfer (Stanton number) and to determine the Reynolds factor in the Reynolds analogy. In addition, the DNS method should be extended to flow over sharp cones. The database would help to determine the Mangler transformation required to transform compressible turbulent flow for the axisymmetric case to the 2D case.

3.5. Updated hypersonic turbulence model validation database

In this section we present our recommendations for the current 2D/axisymmetric experimental database for validating turbulence models. We adhere to

Settles and Dodson's *necessary criteria* for acceptance of experiments into the validation database [1–4] with one exception. Here we relax criteria #4 (well-defined experimental boundary conditions) and allow cases where the boundary layer is not characterized upstream of the interaction region as long as this upstream boundary layer can be adequately predicted by turbulence models or correlations (i.e., for flat plates, cylinders, or sharp cones where an equilibrium boundary layer has been established). Note that in the original Settles and Dodson validation database, they also appear to have relaxed this requirement for the Coleman and Stollery/Elfstrom [31,66,67] compression corner experiment.

3.5.1. Previous flow geometries with adverse pressure gradient

This section describes the four 2D/axisymmetric hypersonic flow geometries that were assessed in the Settles and Dodson database [1–4]. For each of these flow geometries, we present both the experiments that were included in the Settles and Dodson database, as well as new experiments conducted since 1994 which we recommend for inclusion in a 2D/axisymmetric hypersonic validation database. The experiments discussed in this section are included as Cases 1–4 in Table 1.

3.5.1.1. Case 1: 2D compression corner.
There are two hypersonic experiments for the 2D compression corner which are deemed acceptable with some caveats. The first experiment was conducted in the Mach 9 nitrogen gun tunnel and includes heat transfer measurements (see [31,66]) and surface pressures from a separate experiment (see [67]). The second experiment was conducted at the Calspan 48 in and 96 in shock tunnels at Mach 8 by Holden [48].

Coleman and Stollery/Elfstrom experiment [31,66,67]: Elfstrom [67] reported surface pressure measurements and Coleman and Stollery [31] and Coleman [66] reported surface heat transfer measurements for a Mach 9.22 flow over a 2D wedge/compression corner. The wedge angle was varied between $15°$ and $38°$, and includes flows which are nominally attached, at incipient separation, and fully separated. It is not fully clear whether or not the pressure [67] and heat transfer [31] measurements had the same upstream length for the flat plate. While this experiment is considered acceptable by Settles and Dodson, there are no numerical

Table 1
Turbulence validation database for 2D/axisymmetric hypersonic flows

Case no.	Flow geometry	Experiments
1	2D compression corner	Coleman and Stollery/Elfstrom [31,66,67] Holden [48]
2	Cylinder with conical flare	Kussoy and Horstman [32] Babinsky and Edwards [68,69]
3	Cone with conical flare	Holden [44]
4	Axisymmetric impinging shock	Kussoy and Horstman [35,70,71] Hillier et al. [72–75]
5	2D impinging shock	Kussoy and Horstman [38] Schulein et al. [76–78]
6	Flat plate/cylinder	Van Driest (VDII)[a] [51] Huang et al. (HBC)[a] [54] Aupoix et al. (AVC) [8] Hopkins and Keener [79–81] Horstman and Owen [82–84] Coleman et al. [85] Kussoy and Horstman [36,38] Hopkins et al. [86,87] Holden et al. [42,45,46,48,88]
7	Sharp circular cone	Van Driest (VDII)[a][51] and White[a] [56] Kimmel [89,90] Rumsey et al. [91,92] Chien [93] Hillier et al. [94–97] Holden et al. [42–44,46,48,98]

[a]Denotes a data correlation.

uncertainties on the surface quantities given in Refs. [31,67], nor are any uncertainties presented in the Settles and Dodson reviews [1,4]. Holden [48] points out that the interaction region in the Coleman and Stollery/Elfstrom experiments may be too close to the transition zone, resulting in a different trend of separation zone size versus Reynolds number than seen in equilibrium turbulent boundary layers, which require a distance of approximately 50–100 boundary-layer thicknesses between the transition point and the interaction region. Once the oncoming turbulent boundary layer has reached an equilibrium state, the trend should be a decrease of separation zone size (and incipient separation point) with increasing Reynolds number, while these experiments showed the opposite trend.

Holden experiment [48]: Due to the concerns regarding the equilibrium nature of the upstream boundary layer, the compression corner experiments conducted by Holden [48] are also included here, although they too fail to report uncertainties on the surface measurements. While no upstream boundary-layer profile is measured in this experiment, the surface quantities compared well to the Van Driest II correlations [99]; furthermore, the transition location can be easily determined from the surface skin friction and heat transfer measurements made on a flat plate and reported in the same reference. The freestream Mach number for this case is approximately 8, and the ratio of wall temperature to the freestream stagnation temperature was 0.3. The Reynolds number based on the boundary-layer thickness at the interaction location was varied between 100,000 and 10 million. Measurements are reported for surface pressure, skin friction, and heat transfer in the interaction region for wedge angles of $27°$, $30°$, $33°$, and $36°$ and along the flat plate in a configuration without the wedge. Span effects were also investigated and shown to be negligible. This was the first experiment to show the reversal of the separation zone size and incipient separation with Reynolds number within the same experiment. To our knowledge, this experiment has not been employed for validating turbulence models.

3.5.1.2. Case 2: cylinder with conical flare.

There are two experiments which meet the Settles and Dodson criteria for the axisymmetric cylinder-flare geometry. The first was included in the Settles and Dodson review and was performed by Kussoy and Horstman [32] at NASA-Ames Research Center. The second is a more recent experiment performed in the HSST supersonic blow-down wind tunnel and is detailed by Babinsky [69] and Babinsky and Edwards [68].

Kussoy and Horstman Experiment [32]: Kussoy and Horstman [32] studied the flow over axisymmetric ogive-cylinder-flares at a freestream Mach number of 7 for flare angles between $20°$ and $35°$. Data include surface pressure and surface heat transfer both upstream of the shock/boundary-layer interaction (see Case 6: flat plate/cylinder flow) and in the interaction region. Pitot-probe surveys through the boundary layer are presented at various axial locations for the $20°$ flare case only, with the boundary-layer surveys upstream of the interaction confirming a fully-developed turbulent boundary

layer. Information is given on freestream RMS values for stagnation temperature and mass flux as well as temperature for the water-cooled model surface. The data set includes experimental uncertainty estimates for each measured quantity. Derived boundary-layer quantities (displacement thickness, momentum thickness, etc.) are also reported upstream of the interaction. Surface data were taken at $90°$ locations to confirm that the flow was axisymmetric, and multiple runs were conducted to reduce run-to-run uncertainty. A relatively long model was employed to allow for natural (non-tripped) transition to occur at approximately 0.4 to 0.8 m from the tip, which is at least 0.6 m upstream of the interaction region.

Babinsky and Edwards Experiment [68,69]: Babinsky and Edwards [68] conducted careful experimental studies of cylinder-flare flows at Mach 5.1 for flare angles between $3°$ and $20°$, with additional details presented by Babinsky [69] for flare angles of $15°$ and $20°$. The experiments were conducted in the supersonic blow-down wind tunnel (HSST) at DRA Fort Halstead, Great Britain using a Mach 5 nozzle that included a cylindrical centerbody which extended upstream of the test section to the nozzle throat. This centerbody was deemed necessary to allow for the formation of a fully-developed turbulent boundary layer without the use of flow-intrusive boundary-layer tripping mechanisms. However, the use of the centerbody led to the presence of non-negligible axial gradients of pitot pressure (10% variation) and Mach number (3% variation) in the test section. Data were presented for surface pressure, surface heat transfer (via high-resolution liquid crystal thermography), and pitot pressure through the boundary layer at various axial stations. Detailed experimental uncertainties were also provided for each of the measured quantities. Derived quantities presented include velocity profiles, skin friction, boundary-layer thickness, and displacement thickness. Conventional theory suggests that for flare angles of $20°$ and below, no separation will occur. However, investigations using shear stress sensitive liquid crystals showed a small separated region (possibly in the laminar sublayer) for both the $15°$ and $20°$ flare cases. The authors suggest that the presence of this small separation zone destroys the similarity between pressure and heat transfer.

3.5.1.3. Case 3: cone with conical flare.

There is only one experiment for the cone/conical flare case

that is appropriate for turbulence model validation. Holden [44] performed experiments in Calspan's 96 in shock tunnel at Mach numbers of 11 and 13. This is one of Settles and Dodson's accepted hypersonic experiments; however, there is some discrepancy regarding the references. Settles and Dodson [1,4] reference a 1984 AIAA Paper [34], a 1986 CUBRC internal report [33], and a 1988 AFOSR technical report [100], all by Holden and coworkers. However, the initial reporting of these cone/conical flare experiments was not until 1991 in Ref. [44], and this is confirmed by examining Refs. [42,101] which are reviews of the experimental hypersonic program conducted at Calspan. In any case, the data presented by Settles and Dodson [1] does appear to be the same data given in Refs. [44,101]. It should be noted that there is also some question regarding the flare angle for this case. Ref. [44] does not make it clear whether the flare angle is measured from the symmetry axis or from the initial cone angle of 6°, while Ref. [101] clearly shows that the flare angle should be measured from the symmetry axis. However, Settles and Dodson [1] state that the flare angles should be measured from the 6° forecone, and crude angles measured from Schlieren photographs in Refs. [44,101] seem to support this conclusion. Subsequent communications with the author of Ref. [44] confirmed that the *flare angle should be measured from the 6° cone*, not the symmetry axis [102].

Holden experiment [44]: Holden [44] studied the flow over 6° (half angle) cones with conical flares at freestream Mach numbers of 11 and 13 for flare angles of 30° and 36° as measured from the forecone (36° and 42° from the symmetry axis). The smaller flare angle represents an incipient separated flow case, while the larger angle a fully separated flow. Data include surface pressure and heat transfer as well as pitot pressure and total temperature within the interaction region. Experimental uncertainties are given for the freestream conditions as well as heat transfer coefficient (±5%) and pressure coefficient (±3%).

3.5.1.4. Case 4: axisymmetric impinging shock. There are two different axisymmetric impinging shock experiments which are deemed acceptable for turbulence model validation. The first is a series of experiments conducted by Kussoy et al. at a Mach number of 7 on a cone-ogive-cylinder model [35,70,71]. The second is a more recent experimental

investigation by Hillier et al. at Mach 9 on a hollow cylinder model [72–75].

Kussoy and Horstman Experiment [35,70,71]: Kussoy and Horstman studied the flow over an axisymmetric cone-ogive-cylinder model at a freestream Mach number of 6.9. Axisymmetric cowls of 7.5° and 15° were used to impinge axisymmetric shock waves onto the turbulent boundary layer on the cylinder. Surface data include surface pressure, heat transfer, and skin friction [35,70]. Pitot pressure, static pressure, and total temperature were surveyed throughout the interaction region [35,70]. Ref. [71] also presents turbulence intensity and Reynolds stress profiles for these two cases. The cowl length is relatively short, thus the leading shock wave and subsequent expansion fan merge before the shock impinges on the surface. It is therefore strongly recommended that future computations of this experiment also include the viscous boundary layer on the outer cowl itself. The length of the model cylinder is 3.3 m, thus suggesting a fully-developed turbulent boundary layer is formed well ahead of the interaction region. The model surface is water-cooled to maintain a temperature of 300 K. The data set includes experimental uncertainty estimates for each measured quantity, with the exception of the turbulence measurements of Ref. [71]. Derived boundary-layer quantities (displacement thickness, momentum thickness, etc.) are also reported upstream of the interaction. Settles and Dodson [1] give the experimental data for the 15° shock generator case in tabular form.

Hillier et al. Experiment [72–75]: Hillier et al. [72] studied the flow over an axisymmetric cone-ogive-cylinder model at a freestream Mach number of 8.9 and Reynolds number of 52×10^6/m. An axisymmetric cowl with a quadratic expression for the shock-generating surface is used to impinge an axisymmetric shock wave onto the turbulent boundary layer formed on the cylinder. Surface data include surface pressure and heat transfer. Transition of the boundary layer on the cylinder begins at 80 mm and ends at 170 mm, with the shock interaction occurring at roughly 520 mm. Due to the curved nature of the shock-generating cowl, it is recommended that computations of this experiment also include the viscous boundary layer on the outer cowl itself. Although not reported in the experimental description, the model surface temperature was 300 K [103]. The data set includes experimental uncertainty estimates for the surface pressure and heat transfer. An additional discussion of the

experimental uncertainties is given in Ref. [73] which quotes uncertainties of ±4% and ±7% for surface pressure and heat transfer, respectively. More recent data for shock generator angles of 4.7° (attached flow) and 10° (separated flow) are given by Murray and Hillier [74,75] for a hollow cylinder forebody. Although no experimental uncertainties were quoted in these last two references, the same experimental techniques that were used in Refs. [72,73] were employed. Personal communication with one of the authors confirmed the uncertainty levels given above [103]. For the 10° shock generator case, the length of the shock-generating outer cowl had to be reduced to prevent choking of the shock system. This recent experiment has not yet been used in the validation of one- or two-equation turbulence models but is recommended.

3.5.2. New flow geometries with and without pressure gradient

In this section we discuss the three new flow geometries which should be added to the 2D/axisymmetric hypersonic turbulence database. The first is the 2D impinging shock problem and is referred to as Case 5. Cases 6 and 7 are zero-pressure gradient flows (flat plate/cylinder and cone flow) where the simplicity of the flow also allows the development of theoretical correlations.

3.5.2.1. Case 5: 2D impinging shock. A 2D imping-ing shock occurs when an externally generated oblique shock impinges on a flat plate boundary layer. There are two experimental data sets that satisfy the Settles and Dodson criteria: Kussoy and Horstman [38] conducted a careful experimental study of the 2D impinging shock case in the Ames 3.5 ft Hypersonic Wind Tunnel at Mach 8.2, and Schulein et al. [76–78] studied a similar geometry at Mach 5.

Kussoy and Horstman Experiment [38]: Kussoy and Horstman [38] studied a 2D oblique shock impinging on a turbulent flat plate boundary layer at a freestream Mach number of 8.2 for effective wedge angles of 5°, 8°, 9°, 10°, and 11°. Data include surface pressure and heat transfer both upstream of the shock/boundary-layer interaction (see Case 6: flat plate/cylinder flow) and in the interaction region. Mean flow surveys through the boundary layer are given for the undisturbed boundary layer (i.e., without the shock generator) in the vicinity of the shock interaction. Surveys in

the interaction are alluded to in the report but are not presented (these may be included on a computer disk which is mentioned in the report). The model is water-cooled to maintain a surface temperature of 300 ± 5 K. The data set includes extensive experimental uncertainty estimates for each measured quantity, but not for the freestream conditions. A relatively long 2.2 m model was employed to allow for natural (non-tripped) transition to occur approximately 0.5 to 1 m from the leading edge, which is at least 0.5 m upstream of the interaction region. The model length results in a fully developed, equilibrium turbulent boundary layer (confirmed by the flow-field surveys) that is nearly 4 cm thick near the interaction region.

Schulein et al. Experiment [76–78]: Schulein and coworkers [76–78] have also studied a 2D oblique shock impinging on a turbulent flat plate boundary layer. The flow is at Mach 5 and wedge angles of 6° to 14° were studied. The flat plate was 0.5 m long and 0.4 m wide, with natural transition occurring 0.1 m from the leading edge, as judged by peak skin-friction. For all shock generator angles, the inter-action occurs approximately 0.35 m from the lead-ing edge. The spanwise extent was chosen to ensure 2D flow, which was further confirmed by surface pressure and pitot survey data taken at various spanwise locations. The Reynolds number based on distance from the leading edge at the interaction region was 13×10^6, and the boundary-layer thick-ness at this location was approximately 5 mm. The wall temperature is 300 ± 5 K. The original report [76] gives pitot surveys in the interaction region, as well as wall static pressures with an estimated uncertainty of ±5% [78]. Surface skin friction (obtained via optical means) and heat transfer data are also available in Ref. [77] and uncertainties in the interaction region for both are given as ±10% [78].

3.5.2.2. Case 6: flat plate/cylinder. The uniform viscous flow over a flat plate or cylinder is considered, where a laminar to turbulent boundary layer develops along the surface. The 2D zero-pressure gradient turbulent boundary-layer flow problem is unique. Theoretical analyses of this case for perfect gas flows have been performed which result in correlations of the experimental results. The turbulent properties of interest are the wall skin friction, heat transfer, and profiles of velocity and temperature across the boundary layer.

A survey has been performed of authors that have used hypersonic turbulent boundary-layer experimental data with zero-pressure gradient to validate correlations of skin friction and Stanton number and correlations of velocity and temperature profiles. Tabulation of the survey is given in Table 2

Table 2
Model geometries and freestream conditions for hypersonic flat plate/cylinder database

Investigator/geometry	Date	M_e	C_f	St	Profiles	Tabulated data reference
Sommer–Short [104] (hollow cylinder, flight range)	1953	5.63, 6.9, 7.0	Yes	No	No	Peterson [105]
Korkegi [106]	1956	5.79	Yes	AdW	No	Peterson [105]
Hill [107] (conical nozzle, nitrogen gas)	1956	8.3–9.1	Yes	Yes	Yes	F&F 5901
Hill [108] (conical nozzle, nitrogen gas)	1959	8.27, 9.07, 10.04	Yes	Yes	No	Hill [108], Peterson [105]
Tendeland [109] (cone-cylinder)	1958	5.04	No	Yes	No	Spalding–Chi [110], Author
Brevoort–Arabian [111] (downstream inside cylinder)	1958	5.05	No	Yes	No	Spalding–Chi [110], Author
Winkler–Cha [112]	1959	5.14, 5.22, 5.25	Yes	Yes	Yes	F&F 5902
Winkler–Cha [112]	1961	5.14, 5.22, 5.25	No	Yes		Authors [112], Peterson [105]
Matting et al. [113] (flat wind tunnel wall, helium gas)	1961	6.7, 9.9	Yes	AdW	Yes	Peterson [105]
Moore [114]	1962	5	No	No	Yes	F&F 6201
Young [115]	1965	5	Yes	Yes	Yes	F&F 6506
Wallace–McLaughlin	1966	7.4, 8.1, 10.7	Yes	Yes	No	Cary–Bertram [53]
Wallace [117]	1967	7.4, 8.1, 10.7	No	Yes	No	No tabulation
Heronimus [118]	1966	4.6 to 11.7	Yes	Yes, AdW	No	Cary [119]
Neal[120]	1966	6.8	Yes	Yes	No	No tabulation
Cary–Morrisette [121] (wedge $\alpha = -5, 0, 5$)	1968	6.8, 6.0, 5.3	No	Yes	No	Cary–Bertram [53]
Hopkins et al. [86]	1969	6.5	Yes	AdW	Yes	Authors [86]
Hopkins et al. [87]	1970	6.5	Yes	Yes	Yes	Authors [87]
Hopkins et al. [122]	1972	6.5	Yes	Yes	Yes	Authors [122]
Cary [123]	1970	6	No	Yes	No	Cary–Bertram [53]
Weinstein [124] (10 deg wedge)	1970	8, 6.8, 6, 5.2	No	Yes	No	Cary–Bertram [53]
Hopkins–Keener [80] (tunnel wall)	1972	7.4	Yes	No	Yes	F&F 7203
Keener–Hopkins [81] (thermally perfect gas)	1972	6.2–6.5	Yes	No	Yes	F&F 7204
Owen–Horstman [82] (cone-ogive-cylinder)	1972	7.2	Yes	Yes	Yes	F&F 7205, Authors [82]
Horstman–Owen [83] (cone-ogive-cylinder)	1972	7.2	Yes	Yes	Yes	Authors [83]
Owen et al. [84] (cone-ogive-cylinder)	1975	7.0	Yes	Yes	Yes	No tabulation
Holden [45]	1972	6.8–13	Yes	Yes	No	Author [45]
Holden electronic database [46]	2003					Author [46]
Coleman et al. [85] (flat plate negative angle)	1972	7.15–9.22	No	Yes	Yes	Cary–Bertram [53]
Watson et al. [125] (wedge, helium)	1973	9–10	Yes	Yes	Yes	F&F 7305
Watson [126] (wedge, helium)	1978	10–11.6	Yes	Yes	Yes	F&F 7804
Laderman–Demetriades[127] (wind tunnel wall)	1974	9.4	Yes	No	Yes	F&F 7403
Kussoy–Horstman [38]	1991	8.18	Yes	Yes	Yes	Authors [38]
Kussoy–Horstman [36]	1992	8.28	Yes	Yes	Yes	Authors [36]

AdW, adiabatic wall; F&F x, Fernholz and Finley case x.

where the experiments are for flat plate flows in air unless indicated otherwise. Since the correlations have been developed for perfect gas flows and fully developed zero-pressure gradient flow, the experimental database is limited to flat plates, wedges, wind tunnel walls and cylindrical body flows. Also the flow properties should be measured sufficiently far downstream where the turbulent flow is fully developed. Upstream history effects can significantly influence the database as the non-equilibrium turbulent effects sometimes persisting 1000s of boundary-layer thicknesses downstream [48].

For validation of correlation theory and turbulence models, direct measurement of skin friction, heat transfer, velocity profiles, and temperature profiles should be made. In addition, the hypersonic experimental database should be limited to the same flow geometry (flat plate) with zero-pressure gradient and same freestream perfect gas model. The sharp wedge and flat plate produce the same turbulent boundary layer as the flow Reynolds number approaches infinity. Flow along hollow cylindrical geometries with decreasing transverse curvature effects approaches flat plate flow. While cylindrical geometries with conical or ogive nose geometries produce initial disturbances that influence the boundary layer, far downstream a flat boundary layer is obtained. Wind tunnel wall boundary layers also have upstream history effects that impact the attainment of a flat plate flow.

Many of the earlier experiments did not measure both the skin friction and the wall heat transfer and are not as useful. While most experiments are performed in air, two experiments use helium gas and one uses nitrogen gas. The ideal hypersonic experimental database for validation of correlation theories becomes very small if one applies all of the restrictions mentioned above. However, many of the experiments in Table 2 have been useful in establishing the accuracy of the correlation theories and determining the validity of turbulence models (see Section 4.5.2). Many of the experiments are useful in direct comparison between turbulent model predictions and experimental results to establish turbulent model validation. This approach is a significantly larger computational effort, but would also help in the evaluation of the importance of the differences in the experiments.

An extensive database of compressible turbulent flows in a standard form has been compiled by Fernholz and Finley [28–30] as discussed in 3.2.1. This database is limited to 2D flows where flow

profile data are available in tabular form. Assessment of the data quality or significance of the data is not complete. Tabulated data is given for the edge and wall flow properties and survey properties across the boundary layer. The hypersonic database given in the Fernholz and Finley reports include a number of experiments where either real gas effects were an issue, a fully turbulent boundary layer was not established after transition process, or the wind tunnel side wall was used to generate the boundary layer (thus bringing the equilibrium nature of the boundary layer into question). As a result, the Fernholz and Finley reports are of limited value.

Two experiments which will be included from the Fernholz and Finley database are those of Hopkins–Keener and Horstman–Owen (discussed in detail below). Additional hypersonic experiments that have not been included in earlier database reviews and are considered useful are discussed below.

Hopkins– Keener [79–81] (*Fernholz & Finley Cases 6601, 7203 and 7204*): The initial work by Hopkins and Keener [79] was concerned with measuring the properties of the turbulent boundary layer on the *side wall* of the NASA Ames 8×7 ft supersonic wind tunnel at Mach 2.4–3.4. The next investigations were performed in the NASA Ames 3.5 ft hypersonic wind tunnel. Hopkins and Keener [80] measured the local skin friction, total-temperature profiles, and pitot-pressure profiles on the hypersonic *wind tunnel wall*. Although the pressure gradient is small near the measurement location, there appears to be significant upstream history effects in this experiment. Keener and Hopkins [81] investigated the wind tunnel air flow over a *flat plate* at Mach 6.2–6.5. The total temperature of the freestream was 764–1028 K and the temperature at the edge of the boundary layer was 73 K or greater. The analysis of the air flow properties included corrections for calorically imperfect gas effects. The boundary-layer properties were investigated with forced and natural transition. Surface properties measured: pressure, temperature, and wall shear stress. Properties measured across boundary layer: static pressure, pitot pressure, and total temperature.

Horstman– Owen [82–84] (*Fernholz & Finley Case 7205*): This investigation was performed for air flow over an *axisymmetric cone-ogive-cylinder* at Mach 7.2 in the NASA Ames 3.5 ft hypersonic wind tunnel. The total temperature of the freestream air was 667 K and the temperature at the edge of the

boundary layer was 59 K. Natural transition occurred along the body and the boundary layer became an equilibrium, constant pressure flow downstream on the body. The transverse curvature effects are considered to be negligible for this geometry. Fluctuating properties of the flow were also measured and $\langle u' \rangle / u_\tau = 0.17$ at $y/\delta = 1.1$, which gives an indication of the turbulent intensity in the freestream flow. Surface properties measured: pressure, temperature, wall shear stress. Properties measured across boundary layer: pitot pressure, total temperature.

Additional experiments that have not been included in the Fernholz and Finley database [28,30] follow below.

Coleman–Elfstrom–Stollery [85] (*see also Refs.* [31,66,67]): The compressible turbulent boundary layer on a *flat plate* was studied at a freestream Mach number of 9 in the Imperial College no. 2 gun tunnel. The total temperature of the freestream air was 1070 K. The local boundary-layer edge Mach number was varied (Mach 3, 5, and 9) by changing the incidence of the plate from $0°$ to $26.5°$. Both natural and tripped boundary layer flows were investigated. Theory based on Spalding–Chi skin-friction and Reynolds analogy was used to predict the Stanton number for the three Mach numbers. There was an increased discrepancy between measurements of heat transfer and the prediction of the theory as the Mach number was increased. Surface properties measured: static pressure and heat transfer. Properties measured across boundary layer: pitot pressure.

Kussoy– Horstman [36,38]: The experiments were conducted with flow over a water-cooled *flat plate* in the NASA Ames 3.5 ft hypersonic wind tunnel at Mach 8.2. The flat plate without a sharp fin is the database that is being considered. The plate surface was maintained at a constant surface temperature of 300 ± 5 K. In the first experiment [38], the properties of the boundary layer 1.87 m from the leading edge were determined. In the second experiment [36], the properties of the boundary layer 1.62 m from the leading edge were determined. Natural transition occurred between 0.5 and 1.0 m from the leading edge. A fully developed, equilibrium boundary layer was established at the measurement location. Tabulated results are presented for boundary-layer surface and edge properties. Tabulated results for the velocity, density and temperature profiles are also given for the measurement location. Surface properties measured: static

pressure and heat transfer. Properties measured across boundary layer: pitot pressure, static pressure, and total temperature.

Hopkins et al. [86,87,122]: The initial experiments were performed by Hopkins et al. [86] on simple shapes for turbulent boundary layers with nearly zero-pressure gradient in the NASA Ames 3.5 ft hypersonic wind tunnel. Local skin friction and heat transfer data were measured on flat plates (Mach 6.5 and 7.4), cones (edge Mach 4.9, 5.0, and 6.6), and the wind tunnel wall (Mach 7.4). Skin-friction data are given in tabulated form. The next experiments were performed by Hopkins et al. [87] on a sharp leading edge flat plate in the same Ames facility. Flat plate skin-friction was measured directly with an edge Mach number of 6.5. The skin-friction experimental database at various momentum thickness Reynolds numbers and adiabatic wall temperature ratios are given in tabulated form. Hopkins et al. [122] conducted further flat plate experiments in the same Ames facility. This study provides additional results to those previously reported by Keener and Hopkins [81], but at a higher Reynolds number. The model was injected into the airstream at various angles of attack, which resulted in local Mach numbers at the measuring station of 5.9, 6.4, 6.9, 7.4, and 7.8. No boundary-layer trips were used. The model surface temperature was nearly isothermal. Direct measurements of skin friction and velocity profiles were made for the various Mach numbers and for $T_w/T_{aw} = 0.3$ and 0.5. Real gas corrections as given in Ref. [128] were used in the analysis of the data. Tabulated results of the database are given in the article. Surface properties measured: wall shear stress with a skin-friction balance. Properties measured across boundary layer: pitot pressure.

Holden [42,45,46,48,88]: Experiments [48,45] were conducted on a flat plate in the Calspan 48 in and 96 in shock tunnels at Mach numbers 6.8–13. Steady flow was established in these facilities in 1 or 2 ms. The investigation measured the wall shear stress and the heat flux. The wall skin friction and heat transfer results were transformed with the Van Driest, Eckert, and Spalding–Chi methods and compared in figures to the incompressible results. The experimental data is approximately within 30% of the incompressible results, which is more scatter than expected from experimental results. The paper [45] provides tabulated test conditions, heat transfer, and skin-friction. Another experiment [88] was conducted in the Calspan tunnels on a flat plate

with a constant curvature surface downstream with a freestream Mach number of 8. The upstream part of the database on the flat plate could be useful, but needs further evaluation. A brief summary of experiments performed on flat plates is given by Holden and Moselle [42]. An electronic database [46] of results from the many experiments performed by Holden is now available on the internet to qualified users. A further evaluation of the usefulness of the Holden flat plate database needs to be performed.

3.5.2.3. *Case 7: sharp circular cone.* The sharp cone model is defined by the cone half-angle (angle between cone axis and cone surface) and the length L along the cone axis. The axial distance along the center of the cone from the tip is defined as X and distance along the cone surface from the tip is defined as x to be consistent with flat plate notation. The basic flow properties in the freestream are defined by specifying the Mach number, total temperature, and freestream unit Reynolds number $Re_{u\infty}$, which are tabulated in Table 3 for the current sharp cone experimental database being evaluated. The cone surface temperature is obtained from the specification of the wall to total temperature ratio. The other properties of the freestream flow are obtained from the following perfect gas relations:

$$T_\infty = T_0 \left[1 + \left(\frac{\gamma - 1}{2}\right) M_\infty^2\right]^{-1},$$

$$T_w = (T_w/T_0)T_0, \quad \gamma = 1.4,$$

$$a_\infty = \sqrt{\gamma R T_\infty}, \quad u_\infty = a_\infty M_\infty,$$
$$\rho_\infty = \mu_\infty Re_{u\infty}/u_\infty,$$

$$p_\infty = \rho_\infty R T_\infty = p_0 \left[1 + \left(\frac{\gamma - 1}{2}\right) M_\infty^2\right]^{-\gamma/(\gamma-1)}.$$

The nose radius R_n of the sharp cones is only available for the Kimmel experiment.

Rumsey et al. [91,92]: Rumsey and coworkers [91,92] performed a number of flight tests with vehicles with a sharp-cone nose and at various supersonic/hypersonic Mach numbers. The Rumsey and Lee [91] report has data at Mach 5.15 and has been included as a potential part of the present sharp cone database. The authors present much of the needed database information in figures. The freestream unit Reynolds number is not consistent with the value determined from the 1976 Standard Atmosphere conditions with the altitude given (10% difference). The accuracy of this database has not been estimated, but it is valuable as limited hypersonic flight data is available.

Stainback et al. [129]: The experimental results [129] were obtained in the NASA Langley 20 in hypersonic wind tunnel in air. The authors obtained the Stanton number along the surface of a 10° sharp cone at Mach 6 and 8. The Mach 6 results are given in their Figs. 3 and 13. The study was also concerned with boundary-layer transition to turbulent flow and the authors measured the unsteady wall pressure. Tabulated test conditions and boundary-layer edge properties are given. This database has been used for validation of transition models.

Chien [93]: Chien [93] performed a wind tunnel investigation on the skin friction and heat transfer on a 5° half-angle sharp cone of length 0.656 m at a freestream Mach number of 7.9. The experimental investigation was conducted in the Naval Ordnance Laboratory Hypersonic Wind Tunnel in air. Chien has tabulated the test conditions for 11 runs. The

Table 3
Model geometries and freestream conditions for cone database

Investigator	Cone half-angle	Cone length (m)	$R_n \times 10^5$ (m)	M_∞	T_0 (K)	T_w/T_0	$Re_{u\infty}/m \times 10^{-6}$
Rumsey et al. [91,92]	7.5°	0.7874	—	5.15	1265	0.591	31.0
Stainback et al. [129]	10°	≈ 0.5	—	6	500	0.6	32.9
Chien [93]	5°	0.656	—	7.90	816	0.351	35.2
Kimmel [89,90]	7°	1.016	5.0	7.93	722	0.420	6.60
Hillier et al. [94–96,130]	7°	0.5783	—	9.16	1063	0.273	55.0
Holden: cone [42,43,46,48,98]	6°	0.7073	—	13.04	1739	0.173	15.60
Holden: cone-flare [44]	6°	2.667	—	10.96	1509	0.199	12.07
Pruett (DNS) [62]	7°	1.427	0	8.0	733	0.834	3.407
Pruett (DNS) [64]	7°	0.254	0	6.0	450	0.865	8.950

Stanton number as a function of the boundary-layer edge properties and surface distance is tabulated for the 11 runs with different freestream conditions. In addition, surface skin-friction measurements were obtained in four of the runs and these values are also tabulated. The measured Stanton numbers are compared to four analytical turbulence models.

Kimmel [89,90]: The experiment by Kimmel [89,90] was conducted in the Hypersonic Wind Tunnel B at Arnold Engineering Development Center where six test conditions were used. The investigation is concerned with boundary-layer transition on a $7°$ sharp cone model of length 1 m at Mach 7.9. In addition, the aft part of the model could be flared or an ogive. Results of this experimental investigation were initially published in the proceedings of an ASME meeting [89] and later published in Ref. [90] with limited changes. The flow conditions are specified with the Mach number and total temperature held constant, while the unit freestream Reynolds number is varied by changing the total pressure. The surface pressure, surface temperature, and wall heat transfer were measured along the model. The heat transfer measurements are given in figures as the Stanton number as a function of x/L or boundary-layer edge Reynolds number with length scale x. The sharp cone results for a freestream unit Reynolds number 6.6 million per meter can be more readily obtained from this article. Boundary-layer edge conditions are not specified.

Hillier et al. [94–96,130]: At the Antibes Workshop on Hypersonic Re-entry Flows, which is documented in the books by Desideri et al. [94], the sharp cone is the first hypersonic turbulent flow problems to be solved by participants. Denmann et al. [95] obtained the experimental database in the Imperial College Number 2 Gun Tunnel, where Mach 9.2 nitrogen flow over a $7°$ cone of length 0.58 m is investigated. The flow in the nozzle is not uniform, but is like a spherical source flow, which gives a Mach number gradient along the nozzle. Mallinson et al. [96] have performed further calibration of the gun tunnel flow to determine improved input conditions for hypersonic flow computations. Measurements obtained are pressure and heat transfer (Stanton number) along the cone surface. The pitot pressure is measured across the boundary layer at two locations along the cone. With the assumption that the static pressure is constant across the boundary layer, the Mach number across the boundary layer is obtained from the Rayleigh pitot formula. The wall pressure and Stanton number along the cone surface are given. Lawrence [130] presented at the workshop results that compare his prediction of total pitot pressure across the boundary layer with the experimental data. Hillier et al. [131] have obtained further data for a new cone test model. The authors present the Stanton number as a function of a Reynolds number (distance along the surface and freestream properties). In 1993, Abgrall et al. [132] present an update of the European Hypersonic Database and the number one problem in the database is the sharp cone problem.

Holden [42–44,46,48,98]: Over more than 30 years, Holden has investigated many hypersonic flow problems experimentally and recently created a database of the measured results. Two experiments have been performed that can contribute to the sharp cone database. Holden performed the tests at the experimental facilities at Calspan in the 96 in shock tunnel in air. The testing time in this shock tunnel is approximately 25 ms, which makes the change of the model wall temperature very small during a run. The models used in the two tests are as follows:

6° sharp cone: An initial investigation was performed by Holden [48] in 1977 and has limited information provided on the model description and on the freestream flow properties in the tunnel. Documentation of the next experimental results with the same model is presented in Ref. [43]. This study is mainly concerned with boundary-layer transition on $6°$ sharp and blunt cones at angle of attack in Mach 11 and 13 flows. However, the heat flux as a function of distance along the sharp cone at zero angle of attack is given and the boundary layer has transitioned from laminar to turbulent flow. It appears the distance is along the surface of the cone and measured from the nose-tip junction point, which is not specified. It is estimated that the junction point is 0.15 m from the cone tip and the cone length is 0.71 m. In 1992, Holden [42] reviewed his experiments concerned with hypersonic flow and created a database of work performed from 1965 to 1991. The database includes the sharp cone work reported in the 1985 paper; however, little new information is presented on the turbulent boundary flow properties. Holden performed further experiments on this model in 1995 and Ref. [98] is mainly concerned with the transition issue. Tabulated data of freestream flow conditions for a list of tunnel runs is given and includes the conditions for Run 2.

In addition, tabulated data on the model config-uration, angle of attack, freestream Mach number, and unit Reynolds number for the list of runs are also given. New measured wall pressure and heat flux along the cone surface for the sharp cone at zero angle of attack are given. For these tunnel test runs, the turbulent boundary layer has not become fully turbulent. Described in Ref. [46] is the further development of Holden's hypersonic database. The sharp cone database is available on a CD ROM and on the CUBRC website (http://www.cubrc.org/aerospace/index.html) to qualified applicants. It does not appear that a complete database for experiments performed on the $6°$ sharp cone model is available in the open literature and the informa-tion available at Holden's website has not yet been investigated. Tabulation is needed of the skin friction and heat flux along the cone for the various test conditions. The tabulated properties at the edge of the boundary layer are required for the correla-tion of the skin friction and Stanton number.

$6°$ cone with $30°$ flare: The experimental study by Holden was conducted at Mach 11, 13 and 15 and the results documented in a 1991 AIAA paper [44]. Tabulation of the stagnation and freestream test conditions for the three shock tunnel runs is given. For these flow conditions, the boundary layer is fully turbulent well upstream of the cone/flare junction. The measured wall pressure and heat transfer along the cone/flare model for three runs are given. Holden measured the pitot pressure and total temperature across the boundary layer, and the velocity profiles across the boundary layer have been determined from the measurements. Tabulation of the measured turbulent boundary-layer properties are not available in the references reviewed here. Location of the cone/flare junction point is not specified in this paper but is not necessary for the solution on the $6°$ cone with the reasonable assumption that the upstream effect of the flare can be neglected. However, for the profile data, distance is measured from the cone/flare junction point. In the 1992 and 2003 database papers, Holden et al. do not provide additional information on the cone/flare experiment.

For Holden's experiments, the total temperature is sufficiently high that freestream conditions may include real gas effects due to vibrational excitation. Holden has assumed the gas is in thermodynamic equilibrium in the shock tunnel so vibrational nonequilibrium effects are neglected. This review assumes that the wall temperature of the model is at room temperature of 300 K.

3.6. Conclusion and recommendation of adequacy of experimental database

The current recommended database for 2D/axisymmetric hypersonic experiments is composed of seven different geometries. The two zero-pressure gradient geometries, the flat plate/cylinder (Case 6) and the sharp cone (Case 7), have seen the most extensive experimental study. As a result, theory-based correlations exist for these two cases. These correlations are expected to be more accurate than any single experimental data set since they have been shown to match a wide range of experimental data and tend to mitigate the effects of experimental bias errors due to the choice of measurement technique and facility (e.g., flowfield non-uniformity).

For the five geometries involving shock/turbulent boundary-layer interactions there are a total of nine recommended experiments. In general, these experi-ments include surface pressure and surface heat flux measurements, and a few also have skin-friction measurements. Most of these experiments include flow-intrusive pitot/static surveys in the interaction region. Given the elliptic mathematical character of the separated flow region, these pitot surveys should be used with caution.

Since the designer of hypersonic vehicles is primarily interested in the prediction of surface pressures for vehicle aerodynamics and surface heat flux for thermal protection systems, the current 2D/axisymmetric database for shock/turbulent bound-ary-layer interaction appears to be sufficient. How-ever, if this database is to be used to improve the turbulence models (see Section 4), then additional experiments are required. In addition to surface quantities, future experiments should measure profiles of both mean properties and turbulence statistics (rms velocities, Reynolds stresses, turbu-lent kinetic energy, etc.) in the interaction region, preferably using non-intrusive measurement techni-ques. More detailed turbulence information from experiments or DNS might aid in the determination of where these turbulence models break down, ideally on a term-by-term basis. Significant efforts should be made to quantify and reduce the experimental uncertainties in the measurement and freestream quantities. Approaches for converting experimental bias errors into random uncertainties

(e.g., Ref. [27]) should also be employed. Finally, preference should be given for axisymmetric geometries instead of 2D ones due to the possibility of 3D end wall effects.

4. Usage of the hypersonic validation database

4.1. Validation of theory-based correlations

4.1.1. Flat plate/cylinder

The first step in using the flat plate/cylindrical experimental or DNS database is concerned with the validation of the accuracy of the theoretical correlations for skin friction, heat transfer, velocity profiles, and temperature profiles. Theories have been developed to correlate the skin friction or Stanton number of compressible turbulent boundary-layer flows with zero-pressure gradient into a single correlation curve. In addition, the velocity and temperature profiles in the inner or outer regions of the turbulent boundary layer can also be correlated into a single profile (see Section 3.3 and Appendix B). The correlation curves or profiles are based on analysis and validation with a large database to establish the accuracy of the various theories. The following investigators have used the hypersonic experimental data given in Table 2 to assess the accuracy of theoretical correlations for turbulent boundary layers with zero-pressure gradient.

Van Driest [133,134]: In the initial article [133] (Van Driest I) a theory is developed for predicting properties of compressible turbulent boundary-layer flows with the Prandtl mixing-length model, but no comparison of theory to experimental data is given. In the second article [134] (Van Driest II) the theory is modified to incorporate the von Karman mixing-length turbulence model. The turbulent Prandtl number is still assumed to be one, but in the temperature relation the recovery factor is introduced. The usual approach of plotting normalized skin-friction as a function of Mach number was used by Van Driest and he compared the two theories to experimental data. The experimental database included supersonic data of Coles [135] and Chapman–Kester [136] and hypersonic data of Sommer–Short [104] and Korkegi [106]. With this supersonic/hypersonic database, no conclusion could be made on which of the two Van Driest theories provided the best prediction of skin friction.

Peterson [105]: Peterson [105] compares seven theories for predicting the skin friction with an experimental database for turbulent boundary-layer flows with zero-pressure gradient. The theories transform the experimental skin friction and Reynolds number to incompressible (transformed) values. The theoretical prediction of the incompressible skin friction as a function of incompressible Reynolds number is obtained from the Karman–Schoenherr formula, which is considered the most accurate fit of the incompressible experimental database. Peterson uses an experimental compressible skin-friction database obtained from 21 references and the data from the references are tabulated. For hypersonic flow, there are two references for an adiabatic wall [106,113] and there are four references for a non-adiabatic wall [112,104,107,108]. The significance of this paper is that the author uses the transformations of the various theories to correlate all of the experimental data at different Mach numbers, wall temperature ratios, and Reynolds numbers into a single curve. Also, Peterson recognizes the work of Wilson [137] where he developed a skin-friction transformation for zero heat transfer with the von Karman mixing-length law. Van Driest [133] developed a skin-friction transformation with the Prandtl mixing-length (now referred to as Van Driest I). Van Driest [134] extended the theory of Wilson to the case with heat transfer (Van Driest II, or more appropriately, Peterson refers to this theory as Wilson–Van Driest).

Spalding–Chi [110,138]: Spalding–Chi [110] developed an analytical prediction theory for the skin friction on a smooth surface with zero-pressure gradient at various momentum thickness Reynolds numbers ($400 < Re_\theta < 7500$), Mach numbers ($M < 10$), and surface temperatures to free stream temperature $[0.1 < (T_w/T_\infty) < (T_{aw}/T_\infty)]$. A significant number of the experiments are at hypersonic Mach numbers but the wall temperature range is limited. The hypersonic database includes investigations by Sommer–Short [104], Korkegi [106], Hill [107,108], Brevoort and Arabian [111], Matting et al. [113], and Winkler [112]. The RMS value of $(C_{f,exp} - C_{f,th})/C_{f,th}$ for the total database used in this paper is 11% for van Driest II and 9.9% for the Spalding–Chi theory.

Chi and Spalding [138] developed a theoretical analysis to correlate Stanton number (heat transfer) as a function of the Reynolds number. The compressible Stanton and Reynolds numbers for

experimental data points are transformed into incompressible values and should reduce into a single curve. The authors use a database of 11 experiments on isothermal surfaces in air flow with zero-pressure gradient to establish the accuracy of the theoretical correlation. The Chi–Spalding theory is shown to be reasonably accurate. Three of the experiments are for $5.04 < M < 5.25$ with the data from Brevoort and Arabian [111], Tendeland [109], and Winkler [112]. The experiment of Hill [108] provides data at Mach 8.27, 9.07, and 10.04 which was obtained in a conical nozzle with nitrogen gas flow. The Brevoort–Arabian geometry is an axially symmetric annular nozzle which consists of an inner shaped center body and an outer cylindrical sleeve. Boundary-layer measurements were made on the inside of the sleeve which gives essentially flat plate results. The Tendeland experiment uses the turbulent boundary layer along a cone-cylinder geometry. In the determination of the Stanton number, a Reynolds analogy factor of 1.16 is used for the complete database. Further details of the Spalding–Chi theory is given in Appendix B.

Hopkins et al. [81,86,87,139]: Hopkins et al. [86] investigated the accuracy of the correlation theories of Sommer and Short, Spalding and Chi, Van Driest II, and Coles for the local skin friction. The prediction of heat transfer for these theories was also investigated. Hopkins et al. [87] investigated eight local skin-friction transformation theories of Van Driest II, Spalding–Chi, Sommer–Short, Eckert, Moore, Harkness, Coles, and Baronti–Libby. These theories were assessed against the Mach 6.5 experimental database of the authors. It was concluded that the methods of Van Driest II and Coles predict the skin friction within about 5%. The other six theories underpredicted the skin friction from 10% to 25% for this experimental data set. The survey article by Hopkins and Inouye [139] is based on a NASA Technical Note [86] and includes additional skin friction and heat transfer data. Four theories are investigated further and these theories are described in the survey article. The incompressible skin-friction formula of Karman–Schoenherr is used to determine the skin friction as a function of the momentum thickness Reynolds number. The hypersonic database for the *adiabatic flat plate* is only the experiment of Korkegi [106] while the database for the non-adiabatic flat plate is Sommer and Short [104] (hollow cylinder), Hopkins et al. [86], Hopkins–Keener–Louie [87], Wallace–McLaughlin [116], Young [115], and Neal [120].

The authors suggested for hypersonic flat plate flows that Van Driest II theory be used to predict turbulent skin friction, and that heat transfer be obtained with a Reynolds analogy factor equal to 1.0 and a recovery factor equal to 0.9. In the ensuing article by Hopkins et al. [122], the four theories for correlating experimental skin-friction data were further investigated. Their experimental data was compared to numerical turbulent boundary-layer solutions with an algebraic eddy viscosity model of Cebeci. In addition the Baronti–Libby and Van Driest methods for correlating mean velocity profiles were investigated. The authors determined that the Van Driest II, Coles, and numerical turbulent boundary-layer solutions give the best predictions of skin friction and are within ±10%. The authors state "The Van Driest theory gave the most satisfactory transformations of the velocity–profile data onto the incompressible law of the wall and velocity–defect curves." Keener and Hopkins [81] have investigated five velocity profile correlation methods for their Mach 6.5 database: wall reference temperature, T' method of Sommer and Short, Coles, Baronti–Libby, and Van Driest transformations. It is stated that the use of either the Prandtl mixing length (Van Driest I) or the von Karman mixing length (Van Driest II) result in identical transformation functions. The Van Driest method gives the best correlation for both the law of the wall and velocity–defect law when compared to Coles' incompressible velocity profile data. However, the correlations deteriorate with decreasing momentum thickness Reynolds number.

Cary and Bertram [53]: Cary and Bertram [53] made an investigation of the Reynolds analogy and prediction methods for skin friction and heat transfer on flat plates and cones for high speed flows. The incompressible local skin friction in this paper is obtained from the Spalding–Chi relation. The Spalding–Chi relation is 2.0% lower than the Karman–Schoenherr equation at $Re_\theta = 10^3$ and 2.4% high at $Re_\theta = 10^6$. The database used in this work has a Mach number range from 4 to 13 and ratio of wall to total temperature from 0.1 to 0.7. The Reynolds analogy factor for Mach numbers less than approximately 5 is adequately approximated with $R_{af} = 1.16$ for the available wind-tunnel database. For turbulent flow with significant wall cooling and Mach numbers greater than 5 at any ratio of wall to total temperature R_{af} is ill defined. The von Karman expression for R_{af} is approximately 10% higher than experimental data of Keener and Polek [140] and

Holden [141]. In the authors' summary, they state that the Spalding and Chi transformation method incorporating virtual-origin concepts was found to be the best prediction method for Mach numbers less than 10. The Spalding and Chi transformation method using Karman's Reynolds analogy was shown to give the best predictions based on either the length or momentum thickness Reynolds number when the proper virtual origin was specified. The small amount of experimental data for Mach numbers greater than 10 were not correlated well by any of the transformation approaches. The hypersonic database used in this investigation of the accuracy of correlation theories was obtained from the data of Heronimus [118], Wallace [117], Cary and Morrisette [121], Hopkins et al. [86], Cary [123], Weinstein [124], Hopkins et al. [122], Holden [45], and Coleman et al. [66,85].

Owen et al. [84]: Boundary-layer measurements were made downstream on a cone-ogive-cylinder model at a freestream Mach number of 7.0 [84]. Fluctuating and mean flow measurements were obtained at one location sufficiently far downstream where the pressure gradient is zero. Mean velocity and total temperature boundary-layer profiles are given. The relation between T^* (the total temperature in non-dimensional form, see Appendix B) and velocity is linear except in the region close to the wall. The velocity profile was transformed to the incompressible form with Van Driest theory and compared to the incompressible velocity correlation curve of Coles. The data are in good agreement with the incompressible law of the wall correlation. In the outer region of the boundary layer, the data are in good agreement with the incompressible velocity–defect correlation.

Fernholz and Finley [29]: The authors investigated the accuracy of some of the cases in the compressible experimental database for the turbulent mean temperature and velocity profiles with comparison to theoretical correlations [29]. The hypersonic cases investigated are as follows:

Keener and Hopkins [81] (Fernholz & Finley Case 7204): The *sharp flat plate* experiments have zero-pressure gradient with no upstream history effects. The static temperature is in good agreement with the theoretical correlation in the outer part of the boundary layer. Five methods are evaluated for correlating the measured velocity profiles with the incompressible form of the law of the wall and the velocity defect law. The Van

Driest method gives the best correlation of the velocity profiles. The experimental velocity profile database is concluded to be in good agreement with the law of the wall and the velocity defect law.

Horstman and Owen [83] (Fernholz & Finley Case 7205): This experiment investigated the turbulent boundary-layer flow over an axisymmetric *cone-ogive-cylinder body* where downstream the Mach number is 7.2 at the edge of the boundary layer. The nose of the body might have introduced a slight favorable pressure gradient. However, it is highly probable that the boundary layer has reached equilibrium at the three measurement stations. Agreement between the velocity profile measurements and the law of the wall is very good. There is good agreement with the outer velocity law. Agreement between measured and theoretical temperature profiles is satisfactory.

Kussoy and Horstman [36,38]: The first flat plate experiment of Kussoy and Horstman [38] without fins or wedges provides data at Mach 8.2 and at one location, 1.87 m from the sharp leading edge. The experimental mean velocity profile was transformed into incompressible coordinates with Van Driest II theory and compared to Coles' universal law of the wall. Since the data and the theory were in reasonable agreement, the authors concluded that the turbulent boundary layer is fully developed. The second experiment [36] is for a flat plate at Mach 8.3 with the data obtained at 1.62 m from the leading edge. Again the transformed mean velocity profile is compared to Coles' law of the wall profile in inner variables. The authors conclude that the turbulent boundary layer is fully developed. Further analysis of the outer region correlation of the boundary layer also needs evaluation.

Huang et al. [54]: In Ref. [54] a self-consistent transformation method (denoted as HBC) was developed to predict skin friction and velocity profiles of compressible boundary-layer flows with zero-pressure gradient. The paper is also concerned with the assessment of the authors' HBC transformation by comparing the predictions to the well accepted Van Driest transformation and experimental data. For an adiabatic and non-adiabatic wall, the prediction of skin friction with the two theories was compared to the experimental database used by Hopkins and Inouye [139]. The database was not sufficiently accurate to determine the better theory. The database of Watson [126] was also used

to assess the accuracy of the two theories for skin friction. The HBC theory was more accurate than Van Driest II for this case. In addition, the predictions obtained with the HBC transformation method are in good agreement with the experimental velocity and temperature profiles of Kussoy and Horstman [38]. The investigation of Fernholz and Finley [29] has shown that the Van Driest II transformation does indeed transform the compressible velocity profile data into a profile that matches the incompressible law of the wall.

4.1.2. Sharp circular cone

One of the problems with the sharp cone is the lack of a sufficiently accurate theoretical correlation of the experimental data to use as a benchmark solution. For laminar flow, the skin friction and heat transfer for a flat plate are multiplied by $\sqrt{3}$ to obtain the cone values. There does not appear to be a well-defined approach to transform the turbulent flat plate results to the cone. However, the flat plate correlation approach for skin friction and heat transfer has been extended to the sharp cone with some approximations. The sharp cone geometry is well suited to wind tunnel testing and avoids the 2D/3D issues involved with flat plate flows.

In the correlation of the surface skin friction and heat transfer, the flow properties at the edge of the boundary layer are required. For high Reynolds number flows, the boundary layer is thin and the edge properties can be obtained from the inviscid conical flow solutions, where the edge properties are approximated with the wall properties. Perfect gas tables of the inviscid surface properties as a function of Mach number and cone half-angle have been developed by Sims [142] (Sims discusses earlier tables developed by Taylor–Maccoll and Kopal.). As interpolation is required with the use of the tables, the wall properties obtained from the numerical solution of the governing ordinary differential equations is a better approach. The conical inviscid perfect gas flow is determined with the cone half-angle θ_c and the freestream Mach number M_∞ specified. The following cone surface properties are obtained from the tables with linear interpolation: M_e, T_e/T_∞, and p_e/p_∞. Then the edge properties are obtained from the relations

$$T_e = T_\infty(T_e/T_\infty), \quad p_e = p_\infty(p_e/p_\infty),$$

$$a_e = \sqrt{\gamma R T_e}, \quad u_e = M_e a_e,$$

$$\rho_e/\rho_\infty = (p_e/p_\infty)/(T_e/T_\infty), \quad \rho_e = p_e/RT_e,$$

$$\mu_e = \mu(T_e), \text{ Sutherland or Keyes viscosity,}$$

$$Re_{u_e} = \rho_e u_e/\mu_e, \text{ Unit Reynolds number.}$$

The shear stress τ_w and heat flux q_w at the surface of the cone are two of the quantities desired from the experiments, turbulence modeling, and the numerical solutions. The wall shear stress is usually written as the non-dimensional skin-friction parameter, which is defined in two forms

$$C_{f\infty} = 2\tau_w/\rho_\infty u_\infty^2, \quad C_{fe} = 2\tau_w/\rho_e u_e^2.$$

The wall heat flux is usually written as the non-dimensional Stanton number, which is defined in two forms

$$St_\infty = q_w/\rho_\infty u_\infty c_p(T_{0\infty} - T_w), \quad c_p = \gamma R/(\gamma - 1),$$

$$St_e = q_w/\rho_e u_e c_p(T_{aw} - T_w) = q_w/\rho_e u_e(H_{aw} - H_w),$$

$$H = c_p T + \frac{u^2}{2}. \tag{9}$$

The second form of the Stanton number becomes indeterminate when the heat flux is zero. The heat transfer coefficient h_c is also sometimes used and is defined as $q_w = h_c(T_{aw} - T_w)$. The flow properties across the turbulent boundary layer are also useful in the evaluation and validation of turbulence modeling.

Hopkins–Inouye [139]: Hopkins and Inouye [139] have assessed four transformation theories for flat plate hypersonic flows which already have been discussed. However, in the database, the heat transfer on sharp circular cones obtained by Mateer [86,143–145] is included. In a NASA Technical Note, Hopkins et al. [86] have shown that the experimental data for the Stanton number as a function of energy thickness Reynolds number for the cone and a flat plate are essentially the same when the edge Mach numbers and wall temperature ratio (T_w/T_{aw}) are nearly the same. A Reynolds analogy factor of 1.16 was used for this case. No indication of the use of a geometry transformation factor is mentioned.

Chien [93]: Chien [93] measured skin friction and heat transfer (Stanton number) along the cone surface and compared the data to four theories for predicting skin friction and heat transfer for zero-pressure gradient boundary-layer flows. The Karman formula for the Reynolds analogy factor with the Bertram–Neal modification is used to determine

heat transfer. The paper does not indicate that any Mangler-type transformation is used to modify the flat plate predictions to the cone case. The methods of Spalding–Chi, Van Driest II, Sommer–Short, and Clark–Creel are evaluated. The Van Driest II and Clark–Creel skin-friction predictions are within about 10% of the experimental data. The Van Driest II method gives reasonable prediction of heat transfer for $T_w/T_0 > 0.2$. For $T_w/T_0 = 0.11$, Spalding–Chi method results are within 10% for the heat transfer.

Holden [44,48]: The experimental database obtained by Holden [48] in 1977 is used to correlate the heat transfer expressed as Stanton number as a function of Reynolds numbers Re_x and Re_θ. The transformation models that transform the compressible Stanton number and Reynolds number to incompressible values are Spalding–Chi, Van Driest II, and Eckert. It is concluded that Van Driest II method gives the best overall agreement with the experimental database. Holden [44] has presented the cone correlation again in a 1991 AIAA paper where a better plot is given for the Van Driest II correlation of Stanton number as a function of Re_x. There is approximately a 30% scatter of the experimental data about the theoretical incompressible correlation curve. For further discussion see Appendix C.

Dinavahi [97]: A boundary-layer computer code with a Baldwin–Lomax algebraic turbulence model is used by Dinavahi [97] to predict the laminar to turbulent flow on a sharp cone at Mach 6. The experiment of Stainback et al. [129] for a $10°$ half angle cone is used to evaluate the transition and turbulent models. The prediction and experimental results for the Stanton number along the cone surface are in reasonable agreement; however, the length of the measured turbulent region is short and the turbulent flow might not be fully developed.

Pironneau [94]: Pironneau ("A Synthesis of Results for Test Case 1 and 2: Hypersonic Boundary layer and Base Flow," pages 92–94 in Desideri et al. [94]) reviewed the work on the first test case in the modeling and computational Workshop on Hypersonic Flows for Reentry Problems. The first test case is the perfect gas turbulent boundary-layer flow on a cone. The cone model experiment was performed by Denman et al. [95] in a contoured Mach 9 axisymmetric nozzle which produced a weak source-like (spherical) flow that should be modeled in the computation. Lawrence [130] solved the flow field with a Parabolized Navier–Stokes code and the algebraic turbulence model of Baldwin–Lomax was used. The cone surface static pressure and Stanton number were measured and predicted. In addition, boundary-layer profile data for pitot pressure were measured and predicted. Pironneau concluded that the investigations were extremely well done by all investigators with the influence of all parameters carefully studied, yet there was a 10% difference between computational and experimental results. Their results were inconclusive since it is unclear whether the discrepancies arise due to modeling deficiencies or uncertainty in the experimental data.

McKeel et al. [146]: McKeel et al. [146] are concerned with modeling the transition problem with the Baldwin–Lomax algebraic model, Wilcox 1988 k–ω two-equation model, and k–ε Lam–Bremhorst model. One of the problems investigated is transition on a sharp cone in hypersonic flow using the database of Stainback et al. [129], where the free stream Mach number is 6 (see Section 4.5.3). This database gives the Stanton number variation along the surface of the cone. The authors compare the transition/turbulent model predictions with the experimental heat transfer measurements. The turbulent predictions with the three models are in reasonable agreement with the data, and the k–ω model is a little more accurate.

4.2. Validation of turbulence models

There are 18 different turbulence models that are assessed in the current work. These models are listed in Table 4 along with the notation used to reference the model. Recall that we focus only on one- and two-equation turbulence models where integration to the wall is employed (i.e., no wall functions) and which have also been previously validated for a wide range of non-hypersonic flows. We thus omit compressibility corrections which have not yet been applied to a comprehensive low-speed validation database, or which do not vanish at lower speeds.

The turbulence models that have been evaluated for 2D/axisymmetric hypersonic flows are listed below, along with the shorthand notation for the models used throughout this review. Note that the discussion of the turbulence models given here is brief. The interested reader is encouraged to see the original references for specific details of the models. Of these 18 turbulence models, only six have seen extensive validation for the current 2D/axisymmetric

Table 4
Turbulence model notation

Turbulence model	Notation
One-equation models	
Spalart–Allmaras [147,148]	SA
Goldberg [149,150]	UG
Menter [151]	MTR
Two-equation models	
k–ε Jones–Launder [152]	$k\varepsilon$JL
k–ε Launder–Sharma [153]	$k\varepsilon$LS
k–ε Chien [154]	$k\varepsilon$CH
k–ε Nagano and Hishida [155]	$k\varepsilon$NH
k–ε Rodi [156]	$k\varepsilon$R
k–ε So [157,158]	$k\varepsilon$SO
k–ε Huang–Coakley [11]	$k\varepsilon$HC
k–ω Wilcox (1988) [159]	$k\omega$88
k–ω Wilcox (1988) low Reynolds number [159]	$k\omega$88LR
k–ω Wilcox (1998) [6]	$k\omega$98
k–ω Menter with SST [160]	SST
k–ω Menter with BSL [160]	BSL
k–l Smith [161,162]	kl
k–ζ Robinson–Hassan [163,164]	$k\zeta$
q–ω Coakley [165]	$q\omega$

hypersonic validation database: SA, $k\varepsilon$JL, $k\varepsilon$LS, $k\varepsilon$R, $k\omega$88, and $q\omega$.

4.2.1. One-equation models

4.2.1.1. Spalart–Allmaras (SA). A transport equation for determining the eddy viscosity with near-wall effects included has been developed by Spalart and Allmaras [147,148]. The accuracy of the predictions with the Spalart–Allmaras (SA) model is fairly insensitive to the y^{+} spacing at the wall relative to the two-equation models, at least for high-speed flows [166]. Our experience with this model suggests that it has a good combination of accuracy and robustness for attached flows. While stable for large y^{+} values, the maximum for accurate solutions should be roughly $y^{+} \leqslant 1$.

4.2.1.2. Goldberg (UG). Goldberg has developed the one-equation R_{t} turbulence model [149,150]. This model has been shown to provide good predictions for the hypersonic compression ramp (Case 1), but has not yet seen widespread application to the experimental hypersonic database. This model does not require a wall distance to be calculated.

4.2.1.3. Menter one-equation model (MTR). Menter has developed a one-equation eddy viscosity

transport model [151]. This model is derived from the standard k–ε model, and this relationship is explored in detail in Ref. [151].

4.2.2. Two-equation models

4.2.2.1. Jones and Launder high Reynolds number k–ε ($k\varepsilon$JL). The basic k–ε model was developed by Jones and Launder [152] in 1972. The model constants were later refined by Launder and Sharma [153] (see below).

4.2.2.2. Launder and Sharma (standard) k–ε ($k\varepsilon$LS). The Jones and Launder k–ε model [152] was revised by Launder and Sharma [153] in 1974. It is this 1974 revised model that is generally referred to as the "standard" k–ε model. This model is generally good for free shear flows, but will not be as accurate for wall-bounded flows as the k–ω models, especially in the presence of adverse pressure gradients. Marvin and Huang recommend that the y^{+} values at the wall be kept below 0.3 for this model [5].

4.2.2.3. Chien k–ε ($k\varepsilon$CH). Chien has developed a low Reynolds number k–ε model [154]. This model was shown to provide better predictions of peak turbulent kinetic energy than the Jones–Launder model when applied to fully-developed channels and turbulent flat plates.

4.2.2.4. Nagano and Hishida k–ε ($k\varepsilon$NH). Nagano and Hishida have developed a low Reynolds number k–ε model [155]. While this model has been investigated for zero-pressure gradient cases at hypersonic speeds, it has seen little validation usage for shock interaction flows.

4.2.2.5. Rodi k–ε ($k\varepsilon$R). Rodi has developed a two-layer low Reynolds number k–ε model [156]. In the outer layer, the standard dissipation rate ε equation is used, while in the inner layer, an analytic expression for ε is used. This model has seen extensive validation usage for the hypersonic experimental database.

4.2.2.6. So k–ε ($k\varepsilon$SO). So et al. have developed a low Reynolds number k–ε model [157] by modifying the near-wall behavior of ε based on DNS and experimental data.

4.2.2.7. Huang and Coakley k–ε (kεHC). Coakley and Huang have developed a low Reynolds number k–ε model [11] which is based on DNS data.

4.2.2.8. Wilcox 1988 k–ω (kω88). The Wilcox 1988 k–ω model [159] is generally better than the k–ε model for wall-bounded flows, especially in the presence of adverse pressure gradients. It is recommended that the y^+ values at the wall be kept well below one. One problem with this original Wilcox k–ω model is the sensitivity of the results to the freestream ω levels.

4.2.2.9. Wilcox 1988 k–ω low Reynolds number (kω88LR). Wilcox has also developed a low Reynolds number version of his 1988 k–ω model (see Chapters 4.9.2 and 4.9.3 of Ref. [6] for details).

4.2.2.10. Wilcox 1998 k−ω (kω98). In 1998, Wilcox updated his original k–ω turbulence model to more accurately predict free shear flows [6]. This updated version will be referred to as the Wilcox 1998 k–ω model, or kω98, herein. While the sensitivity of the results to the freestream ω levels is indeed reduced in the 1998 version of the model [6], some sensitivity effects remain, at least for high-speed flows [16].

4.2.2.11. Menter baseline k–ω (BSL). The baseline (BSL) Menter k–ω model is a blending of the Wilcox 1988 k–ω model [6] near walls and a transformed k–ε model in shear layers and the freestream [160]. The BSL model utilizes the blending to reduce the sensitivity to freestream turbulence levels that afflicts the Wilcox k–ω model. This model has obtained good results for a wide range of flows.

4.2.2.12. Menter shear stress transport k–ω (SST). The Menter Shear Stress Transport (SST) k–ω model utilizes the same blending between the k–ω and k–ε models as the BSL model; however, the SST model also employs a modified form of the eddy viscosity definition which accounts for the transport of the Reynolds stress [160]. This modification improves the SST model's predictive accuracy for flows with adverse pressure gradients.

4.2.2.13. Smith k−l (kl). Smith has developed a two-equation k−l model [161,162] as an improvement to an earlier k−kl model [167]. This model has been shown to provide accurate velocity profiles on

compressible flat plate flows where typical k–ε models fail.

4.2.2.14. Robinson and Hassan k−ζ (kζ). It is generally acknowledged that the failure of the standard k–ε model to accurately predict a wide variety of flows is due to inadequate modeling of the dissipation equation. Robinson and Hassan [163,164], have developed a new two-equation turbulence model based on the vorticity variance (enstrophy) equation which has demonstrated good predictive capability for a wide-variety of flows. A number of modeled terms in the enstrophy equation are included with the goal of incorporating additional physics into the equation governing the dissipation of turbulent kinetic energy. The k−ζ model does not employ damping or wall functions.

4.2.2.15. Coakley q−ω (qω). A two-equation q−ω model ($q = k^{1/2}$) was developed by Coakley [165] to predict low-Reynolds number transition and increase numerical robustness over other two-equation models. This model has been demonstrated to have more favorable numerically stability behavior than standard k−ω models when integrated to the wall.

4.2.3. Physical freestream turbulence quantities

One method for determining the freestream turbulence properties is as follows. For the two-equation models, the specification of a freestream turbulence intensity (Tu) can be used to determine the turbulent kinetic energy in the freestream from

$$k = \frac{1.2}{2}(TuV_\infty)^2, \qquad (10)$$

where, for example, $Tu = 0.1$ corresponds to a freestream turbulence intensity of 10%. However, the experimental measurement of ε (or ω, ζ etc.) is extremely difficult. As a result, the dissipation variable is often determined by specifying the ratio of turbulent to laminar viscosity, μ_T/μ, i.e.,

$$\varepsilon = \frac{C_\mu \rho k^2/\mu}{\mu_T/\mu} \qquad (11)$$

or

$$\omega = \frac{\rho k/\mu}{\mu_T/\mu}. \qquad (12)$$

For one-equation eddy viscosity turbulence models, the transported variable is simply found from the μ_T/μ ratio.

4.2.3.1. Effects on transition. High freestream turbulence intensity levels can lead to early transition from laminar to turbulent flow. This phenomenon is often referred to as bypass transition (since the natural transition mechanisms are bypassed), or more recently as transition due to a high disturbance environment [168]. While some turbulence models also provide a transition prediction capability, the transition process is complex, especially for high-speed flows, and its modeling is beyond the scope of the current work.

4.2.3.2. Effects on turbulence. Experimental evidence [25,169] suggests that surface properties (e.g., shear stress) in the fully-developed turbulent region are generally not affected by freestream turbulence intensity, at least in the case of low-speed flows. Thus, it is expected that there should be little or no effect of the freestream turbulence levels on the mean flow predictions. Note that this is not the case in free shear layers, where the freestream turbulence levels can have a significant effect on the flow.

4.3. Turbulence model application to the hypersonic validation database

A listing of hypersonic validation experiments is presented in Table 5 along with the turbulence models from Table 4 that have been used with each experiment for validation purposes. The flow geometries in Table 5 include the accepted 2D/axisymmetric experiments of Settles and Dodson [1–4] as Cases 1–4. Case 5 should also become a standard benchmark case for hypersonic shock/turbulent boundary-layer interaction flows. Cases 6 and 7 are zero-pressure gradient flows and have received extensive validation usage. For the sharp circular cone (Case 7), an accurate correlation of the sharp cone database similar to Van Driest II for the flat plate is needed.

A summary of the turbulence model validation usage is presented in Table 6. It is clear from the table that of the 18 turbulence models that have been applied to this 2D/axisymmetric hypersonic validation database, only a limited number have seen extensive validation. In fact, only five turbulence models have been applied to the majority of these seven geometries (SA, $k\varepsilon$JL, $k\varepsilon$LS, $k\varepsilon$R, and $k\omega$88). A sixth model, the $q\omega$ model of Coakley, has been applied to three of the five shock interaction geometries (Cases 1–5). Our review will

therefore emphasize the assessments of these six turbulence models, which are summarized in Table 7.

4.4. Previous flow geometries with adverse pressure gradient

4.4.1. Case 1: 2D compression corner

There are two hypersonic experiments for the 2D compression corner which are deemed acceptable with some caveats: the experiments of Coleman and Stollery [31] and Coleman [66] with surface pressures by Elfstrom [67], and the experiment of Holden [48]. An overview of the model validation using the Coleman/Stollery/Elfstrom experiment is summarized graphically in Figs. 1 and 2 for the six turbulence models given in Table 7.

Coleman and Stollery/Elfstrom experiment [31,66,67]: Horstman [170] has used the Coleman and Stollery/Eflstrom experiment (among others) to perform validation computations for two-equation k–ε models. The two turbulence models examined are the high-Reynolds number Jones–Launder k–ε model ($k\varepsilon$JL) and the low Reynolds number k–ε model of Rodi ($k\varepsilon$R). A third k–ε model employing various compressibility corrections was also examined. However, this model was calibrated using some of the hypersonic validation experiments, thus blurring the line between model prediction and calibration. The third k–ε model is not included in this review. A y^+ study was performed on a different (unspecified) geometry for this case using surface heat flux, and showed that the $k\varepsilon$JL model was sensitive to y^+ values above 0.15, while the $k\varepsilon$R model showed some mild sensitivity above 0.5. A grid refinement study was also performed on a few of the test cases (again, which cases were not specified) with no change in the predicted values on grids of 40×100 and 60×150. No sensitivities to the freestream turbulence quantities were discussed. For the 2D compression ramp, the $k\varepsilon$JL model was found to match the pressure well everywhere except for the constant pressure plateau on the ramp where it is overpredicted by 20% (see Fig. 1). The heat transfer predicted by this model is given in Fig. 2 and greatly overpredicts the heating both in the interaction region and in the plateau region, in some locations overpredicting by an order of magnitude or more. The $k\varepsilon$R model performed much better, matching the experimental pressure data within 10% and accurately predicting the heat transfer everywhere except within the interaction region,

Table 5
Turbulence models assessed using the hypersonic validation database

Case no.	Flow geometry	Experiments	Validation usage	Turbulence models assessed
1	2D compression corner	[31,66,67]	[7,11,12]	$q\omega$, $k\omega88$, $k\varepsilon$LS, $k\varepsilon$CH, $k\varepsilon$SO, $k\varepsilon$HC
			[170]	$k\varepsilon$JL, $k\varepsilon$R
			[149,150]	UG, SA, MTR
			[171]	$k\omega88$LR, SA, SST
			[172,173]	$k\zeta$
		[48]	None	
2	Cylinder with conical Flare	[32]	[10,170]	$k\varepsilon$JL, $k\varepsilon$R
			[7,11,12]	$q\omega$, $k\omega88$, $k\varepsilon$LS, $k\varepsilon$CH, $k\varepsilon$SO, $k\varepsilon$HC
			[174]	$k\omega88$
			[175]	SA, SST
		[68,69]	None	
3	Cone with conical flare	[44]	[170]	$k\varepsilon$JL,$k\varepsilon$R
4	Axisymmetric impinging shock	[35,70,71]	[7,12]	$k\omega88$, $k\varepsilon$LS
			[170]	$k\varepsilon$JL, $k\varepsilon$R
			[176]	$q\omega$
		[72–75]	None	
5	2D impinging shock	[38]	[170]	$k\varepsilon$JL, $k\varepsilon$R
			[161]	kl
		[76,78]	[172,173]	$k\zeta$
			[177]	$k\omega88$
6	Flat plate/cylinder	VDII [51]	[178]	Various
			[13]	$k\omega88$, $k\varepsilon$LS, SST, SA
			[171]	$k\omega88$, SST, SA
			[16]	SA, $k\omega98$, $k\varepsilon$NH, BSL
			[175]	SA, $k\omega88$, SST
		HBC [54]	[179]	$k\omega88$, $k\varepsilon$LS
			[13]	$k\omega88$, $k\varepsilon$LS, SST, SA
		AVC [8]	[8]	$k\omega88$, $k\varepsilon$LS
			[180,181]	$k\omega88$, $k\varepsilon$CH, kl, SA
		[79–81]	None	
		[82–84]	None	
		[85]	None	
		[36,38]	None	
		[86,87]	None	
		[42,46,48,88]	None	
7	Sharp circular cone	VDII [51]& White [56]	[16]	SA, $k\omega98$, $k\varepsilon$NH, BSL
		[89,90]	[182,183]	$k\zeta$
			[16]	SA, $k\omega98$, $k\varepsilon$NH, BSL
		[91,92]	None	
		[93]	None	
		[94–97]	None	
		[42–44,46,48,98]	None	

where the model overpredicts the heating by a factor of two.

Coakley, Huang, and coworkers [7,11,12] also used the Coleman and Stollery/Eflstrom experiment for turbulence model validation purposes. A num-ber of different two-equation turbulence models were examined including: the q–ω model of Coakley ($q\omega$), the 1988 k–ω model of Wilcox ($k\omega88$), the k–ε model of Launder and Sharma ($k\varepsilon$LS), the k–ε model of Chien ($k\varepsilon$CH), the $k-\varepsilon$ model of So

Table 6
Summary of turbulence models assessed using the hypersonic validation database

Turbulence model	Case 1	Case 2	Case 3	Case 4	Case 5	Case 6	Case 7
SA	X	X				X	X
UG	X						
MTR	X						
$k\varepsilon$JL	X	X	X	X	X		
$k\varepsilon$LS	X	X		X		X	
$k\varepsilon$CH	X	X				X	
$k\varepsilon$NH						X	X
$k\varepsilon$R	X	X	X	X	X		
$k\varepsilon$SO	X	X					
$k\varepsilon$HC	X	X					
$k\omega$88	X	X		X	X	X	
$k\omega$88LR	X						
$k\omega$98						X	X
SST	X	X				X	
BSL						X	X
kl					X	X	
$k\zeta$	X				X		X
$q\omega$	X	X		X			

Table 7
Summary of turbulence model assessment using the hypersonic validation database for selected models with a significant hypersonic validation history

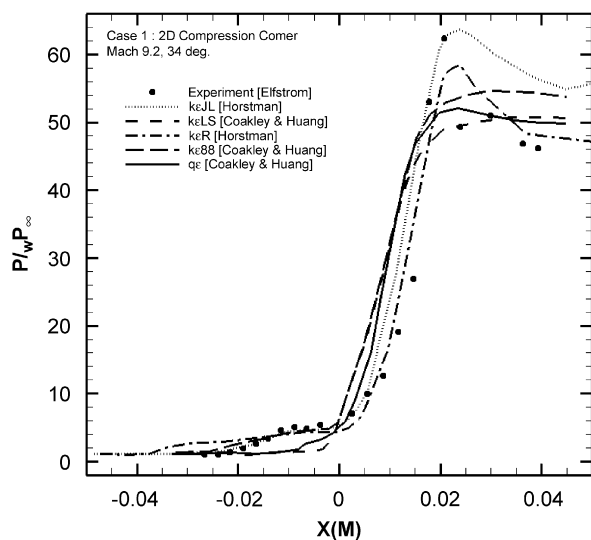| Turbulence model	Case 1	Case 2	Case 3	Case 4	Case 5	Case 6	Case 7
SA	X	X				X	X
$k\varepsilon$JL	X	X	X	X	X		
$k\varepsilon$LS	X	X		X		X	
$k\varepsilon$R	X	X	X	X	X		
$k\omega$88	X	X		X	X	X	
$q\omega$	X	X		X			

Fig. 1. Surface pressure turbulence model comparisons for Case 1: 2D compression corner at 34° (experiment by Elfstrom [67]).
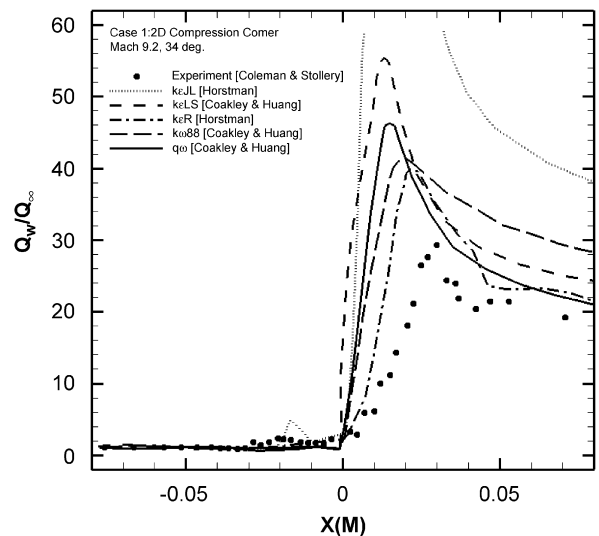

Fig. 2. Surface heat flux turbulence model comparisons for Case 1: 2D compression corner at 34° (experiment by Coleman and Stollery [31]).

(kεSO) which includes compressibility extensions given by Zhang et al. [158], and the k–$ε$ model of Huang and Coakley (kεHC). A number of modeling corrections designed specifically for high-speed separated flows were also investigated by these authors, but it is unclear how these corrections impact the previous validation efforts for the model, especially at low speeds. These corrected models will therefore not be included in the current review. Grid refinement studies were discussed, but no results were presented and no estimates of the discretization error were given. A wall-spacing study showed that y^+ values greater than one gave errors in the skin friction ($>2\%$) and also gave stability problems with some models; however, varying the y^+ values from 0.1 to 1.0 showed no changes. Sensitivities to the freestream turbulence quantities were not addressed. Only the kεLS and kω88 models were examined for the 15° ramp case, and both models gave good predictions of surface pressure as shown in Fig. 1, with a slight underprediction in the interaction region. The heat transfer was not predicted as well (see Fig. 2), with the kεLS model yielding heat transfer levels 25% higher than the data in the interaction region and the kω88 model overpredicting the heating by as much as 50% in the interaction region and in the plateau region on the ramp. All five models were applied to the 34° ramp case, with the kεSO and kεHC models giving accurate predictions for the surface pressure, while the other three models tend to overpredict the pressure in the interaction region and significantly underpredicting the size of the separated region as judged by the initial upstream pressure rise. All five models greatly overpredict the heat transfer in the interaction region by at least a factor of three, and the kω88 model also overpredicts the plateau heating downstream on the ramp by 50%.

Goldberg and coworkers [149,150] have computed the 38° ramp case of Coleman and Stollery/Elfstrom with three one-equation turbulence models: Goldberg (UG), SA, and Menter (MTR). A mesh refinement study was performed for the UG model only using 200×150 and 250×200 cell meshes with some minor effects on the results. While the effects of changing the y^+ values are not discussed, the y^+ values in all cases are kept near 0.1. No effects of the freestream turbulence levels are examined. The SA and MTR models are shown to underpredict the size of the separation zone, thereby predicting an earlier peak in the

pressure. The UG model accurately predicts the pressure and provides fairly good estimates of the wall heating. The SA model also gives good predictions for the surface heating, while the MTR model greatly overpredicts the peak heating levels in the interaction region by as much as a factor of four.

Coratekin et al. [171] have computed the 38° ramp case of Coleman and Stollery/Elfstrom with three turbulence models: a low Reynolds number version of the Wilcox 1988 k–$ω$ model (kω88LR), the SA model, and the hybrid k–$ω/k$–$ε$ model of Menter with the SST option. They also examined various compressibility corrections to the kω88LR model, but these corrections have not been evaluated over a wide variety of flowfields and thus will not be included here. A single grid of 128×64 cells is used for this case, with a grid refinement study using three grid levels being performed on a Mach 3, 24° compression corner and assumed to extend to the hypersonic case. The y^+ values employed are not discussed, and no sensitivity is performed for the freestream turbulence values. The kω88LR and STT models match the surface pressure levels reasonably well, but underpredict the extent of flow separation as judged by the initial rise in surface pressure. The SA model gives good estimates of both the surface pressure and separation extent. The peak surface heat flux levels are overpredicted by a factor of two for all the models, and local values of heat flux are as much as five times the experimental measurements in the interaction region.

Nance and Hassan [172] and Xiao et al. [173] have used the k–$ζ$ turbulence model (kζ) to examine the Coleman and Stollery/Elfstrom experiment. In both papers, a grid sensitivity study is mentioned, but no results are presented. In addition, sensitivities to wall y^+ values and freestream turbulence levels are not discussed. Fairly good agreement with is shown for the 15° ramp [173], but predictions for the 34° and 38° ramps [172] overpredict the magnitude of the initial pressure rise and greatly overpredict (by up to a factor of five) the heating in the interaction region. In all three cases, the recovery pressure and heating appear to be accurately predicted. The later study [173] also examines variable turbulent Prandtl number effects, but with little improvement for this case.

Holden experiment [48]: To our knowledge, this experiment has not been employed for validating turbulence models.

4.4.2. Case 2: cylinder with conical flare

There are two experiments which meet the Settles and Dodson criteria for the axisymmetric cylinder-flare geometry. The first was included in the Settles and Dodson review and was performed by Kussoy and Horstman [32] at NASA-Ames Research Center. The second is a more recent experiment performed in the supersonic blow-down wind tunnel (HSST) at DRA Fort Halstead, Great Britain and is detailed by Babinsky [69] and Babinsky and Edwards [68]. The former experiment has seen extensive validation usage, while to the authors' knowledge, the latter experiment has not yet been computed in the literature. An overview of the turbulence model validation for this case as discussed below is shown graphically in Figs. 3 and 4 for the five of the six turbulence models from Table 7.

Kussoy and Horstman experiment [32]: The Kussoy and Horstman cylinder-flare experiments [32] have been used for turbulence model validation purposes by Horstman [10,170]. A brief synopsis of the results was presented in Ref. [10], while a more detailed discussion is given in Ref. [170]. Horstman examined two different two-equation turbulence models: the low Reynolds number k–ε model of Jones and Launder ($k\varepsilon$JL) and the low Reynolds number k–ε model of Rodi ($k\varepsilon$R) (a third "compressible" k–ε model is omitted from the present discussion as mentioned in Section 4.4.1). Mesh

Fig. 4. Surface heat flux turbulence model comparisons for Case 2: cylinder with conical flare at 35° (experiment by Kussoy and Horstman [32]).

resolution studies were discussed; however, no results were shown, and no estimates of the discretization error were reported. The sensitivity to wall-normal mesh spacing was examined and is reported in Section 4.4.1 above for the 2D compression corner. For the 20° flare case, which was nominally attached flow, both k–ε models gave accurate predictions of the surface pressure. The $k\varepsilon$JL model gave reasonable predictions of the heat transfer (within approximately 30%), while the $k\varepsilon$R model predicted heat transfer within the experimental uncertainty bounds everywhere except possibly in the recovery region where the heat transfer is underpredicted by as much as 25%. For the 35° flare case with flow separation, the surface pressure was reasonably well predicted by both models as shown in Fig. 3. The heat transfer was overpredicted by an order of magnitude or more by the $k\varepsilon$JL model and underpredicted by almost a factor of two by the $k\varepsilon$R model (see Fig. 4). The size of the separation zone for this case is underpredicted by over 50% as judged by the initial pressure rise and the peak pressure.

Coakley, Huang, and co-workers [7,11,12] also used the Kussoy and Horstman cylinder-flare experiments [32] for turbulence model validation purposes. A number of different two-equation turbulence models were examined including: the q–ω model of Coakley ($q\omega$), the 1988 k–ω model of Wilcox ($k\omega$88), the k–ε model of Launder and
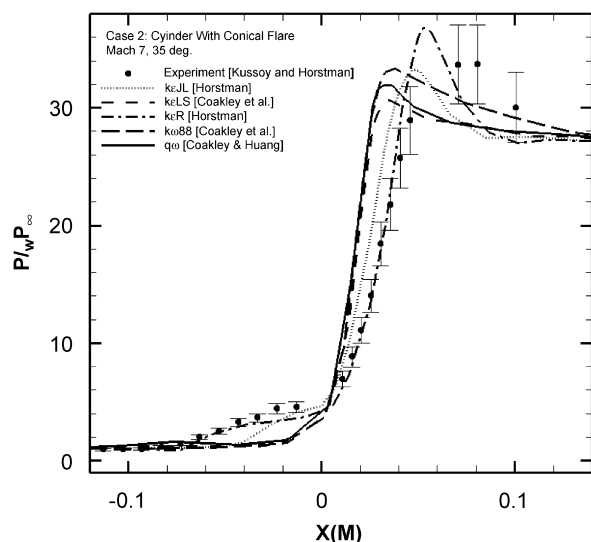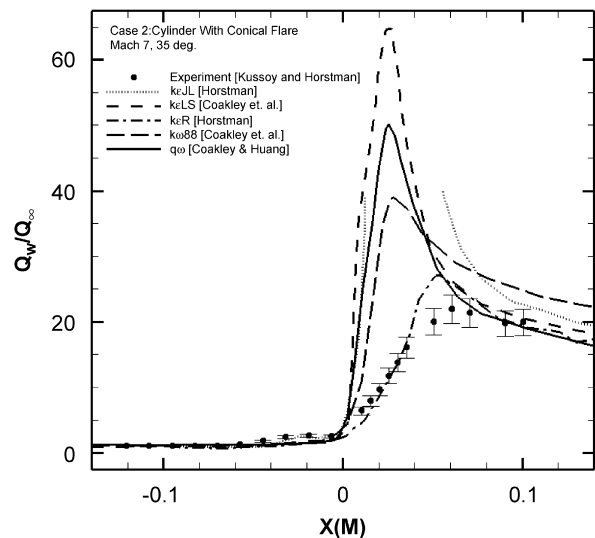

Fig. 3. Surface pressure turbulence model comparisons for Case 2: cylinder with conical flare at 35° (experiment by Kussoy and Horstman [32]).

Sharma ($k\varepsilon$LS), the k–ε model of Chien ($k\varepsilon$CH), the k–ε model of So ($k\varepsilon$SO) which includes compressibility extensions given by Zhang et al. [158], and the k–ε model of Huang and Coakley ($k\varepsilon$HC). For a more detailed discussion of this study, see Section 4.4.1 above for the 2D compression corner. Only the $k\varepsilon$LS and $k\omega$88 models were applied to the 20° flare case [11], and both models provided good predictions of the surface pressure. The heat transfer predictions were as much as twice the experimental values. All six models were applied to the 35° flare case [12]. The $k\varepsilon$LS, $k\omega$88, and $q\omega$ models gave an adequate prediction of the surface pressure levels but underpredicted the size of the separation zone by 60% (see Fig. 3). These models predicted an early peak heating location (Fig. 4), with maximum errors of a factor of 6.5, 3, and 4, respectively. The $k\varepsilon$HC and $k\varepsilon$SO models gave reasonable pressure predictions and only underpredicted the separation zone size by approximately 20%. The peak heating, however, was still overpredicted by a factor of 2.5.

Bedarev et al. [174] used the Wilcox 1988 k–ω model ($k\omega$88) to study the Kussoy and Horstman cylinder flare experiments. They discussed a grid sensitivity study, but did not report the results. In addition, they did not discuss the sensitivities to freestream turbulence levels or y^+ wall spacing. They examined 20°, 30°, and 35° flares. Their results do not appear to be as good as those of Huang and Coakley [12] with the same turbulence model. The reasons for these discrepancies are not known.

Olsen et al. [175] used the SA and Menter k–ω SST model (SST) to study the Kussoy and Horstman cylinder flare experiments. Their domain included the entire ogive-cylinder-flare, and an extensive grid study was performed for a modified k–ε model known as the Lag model. The sensitivities to wall y^+ spacing and freestream turbulence levels were not addressed. Both models perform well for all of the flare angles except 35°, where the upstream pressure and heating rise is not accurately predicted. It is notable that both models give reasonable surface heat flux predictions, even in the interaction region.

Babinsky and Edwards experiment [68,69]: This experiment has not yet been used for turbulence model validation but is recommended.

4.4.3. Case 3: cone with conical flare

There is only one experiment for the cone/conical flare case that is appropriate for turbulence model validation. Holden [44] performed experiments in

Calspan's 96 in shock tunnel at Mach numbers of 11 and 13. As noted earlier, personal communications with Holden (the author of Ref. [44]) confirmed that the *flare angle should be measured from the 6° cone*, not the symmetry axis [102]. An overview of the turbulence model validation for the two models applied to this case (as discussed below) is shown graphically in Figs. 5 and 6.

Holden experiment: The Holden cone/conical flare experiment [44] at Mach 11 with a flare angle of 36° (as measured from the forecone) has been used for turbulence model validation by Horstman [170],
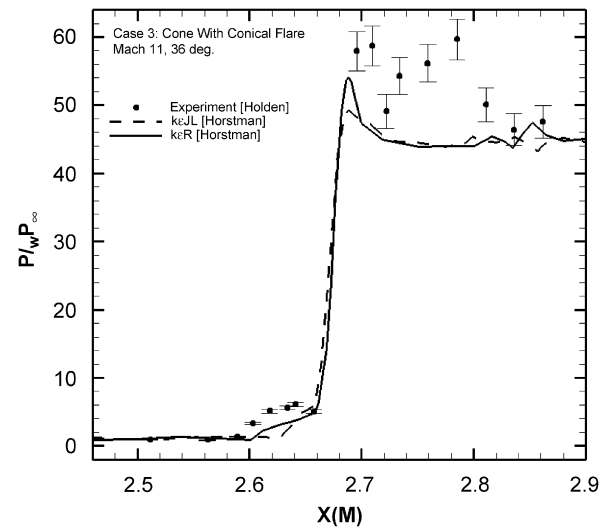

Fig. 5. Surface pressure turbulence model comparisons for Case 3: cone with conical flare at 36° (experiment by Holden [44]).
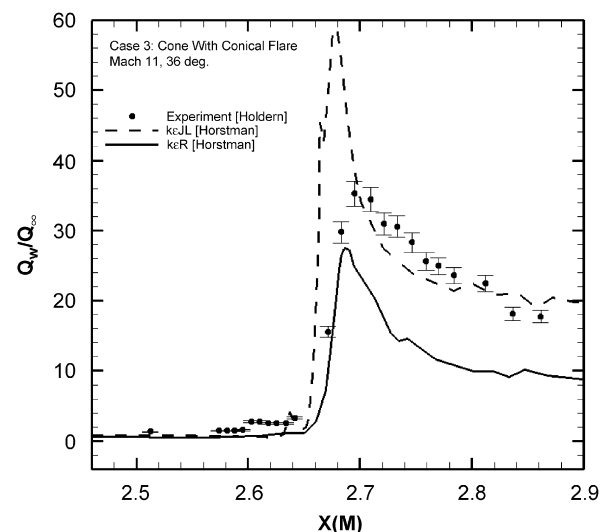

Fig. 6. Surface heat flux turbulence model comparisons for Case 3: cone with conical flare at 36° (experiment by Holden [44]).

who examined two different two-equation turbulence models: the low Reynolds number k–ε model of Jones and Launder ($k\varepsilon$JL) and the low Reynolds number k–ε model of Rodi ($k\varepsilon$R) (a third "compressible" k–ε model is omitted from the present discussion as mentioned in Section 4.4.1). Mesh resolution studies were discussed; however, no results were shown and no estimates of the discretization error were reported. The sensitivity to wall-normal mesh spacing was examined and is reported in Section 4.4.1 above for the 2D compression corner. As shown in Fig. 5, the surface pressure was reasonably well predicted by the $k\varepsilon$R model in the interaction region, with the onset of separation (judged by the initial rise in pressure) occurring slightly downstream of the experimental location. The $k\varepsilon$JL model greatly underpredicts the size of the separated zone, and both models fail to capture a secondary peak in the pressure in the vicinity of the downstream plateau region. The $k\varepsilon$JL model also overpredicts the peak heating level by nearly a factor of two, but accurately matches the heating in the recovery region downstream of the interaction (see Fig. 6). The $k\varepsilon$R model underpredicts both the peak heating and the heating levels in the recovery region by 50%.

4.4.4. Case 4: axisymmetric impinging shock

There are two different axisymmetric impinging shock experiments which are deemed acceptable for turbulence model validation. The first is a series of
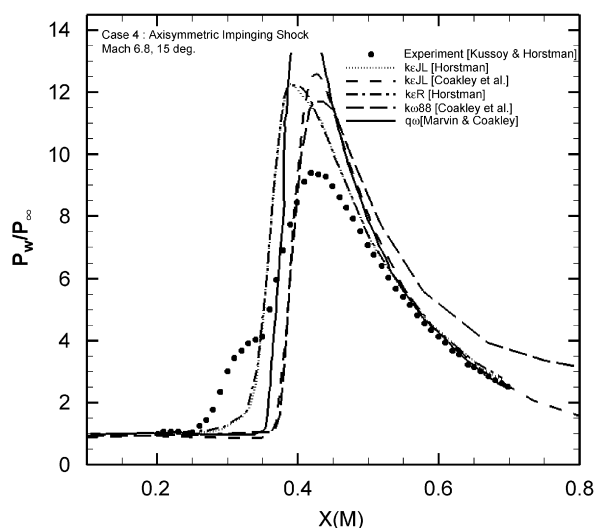

Fig. 7. Surface pressure turbulence model comparisons for Case 4: axisymmetric impinging shock at 15° (experiment by Kussoy and Horstman [35,70]).
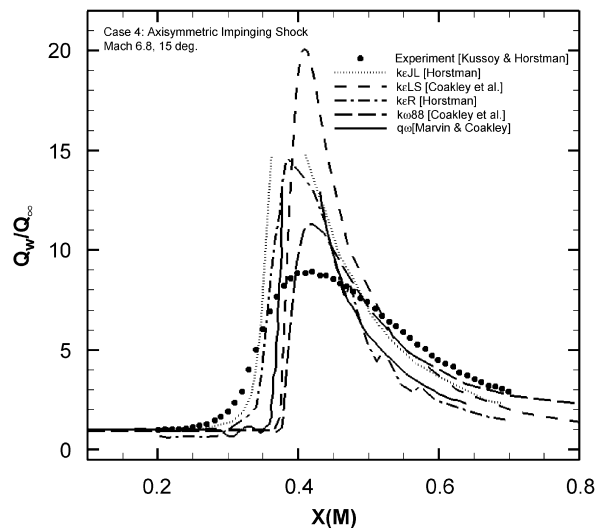

Fig. 8. Surface heat flux turbulence model comparisons for Case 4: axisymmetric impinging shock at 15° (experiment by Kussoy and Horstman [35,70]).

experiments conducted by Kussoy et al. at a Mach number of 7 on a cone-ogive-cylinder model [35,70,71]. The second is a more recent experimental investigation by Hillier et al. at Mach 9 on a hollow cylinder model [72–75]. An overview of the turbulence model validation for this case as discussed below is shown graphically in Figs. 7 and 8.

Kussoy and Horstman experiment [35,70,71]: Marvin and Coakley [176] used the Kussoy and Horstman axisymmetric impinging shock experiment [35,70] with a shock generator angle of 15° for the validation of the q–ω model of Coakley ($q\omega$). The authors fail to report the effects of mesh refinement, variations of the y^{+} values, or the effects of varying the freestream turbulence values. Predictions with the $q\omega$ model are given in Figs. 7 and 8 for surface pressure and heat transfer, respectively. Although a mild amount of flow separation is shown by the experimental data and the $q\omega$ model, the model significantly underpredicts the size of the interaction region. As a result, the model greatly overpredicts the peak levels of pressure, skin friction, and heat flux (although the scale chosen for the original figures does not include the peak values from the model).

The Kussoy and Horstman axisymmetric impinging shock experiment [35,70] with a shock generator angle of 15° has been used for turbulence model validation by Horstman [170] who examined two different two-equation turbulence models: the low Reynolds number k–ε model of Jones and Launder

($k\varepsilon$JL) and the low Reynolds number $k-\varepsilon$ model of Rodi ($k\varepsilon$R) (a third "compressible" k–ε model is omitted from the present discussion as mentioned in Section 4.4.1). Mesh resolution studies were discussed; however, no results were shown, and no estimates of the discretization error were reported. The sensitivity to wall-normal mesh spacing was examined and is reported in Section 4.4.1 above for the 2D compression corner. Neither model is able to predict the mild amount of flow separation indicated by the experimental data, and both also underpredict the size of the interaction region. As a result, the peak pressures are overpredicted by 25% and the upstream pressure rise is not captured at all (Fig. 7). The peak skin-friction levels are overpredicted by a factor of two with the $k\varepsilon$R model and a factor of three with the $k\varepsilon$JL model. Both models match the surface pressure and skin friction in the recovery region well within the experimental uncertainty bounds. The surface heating levels, shown in Fig. 8, are overpredicted by 50% with the $k\varepsilon$R model and by at least a factor of two with the $k\varepsilon$JL model, while the recovery heat flux is underpredicted by 30% with $k\varepsilon$JL and 50% by $k\varepsilon$R.

Huang and Coakley [12] and Coakley et al. [7] used both shock generator angles of the Kussoy and Horstman experiment [35,70] for turbulence model validation. Two two-equation turbulence models were examined: the 1988 k–ω model of Wilcox ($k\omega$88) and the k–ε model of Launder and Sharma ($k\varepsilon$LS). A mesh refinement study was discussed, and the authors state that changing the mesh had no effect of the predictions. While a y^+ sensitivity study was not conducted explicitly, the y^+ values were kept below 0.5, which had been shown to be sufficient for these models in a related study [11]. The effects of changing the freestream turbulence quantities were not assessed in these studies. For the 7.5° shock generator case, both models accurately predict the extent of the interaction region and the surface pressure; however, both models also overpredict the peak heating and skin-friction levels by 35% and 70%, respectively. As shown in Fig. 7 for the 15° shock generator case, the width of the interaction region is underpredicted, and the initial pressure rise in the vicinity of the separated flow region is not captured. The peak levels of pressure and skin friction are overpredicted by approximately 30% and 100%, respectively. The $k\varepsilon$LS model overpredicts the heating by more than a factor of two, while the $k\omega$88 model is 60% higher than the data (Fig. 8). The $k\omega$88 model overpredicts

all three surface quantities by at least a factor of two in the recovery region. The $k\varepsilon$LS model accurately captures the wall pressure and skin-friction in the recovery region, but underpredicts the heating in the recovery region by 50%.

Hillier et al. experiment [72–75]: To our knowledge, this experiment has not been used in the validation of one- or two-equation turbulence models.

4.5. New flow geometries with and without pressure gradient

4.5.1. Case 5: 2D impinging shock

A 2D impinging shock occurs when an externally generated oblique shock impinges on a flat plate boundary-layer. There are two experimental data sets that satisfies the Settles and Dodson criteria. Kussoy and Horstman [38] conducted a careful experimental study of the 2D impinging shock case in the Ames 3.5 ft Hypersonic Wind Tunnel at Mach 8.2. An overview of the turbulence model validation for this case as discussed below is shown graphically in Figs. 9 and 10. Recently, Schulein and coworkers [76,77] also studied the 2D impinging shock case.

Kussoy and Horstman experiment [38]: The Kussoy and Horstman 2D impinging shock experiment [38] with an effective wedge angle of 10° has been used for turbulence model validation by Horstman [170], who examined two different two-equation turbulence models: the low Reynolds

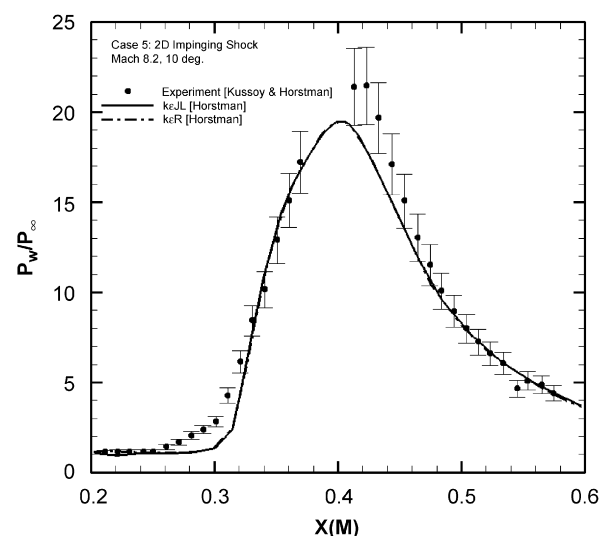Fig. 9. Surface pressure turbulence model comparisons for Case 5: 2D impinging shock at 10° (experiment by Kussoy and Horstman [38]).
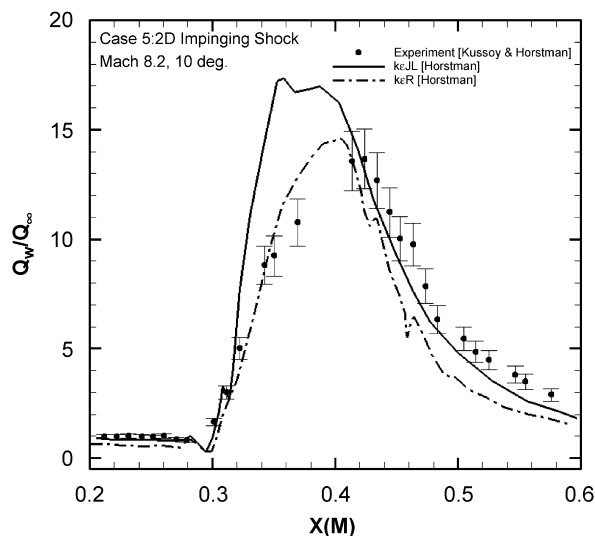
Fig. 10. Surface heat flux turbulence model comparisons for Case 5: 2D impinging shock at 10° (experiment by Kussoy and Horstman [38]).

number k–ε model of Jones and Launder ($k\varepsilon$JL) and the low Reynolds number k–ε model of Rodi ($k\varepsilon$R) (a third "compressible" k–ε model is omitted from the present discussion as mentioned in Section 4.4.1). Mesh resolution studies were discussed; however, no results were shown, and no estimates of the discretization error were reported. The sensitivity to wall-normal mesh spacing was examined and is reported in Section 4.4.1 above for the 2D compression corner. As shown in Fig. 9, the surface pressure was accurately predicted by both models, with the predictions falling just outside the experimental uncertainty bars over the entire interaction region. The models do appear to slightly underpredict the upstream separation point as judged by the initial rise in the surface pressure. The $k\varepsilon$JL model overpredicts the heating by 60% in the interaction region but accurately matches the heating in the recovery region downstream of the interaction (see Fig. 10). The $k\varepsilon$R model accurately predicts the heating in the interaction region but underpredicts the heating levels in the recovery region by up to 20%.

The Kussoy and Horstman experiment [38] for 5° and 10° wedge angles was also used by Smith [161] in the validation of a two-equation k–l model (kl). A compressibility correction designed specifically for high-speed separated flows [7] was also investigated by the author, but it is unclear how this correction impacts the previous validation efforts for the model, especially at low speeds. Results for

the corrected model will therefore not be included here. The transition onset and extent were set to 50 and 100 cm, respectively, (as suggested by the experiment) to achieve the best fit to the undisturbed boundary-layer profile. A grid refinement study was performed for the model with the compressibility correction for the 10° wedge case with minor effects on the surface properties. The y^+ values in each case are discussed, but no y^+ sensitivity was performed and the effects of varying the freestream turbulence levels were not examined. For the 5° wedge case, the surface pressure is accurately predicted by the model, with a slight underprediction of the upstream extent of the pressure rise. The heat transfer was overpredicted by as much as 30% within the interaction region for this case. The results for the 10° wedge were similar.

Schulein et al. experiment [76,77]: Nance and Hassan [172] and Xiao et al. [173] have used the k–ζ turbulence model ($k\zeta$) to examine the Schulein experiment. In both papers, a grid sensitivity study is mentioned, but no results are presented. In addition, sensitivities to wall y^+ values and freestream turbulence levels are not discussed. The 10° and 14° shock generators were studied, and good agreement was found for both wall pressure and skin friction. The heat flux in the interaction and recovery regions was overpredicted, with the peak heating being too high by a factor of two.

Fedorova et al. [177] used the Wilcox 1988 k–ω model ($k\omega$88) to study the Schulein impinging shock experiment for shock generator angles of 6°, 10°, and 14°. No grid study was discussed, and the sensitivities of the results to freestream turbulence levels and wall spacing were not addressed. They found good agreement for the surface pressure at all shock generator angles. The skin friction was accurately predicted for the smaller generator angles, but the recovery skin-friction levels were underpredicted for the 14° case. The peak heating was overpredicted for all cases in the interaction region by roughly a factor of two, but the heating rate in the recovery region appears to be accurate.

4.5.2. Case 6: flat plate/cylinder

For the numerical solution of the hypersonic turbulent flow on a sharp flat plate with a Navier–Stokes code, there are many choices for the grid. It is recommended that a parabolic grid be used as described in Roy and Blottner [166]. The boundary conditions for a parabolic grid are well defined and are continuous without a singularity at the leading

edge. The assessment of accuracy of turbulence models can be performed with numerical predictions for a group of experiments compared directly with the experimental data. However, a better approach is to transform numerical predictions with the correlation theory into a curve which should match the theoretical correlation curve within a small error. The following investigators have used the hypersonic experimental data given in Table 2 to assess the accuracy of one- and two-equation turbulence models for boundary layers with zero-pressure gradient.

Huang et al. [179]: An assessment of two-equation turbulence models has been performed in Ref. [179], and it has been determined that the k–ε Launder–Sharma ($k\varepsilon$LS) and Wilcox 1988 k–ε ($k\omega$88) models do not give the expected law of the wall behavior. The k–ω model is much less sensitive to density effects than the k–ε model. A density correction to the closure coefficients was developed that improved the accuracy of the two-equation models in the logarithmic part of the turbulent velocity profile.

Aupoix et al. [8,180,181]: In the paper by Aupoix and Viala [8] the standard turbulence models are assessed with supersonic and hypersonic boundary-layer flow on an adiabatic flat plate. The authors use the following adiabatic wall experimental database to evaluate the local skin-friction correlations and to obtain *reference test cases* to evaluate turbulent model predictions (note: these cases are referred to as AVC experiments in Table 1):

Supersonic: Coles [135], Kistler [184], Hasting–Sawyer [185], Mabey et al. [186,187], Richmond [188].

Hypersonic: Winkler–Cha [112], Moore [114], Watson et al. [125,126], Laderman and Demetriades [127].

The Van Driest II and HBC approaches correlate the experimental database for adiabatic flat plate flows within a scatter of $\pm10\%$. The data is not sufficiently accurate to determine which correlation is more accurate. Also the authors investigate the influence of the non-dimensional form of y^+ in the wall damping functions. For high Mach number flows, density gradients influence the logarithmic behavior of the velocity profile and the turbulence models require additional modeling to retain the logarithmic region. A density gradient correction to the turbulence models is investigated using the approach of Huang et al. [179]. The database given

above is used to assess the accuracy of density gradient corrections added to standard turbulence models. The Wilcox 1988 k–ω model ($k\omega$88) is less sensitive to density gradient effects than the k–ε models.

The initial work of Catris and Aupoix was given in an AIAA paper [180] and was later published as Ref. [181] with additional work included. The authors have proposed modifications of the diffusion term in the compressible turbulent transport equations for the various turbulence models. The models investigated are the Chien k–ε model ($k\varepsilon$CH), Wilcox k–ω 1988 model ($k\omega$88), the Smith k–l model (kl), and the SA model. The modified turbulence models are assessed for supersonic and hypersonic zero-pressure gradient boundary-layers where the accuracy of the velocity profile and skin friction are determined with the *reference test cases*. Velocity profile predictions with the various turbulence models are compared to the following flat plate experimental databases: Mabey et al. [186] (Mach 4) and Winkler and Cha [112] (Mach 5.3). Skin-friction predictions with the various turbulence models are compared to the following experimental databases: Mabey et al. [187], Winkler and Cha [112], Watson [126] (Mach 10–11.6), and Owen et al. [84] (Mach 7.2). The modified turbulence model solutions generally improve the prediction accuracy.

Bradshaw et al. [178]: As a part of the Stanford Collaborative Testing of Turbulence Models, one of the entry cases is the compressible flow over a flat plate at a Reynolds number of 10^4 based on momentum thickness. The final problem definition requested turbulence modelers to obtain the following solutions: (Case A) Mach 2, 3, 5, and 8 with an adiabatic wall and (Case B) Mach 5 flow with T_w/T_{aw} equal 0.2, 0.4, 0.6, 0.8, and 1.0. The Van Driest II values of compressible local skin friction and Stanton number with Reynolds analogy factor of 1.16 were determined by Bradshaw as the reference solution for comparison. For Case A, the average of the modeler predictions for skin friction were 1% below reference values at Mach 2 and 4% above reference values at Mach 8. For Case B, the average of the modeler predictions for skin friction were 5.2% high for $T_w/T_{aw} = 0.2$ and 2.5% high at $T_w/T_{aw} = 0.8$. Some further refinement of specification of the viscosity law and equation of state for a perfect gas is needed.

Bardina et al. [13]: The Mach 5 boundary-layer flow over an adiabatic flat plate was investigated at momentum thickness Reynolds numbers of 5000,

10,000, 20,000, 50,000, and 100,000. The authors performed careful numerical solutions to ensure that the solutions for four turbulence models (Launder–Sharma $k-\varepsilon$, Wilcox 1998 $k-\omega$, Menter SST $k-\omega$, and Spalart–Allmaras) had small numerical errors. The Van Driest II transformation theory was used with the von Karman–Schoenherr incompressible skin-friction relation to obtain the compressible skin friction for comparison with the numerical predictions from the four turbulence models. For this case, the Van Driest approach provides a good approximation to flat plate skin friction experimental data. The $k\varepsilon$LS model showed a significant underprediction of the skin friction (as much as 20%). In addition, the transformation of HBC gives larger skin friction (5–10%) than the Van Driest II transformation. The compressible velocity profiles for the four turbulence models were transformed to incompressible form and compared to the log law of HBC. The $k\varepsilon$LS turbulence model again gave poor results. The SA turbulence model gave the best overall predictions for the skin friction and the velocity profile.

Roy and Blottner [16]: Roy and Blottner [16] examined Mach 8, calorically perfect gas flow over a flat plate using four different turbulence models: SA, Nagano and Hishida $k-\varepsilon$ ($k\varepsilon$NH), Wilcox 1998 $k-\omega$ ($k\omega$98), and Menter's BSL $k-\omega$ (BSL). The conditions correspond to 15 km altitude and a wall temperature of 1000 K was used. The plate was 1 m long, and transition was specified at 0.12 m to allow a significant amount of both laminar and fully-developed turbulent flow. The simulation results were compared to the accurate laminar and turbulent results obtained for this case by Van Driest [99,133]. The validation methodology discussed in Section 2 was used. Multiple grids were run in order to estimate the discretization error. In the fully-developed turbulent region, the discretization error for the SA model was approximately 0.5%, while the error for the two-equation models was near 1%. These estimates increase to 0.6% and 1.25% when a safety factor of 1.25 is included. The effects of varying the wall y^+ values between 0.01 and 1.0 were studied, and the models were found to be relatively insensitive to y^+ variations below 0.25. Skin friction as a function of Reynolds number in the turbulent region are shown in Fig. 11 for each model. The results appear to reach an approximately constant error relative to the Van Driest correlation by the end of the plate. At this location,
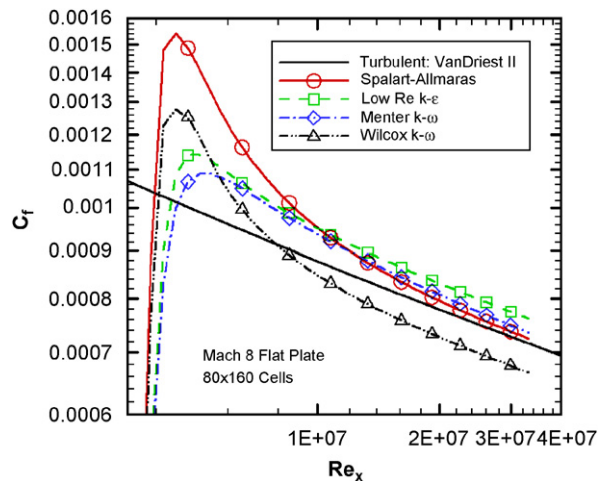

Fig. 11. Skin friction turbulence model comparisons for Case 6: flat plate/cylinder (correlation is Van Driest II [51]).

the Wilcox (1998) $k-\omega$ model underpredicts the Van Driest II curve by 6.7%, while the SA, Menter $k-\omega$, and low Reynolds number $k-\varepsilon$ overpredict the skin-friction by 1.4%, 3.1%, and 6.3%, respectively. Accounting for the grid convergence errors, the skin-friction predictions from the SA and Menter $k-\varepsilon$ models are within the error tolerances, while the low Reynolds number $k-\varepsilon$ and Wilcox (1998) $k-\omega$ models are not. In addition, the surface shear stress values for the Wilcox (1998) $k-\omega$ model showed a sensitivity of up to 4% to the freestream ω values.

Coratekin et al. [171]: The authors have developed a compressible Navier–Stokes code and are concerned with the performance of the numerical scheme and accuracy of three linear turbulence models for hypersonic perfect gas flows [171]. The turbulence models in the code are the following: Wilcox $k-\omega$ model ($k\omega$88) (with two compressible corrections—Coakley et al. [7] have developed a length scale correction for reattachment boundary-layer flows while Coakley and Huang [7,11] have introduced a correction in flow regions with strong compression effects), SA one-equation model, and Menter $k-\omega$ (SST) model. The turbulent boundary layer on an isothermal flat plate at Mach 5 is solved with the code and compared with the Van Driest II [51] correlation of the skin friction. At a given momentum thickness Reynolds number, the turbulent model predictions for skin-friction are lower than the values obtained with the Van Driest II theory.

4.5.3. Case 7: sharp circular cone

The supersonic/hypersonic flow over a sharp cone at zero angle of attack is of interest as the flow properties at the edge of the boundary layer are approximately constant along the cone. The sharp cone is an extension of the flat plate geometry and is basic to the understanding of turbulent boundary-layer flows. From a computational point of view, this geometry is not ideal because the singularity at the sharp tip can make it difficult to obtain accurate numerical solutions. With the appropriate extension of the flat plate type of grid [166], the tip singularity problem can be handled.

McDaniel et al. [183]: McDaniel et al. [183] are concerned with the modeling and prediction of boundary-layer transition in high speed flows. The $k-\zeta$ ($k\zeta$) Robinson–Hassan turbulence model is used for the fully turbulent flow. The experimental database of Kimmel (see Kimmel [89, 4.5.3]) is used to evaluate the validity of the transition model and also shows the accuracy of the $k-\zeta$ model for hypersonic turbulent flow. The turbulent heat flux prediction has an accuracy of approximately 10% and the prediction is smaller than the experimental value.

Roy and Blottner [16]: Flow over a sharp cone with a half angle of $7°$ was examined by Roy and Blottner [16] using four different turbulence models: SA, Nagano and Hishida $k-\varepsilon$ ($k\varepsilon$NH), Wilcox 1998 $k-\omega$ ($k\omega98$), and Menter's BSL $k-\omega$ (BSL). The flow conditions correspond to a wind tunnel test performed by Kimmel [89,90], where transition occurs at approximately 0.5 m downstream of the cone tip. The gas is air, and the temperatures are such that the perfect gas assumption with $\gamma = 1.4$ is appropriate. The discretization error in surface heating for the SA model was estimated to be 0.25% in the turbulent region. The two-equation models had numerical error estimates of less than 1.5% in the turbulent region. The effects of varying the wall y^+ values between 0.01 and 1.0 were studied, and the models were found to be relatively insensitive to y^+ variations below 0.25. In this case, the surface heating values for the Wilcox (1998) $k-\omega$ model showed a sensitivity of up to 4% to the freestream ω values.

Skin-friction predictions versus surface distance Reynolds number are presented in Fig. 12 for the four turbulence models as well as the correlations of Van Driest [55] and White [56]. Taking the average of the two correlations as the true experimental value, all of the models are within the estimated
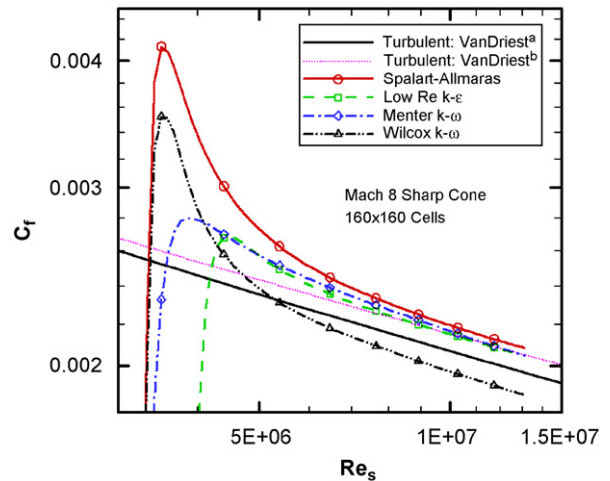

Fig. 12. Skin friction turbulence model comparisons for Case 7: sharp circular cone (correlations are Van Driest[a] [55] and White's cone rule[b] [56]).
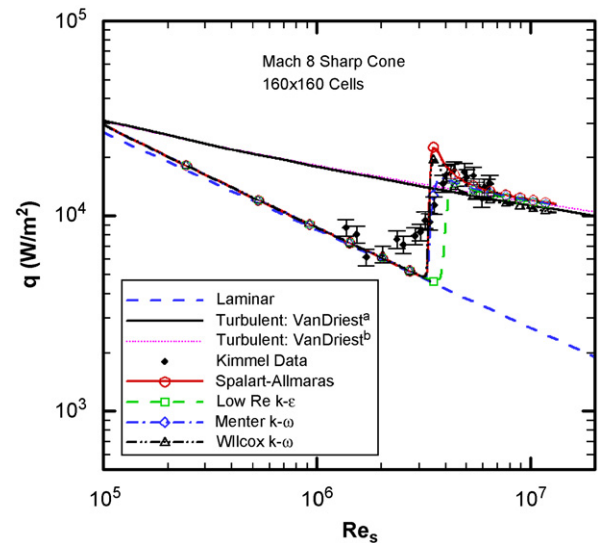

Fig. 13. Surface heat flux turbulence model comparisons for Case 7: sharp circular cone (correlations are Van Driest[a] [55] and White's cone rule[b] [56] and experiment by Kimmel [89,90]).

uncertainty of ±5% except for the Wilcox 1998 $k-\omega$ model, which underpredicts the skin friction by roughly 10%. Surface heating results versus surface distance Reynolds number are presented in Fig. 13 for the four turbulence models along with laminar boundary-layer code results and the turbulent Van Driest cone theory. Note that (a) refers to the transformed Van Driest [55], while (b) denotes White's cone rule [56]. In addition, experimental data is taken from Kimmel [90] and includes the
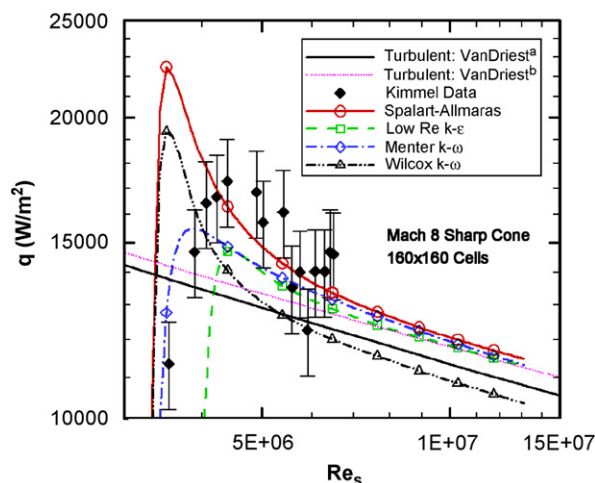
Fig. 14. Surface heat flux turbulence model comparisons (enlarged view) for Case 7: sharp circular cone (correlations are Van Driest[a] [55] and White's cone rule[b] [56] and experiment by Kimmel [89,90]).

conservative 10% error bounds suggested by the author. Although the surface heating predictions in the transitional region do not match the experimental data, the predictions in both the laminar and turbulent regions are generally within the experimental error bounds. An enlarged view of the turbulent heating region is presented in Fig. 14. At the end of the cone, the two theoretical correlations agree to within 4%. This difference is well within the accuracy of the correlations, which is estimated to be approximately ± 5–10%. Taking the theoretical value to be the average of these two curves, the Wilcox (1998) $k-\omega$ model is roughly 5.7% below the theory at the end of the cone. Both the Menter $k-\omega$ model and the low Reynolds number $k-\varepsilon$ model predict heating values approximately 2.5% high, while the SA model is 4.3% high. Accounting for the discretization errors, all of the turbulence models are well within the estimated error bounds.

Summary of turbulence model validation for the sharp cone: The use of the sharp cone for validation of zero-pressure gradient turbulent boundary-layer flows has been limited. Hypersonic cone flow is considered a simple problem that is not computationally expensive as the flow is axisymmetric. The experimental results have been mainly measurements of wall heat transfer, which has been used for validation of turbulence models. The theoretical prediction of surface heat transfer is less accurate than skin-friction prediction as the Reynolds analogy factor and a Mangler transformation are

required, which are of limited accuracy (see Appendix C). There is a need to further predict conical and flat plate flows with various turbulence models and compare the results with experimental measurements. This will help establish turbulence modeling accuracies and the relation between planar 2D and axisymmetric turbulent boundary-layer flows.

4.6. Conclusion and recommendation on turbulence model validation usage

Of the 18 turbulence models examined in this review, only six of them have seen extensive validation usage on the current 2D/axisymmetric hypersonic experimental database. In many cases, the effects of grid refinement on the predictions were not demonstrated. Furthermore, in none of the shock interaction cases were the numerical errors estimated with regard to grid refinement, nor were the sensitivities to the freestream turbulence quantities assessed. We recommend that future model validation efforts include a comprehensive grid refinement study, along with estimates of the discretization error and iterative error.

The ability of the models to predict surface pressure was mixed, with Rodi's $k-\varepsilon$ model performing the best; it was accurate for a majority of the cases with the exception of the region immediately upstream of the interaction. The ability of the models to predict skin friction cannot yet be determined since only a few of the experiments include detailed skin-friction data. The heat flux predictions were generally poor, with the best model (again Rodi's $k-\varepsilon$ model) still off by a factor of two for most of the shock interaction cases. While these model validation results should be used with caution due to the failure of most authors to adequately address numerical errors and model sensitivities, they do suggest that these turbulence models are not yet capable of accurately predicting hypersonic shock/boundary-layer interactions, even for the simple 2D/axisymmetric geometries. This shortfall needs to be addressed before attempting to predict complex, three dimensional (3D) flows involving shock wave/turbulent boundary-layer interaction.

For the two zero-pressure gradient cases (the flat plate and the sharp cone), the available correlations for skin friction are widely accepted as being more accurate than any single experimental data set. For example, the skin-friction correlations for the flat

plate are within ±5%. The correlations for heat flux have additional uncertainties related to the choice for Reynolds analogy factor and require further study, as does the transformation to convert skin friction and heat transfer from the flat plate to the sharp cone for turbulent flows (the current recommend value for this transformation is 1.13 for turbulent flows, see Section 3.3.2).

There is a need for new model validation studies with a focus on the newer experiments in the current 2D/axisymmetric hypersonic database (e.g., [68,69,72–78]). We find it surprising that the Menter's SST [160] model and, to a lesser extent, the SA [147,148] model, have seen only limited assessment with this hypersonic database. These two turbulence models are arguably the most commonly used turbulence models for external flows in the subsonic, transonic, and supersonic speed range.

Compressibility corrections should be implemented in the baseline turbulence models. Some of these corrections (e.g., [180]) vanish as the mean density variations are reduced, thus ensuring prior model validation efforts at low speeds are still valid. For other corrections (e.g., [7]), the low-speed model validation test cases should be revisited (the subsonic through supersonic test cases of Marvin and Huang [5] are recommended). Future modeling efforts should also investigate the effects of shock unsteadiness (e.g., [189,190]) and the effects of variations in the turbulent Prandtl number (e.g., [173,191]). In general, the use of ad hoc model corrections applied to a limited class of flows resembles calibration or parameter fitting and should be avoided for turbulence models that will be applied to general hypersonic flows; thus the effects of any turbulence model modifications should be assessed for a wide range of flows.

5. Conclusions

The current recommended database for 2D/axisymmetric hypersonic experiments is composed of seven different geometries. For the cases involving shock/boundary-layer interaction, we have added one additional geometry, the 2D impinging shock, to the previous hypersonic validation database. There are two new validation experiments discussed on this geometry. For the original four geometries in the Settles and Dodson review [1–4], three new experiments have been added. These new experiments generally provide higher spatial resolution data and use newer measurement techniques, and thus are highly recommended for turbulence model validation. The current 2D/axisymmetric hypersonic experimental database for shock interacting flows appears to be sufficient for validating turbulence models for predicting surface pressure and heat flux; however, there are not sufficient data for validating skin-friction predictions. Furthermore, the current database is not sufficient for improving the turbulence models since there are very few measurements of mean and fluctuating turbulence quantities in the interaction region.

The two zero-pressure gradient cases, the flat plate/cylinder and the sharp cone, have been the subject of extensive experimental investigation. As a result, the available correlations for skin friction on the flat plate are estimated to be accurate to within ±5% and are widely accepted as being more accurate than any single experimental data set. The flat plate correlations for heat flux have additional uncertainties related to the choice for Reynolds analogy factor and require further study. For the flat plate, theoretical results for the mean profiles of velocity and temperature are also available [54]. The correlations for both skin friction and heat transfer for the sharp cone have larger uncertainties due to the difficulties in determining the proper flat plate/cone transformation.

Of the 18 turbulence models examined in this review, only six of them have seen extensive validation usage on the 2D/axisymmetric hypersonic experimental database. For the models that have been assessed on the database, most provide reasonable predictions of surface pressure (and skin friction when available), but not for surface heating. The heating rates are generally overpredicted by the models by as little as a factor of two or as much as an order of magnitude in the interaction region and, to a lesser extent, in the recovery region. In only a minority of cases have these turbulence model assessments included an adequate assessment of numerical errors. In addition, the model assessments rarely included sensitivities to wall y^+ spacing or freestream turbulence quantities.

6. Recommendations

There is an urgent need for new hypersonic flow experiments be conducted. In addition to surface quantities (pressure, skin friction, and heat flux), these experiments should measure profiles of both mean properties and turbulence statistics (rms

velocities, Reynolds stresses, turbulent kinetic energy, etc.) in the interaction region. Despite the difficult challenges (short flow residence times, particle seeding, etc.), these turbulence profiles should be measured with non-intrusive optical techniques if possible. The more detailed turbulence information from non-intrusive experiments or DNS might aid in the determination of where the turbulence models break down, ideally on a term-by-term basis. For any new experiments, significant efforts should be made to quantify and reduce the experimental uncertainties in the measured and freestream quantities.

We recommend that a comprehensive study be undertaken to assess a wide range of turbulence models (including current popular models) on the current 2D hypersonic experimental database. This study should follow the turbulence model validation methodology discussed in Section 2, which includes careful documentation of the test cases and turbulence models employed, estimates of the numerical error, model sensitivities to wall y^+ spacing and freestream turbulence values, and quantitative comparisons with experimental data. The effects of model corrections should also be examined (e.g., compressibility, shock unsteadiness, variations in turbulent Prandtl number), but only in a manner which does not destroy the prior validation history of the model (including low-speed incompressible flows). As detailed experimental measurements and DNS data become available for mean and fluctuating turbulence quantities, the modeling of specific physics in the turbulence models can be examined, and the predictive capability of turbulence models for hypersonic flows can be improved.

Appendix A. Compressibility corrections

With the two-equation turbulent turbulence models, the standard form of these equation is not adequate for obtaining the logarithmic region of the velocity profile for compressible flows (e.g., see [54]). For the $k-\varepsilon$ turbulence model, the standard and modified equations developed by Catris and Aupoix [180] are presented. In addition, the modified equation for the eddy viscosity for compressible flow developed by Catris and Aupoix [180] is also presented.

A.1. Two-equation $k-\varepsilon$ turbulence models

The standard or classical form of the turbulent kinetic energy equation is

$$\bar{\rho}\frac{Dk}{Dt} = \frac{\partial}{\partial t}(\bar{\rho}k) + \frac{\partial}{\partial x_j}(\bar{\rho}u_j k) = D_k + S_{Pk} - S_{Dk},$$
(A.1)

where the diffusion, production, and destruction terms are

$$D_k = \frac{\partial}{\partial x_j}\left[\left(\mu + \frac{\mu_T}{\sigma_k}\right)\frac{\partial k}{\partial x_j}\right], \quad S_{Pk} = P_k, \quad S_{Dk} = \bar{\rho}\varepsilon.$$

In the above P_k is the turbulent kinetic energy production. Huang et al. [179] have shown for two-equation turbulence models, that density corrections to the incompressible closure coefficients are required to obtain a logarithmic region of the velocity profile for compressible flows. Catris and Aupoix [180] have modified the turbulent transport equation for two-equation turbulence models. A compressibility correction to the turbulent kinetic energy equation has been developed by Catris and Aupoix, which gives the same form as Eq. (A.1) except the diffusion term is modified as follows:

$$D_k = \frac{\partial}{\partial x_j}\left[\left(\frac{\mu}{\bar{\rho}} + \frac{\mu_T}{\bar{\rho}\sigma_k}\right)\frac{\partial(\bar{\rho}k)}{\partial x_j}\right].$$

The standard or classical form of the dissipation equation is

$$\bar{\rho}\frac{D\varphi}{Dt} = \frac{\partial}{\partial t}(\bar{\rho}\varphi) + \frac{\partial}{\partial x_j}(\bar{\rho}u_j\varphi)$$
$$= D_\varepsilon + S_{P\varepsilon} - S_{D\varepsilon}, \quad \varphi = \varepsilon,$$
(A.2)

where the diffusion, production, and destruction terms are

$$D_\varepsilon = \frac{\partial}{\partial x_j}\left[(\mu + \mu_T/\sigma_\varepsilon)\frac{\partial\varphi}{\partial x_j}\right], \quad S_{P\varepsilon} = c_{\varepsilon 1}f_1 P_k \frac{\varphi}{k},$$
$$S_{D\varepsilon} = c_{\varepsilon 2}f_2\bar{\rho}\frac{\varphi^2}{k}.$$

A compressibility correction to the dissipation equation has been developed by Catris and Aupoix

[180], which gives the same transport equation as Eq. (A.2) but with $\varphi = \overline{\rho}\varepsilon$. The diffusion term becomes

$$D_\varepsilon = \frac{\partial}{\partial x_j}\left[\left(\frac{\mu}{\sqrt{\overline{\rho}}} + \frac{\mu_T}{\sigma_\varepsilon \sqrt{\overline{\rho}}}\right)\frac{\partial \sqrt{\overline{\rho}}\varphi}{\partial x_j}\right],$$

$$S_{P\varepsilon} = c_{\varepsilon 1}f_1 P_k \frac{\varphi}{k},$$

$$S_{D\varepsilon} = c_{\varepsilon 2}f_2 \frac{\varphi^2}{k}.$$

The production, and destruction terms are the same form as above but $\varphi = \overline{\rho}\varepsilon$.

Spalart–Allmaras model: The transport equation for the eddy viscosity was originally developed by SA. Spalart [192] states, "Note that the S-A paper was silent on large density variations, and therefore...". The transport equation is written with the dependent (working) variable $\varphi = v$ in the following form, which is appropriate for *SA model for incompressible flows*:

$$\frac{D\varphi}{Dt} = \frac{\partial \varphi}{\partial t} + \tilde{u}_j \frac{\partial \varphi}{\partial x_j} = D^* + S_p^* - S_D^*. \tag{A.3}$$

The turbulent eddy viscosity is related to the dependent variable by the relation $\mu_T = \overline{\rho}\varphi f_{v1}$. The diffusion term D^* is

$$D^* = \frac{\partial}{\partial x_j}\left(\mu^* \frac{\partial \varphi}{\partial x_j}\right) + \frac{c_{b2}}{\sigma}\frac{\partial \varphi}{\partial x_j}\frac{\partial \varphi}{\partial x_j},$$

$$\mu^* = [(\mu/\overline{\rho}) + \varphi]/\sigma.$$

The production term is $S_P^* = c_{b1}\tilde{S}_\varphi$ and the destruction term is $S_D^* = c_{w1}f_w(\varphi/d)^2$. The various terms introduced are defined in the original paper of Spalart and Allmaras. The gas density $\overline{\rho}$ does not appear in the transport equation for ϕ except in the viscous sublayer. However, the density does appear in the relation for determining the eddy viscosity.

In fluid dynamics codes, the governing equations are generally written in conservation form. The above kinematic eddy viscosity transport Eq. (A.3) is rewritten in conservation form by multiplying the equation by the density and using the conservation of mass equation to obtain the following *conservation form for the SA turbulence model*:

$$\overline{\rho}\frac{D\varphi}{Dt} = \frac{\partial}{\partial t}(\overline{\rho}\varphi) + \frac{\partial}{\partial x_j}(\overline{\rho}u_j\varphi) = D + S_p - S_D. \tag{A.4}$$

The diffusion term with a variable density included is

$$D = \frac{\partial}{\partial x_j}\left(\mu_{ef}\frac{\partial \varphi}{\partial x_j}\right) + \frac{c_{b2}}{\sigma}\frac{\partial \varphi}{\partial x_j}\frac{\partial \varphi}{\partial x_j} - \mu^*\frac{\partial \varphi}{\partial x_j}\frac{\partial \overline{\rho}}{\partial x_j},$$

$$\mu_{ef} = \overline{\rho} \quad \mu^* = [\mu + \overline{\rho}\varphi]/\sigma.$$

The production term is

$$S_P = \overline{\rho}S_P^* = c_{b1}\tilde{S}\overline{\rho}\varphi. \tag{A.5}$$

The destruction term is

$$S_D = \overline{\rho}S_D^* = c_{w1}f_w\overline{\rho}(\varphi/d)^2. \tag{A.6}$$

The last term in the diffusion term above, which involves the density gradient, is zero for incompressible flows and is usually neglected for compressible flows (see for example: [13,166], and the FLUENT code [193]).

The SA model has been modified by Catris and Aupoix [180] to account for compressibility effects. The resulting *Catris and Aupoix equation for the SA turbulence model for compressible flow* is

$$\frac{D(\overline{\rho}\varphi)}{Dt} = \frac{\partial}{\partial t}(\overline{\rho}\varphi) + u_j \frac{\partial}{\partial x_j}(\overline{\rho}\varphi)$$

$$= D + S_P - S_D,$$

$$\varphi = (\mu_T/\overline{\rho})f_{v1}. \tag{A.7}$$

The diffusion term is

$$D = \frac{\partial}{\partial x_j}\left[\frac{\mu}{\sigma}\frac{\partial(\sqrt{\overline{\rho}}\varphi)}{\partial x_j} + \frac{(\sqrt{\overline{\rho}}\varphi)}{\sigma}\frac{\partial(\sqrt{\overline{\rho}}\varphi)}{\partial x_j}\right]$$

$$+ \frac{c_{b2}}{\sigma}\frac{\partial}{\partial x_j}(\sqrt{\overline{\rho}}\varphi)\frac{\partial}{\partial x_j}(\sqrt{\overline{\rho}}\varphi).$$

The form of Eq. (A.7) in conservation form on the left-hand side becomes

$$\frac{D(\overline{\rho}\varphi)}{Dt} = \frac{\partial}{\partial t}(\overline{\rho}\varphi) + \frac{\partial}{\partial x_j}(\overline{\rho}u_j\varphi) - \overline{\rho}\varphi\frac{\partial u_j}{\partial x_j}$$

$$= D + S_p - S_D. \tag{A.8}$$

The production term is defined in Eq. (A.5) and the destruction term is defined in Eq. (A.6).

Appendix B. Turbulent flat plate correlations

B.1. Correlation of skin-friction data

The standard approach for correlation of compressible skin friction on a flat plate is the van Driest II transformation theory [51]. This approach transforms the compressible skin friction at a given Reynolds number (Re_x or Re_θ) into the incompressible skin friction at an incompressible Reynolds number. A more complete analysis for the correlation of the skin friction has been developed by Hung, Bradshaw, and Coakley (HBC) [54]. The correlation theories transform the experimental

compressible skin friction and Reynolds numbers into incompressible values as follows:

$$C_f^* = F_c C_f,$$

F_c skin-friction transformation function.

$$Re_x^* = F_x Re_x, \quad F_x \text{ surface distance}$$

Reynolds no. transformation function.

$$Re_\theta^* = F_\theta Re_\theta, \quad F_\theta \text{ momentum thickness}$$

Reynolds no. transformation function.   (B.1)

Therefore, if the theory is accurate, the transformed skin-friction C_f^* and Reynolds numbers Re_x^* and Re_θ^* should be the same as the incompressible values.

$$C_f^* \approx C_{f,i}, \quad Re_x^* \approx Re_{x,i}, \quad Re_\theta^* \approx Re_{\theta,i}.$$

The compressible skin friction, Reynolds numbers, and transformation functions for the van Driest II theory are

$$C_f = 2\tau_w / \rho_e u_e^2, \quad Re_x = \rho_e u_e x / \mu_e,$$

$$Re_\theta = \rho_e u_e \theta / \mu_e, \quad (B.2)$$

$$F_c = rm / (\sin^{-1}\alpha + \sin^{-1}\beta)^2,$$

$$F_x = F_\theta / F_c, \quad F_\theta = \mu_e / \mu_w, \quad (B.3)$$

where

$$m = M_e^2(\gamma - 1)/2, \quad F = T_w / T_e,$$

$$A = \sqrt{rm/F}, \quad B = (1 + rm - F)/F,$$

$$r = \text{Recovery factor} = 0.9,$$

$$\alpha = (2A^2 - B)/\sqrt{4A^2 + B^2}, \quad \beta = B/\sqrt{4A^2/B^2}.$$

The local incompressible skin friction is evaluated from the Karman–Schoenherr relation, which is considered one of the most accurate fits to the incompressible experimental data:

$$C_{f,i} = \frac{1}{\log(2\,Re_\theta|_{\text{inc}})[17.075\log(2\,Re_\theta|_{\text{inc}}) + 14.832]}.$$

(B.4)

The accuracy of the theories relative to the experimental C_f data is illustrated by plotting the transformed skin friction $F_c C_f$ as a function of the transformed Reynolds number $F_\theta Re_\theta$. The transformed data should be in close agreement with the Karman–Schoenherr curve plotted on this figure. A more sensitive illustration of the accuracy is to use percent error E of experimental skin

friction relative to theoretical value $C_{f,i}$, which is obtained from

$$E = [(F_c C_f / C_{f,i}) - 1] \times 100.$$

Then the percent error E is plotted versus $F_\theta Re_\theta$. Compressible turbulent model predictions can be treated in the same manner. Correlation of the experimental measured skin friction of compressible flows (Mach < 5) has proven to be reasonably effective with the Van Driest II approach. The correlation approach of Huang et al. [54] gives results of similar accuracy. Squire [52] estimates that the accuracy of the Van Driest II correlation is within ±3% for the flat plate. Based on the sometimes erratic agreement between experiments and the correlation, we feel that this error estimate is somewhat optimistic and should be increased to ±5%.

B.2. Correlation of heat transfer

Reynolds analogy [194] is used to predict the wall heat flux and was developed for incompressible flow. The compressible Reynolds analogy is written in the same form which gives

$$2St/C_f = R_{af} = \text{Reynolds analogy factor},$$ (B.5)

where St is the compressible Stanton number, C_f is the compressible skin friction, and R_{af} is the Reynolds analogy factor. The above is multiplied by F_c which is defined in Eq. (B.3) and gives the incompressible Stanton number and the transformed Reynolds numbers

$$St^* = F_c St = R_{af} C_f^*/2,$$

$$Re_x^* = F_x Re_x, \quad Re_\theta^* = F_\theta Re_\theta.$$ (B.6)

The transformed skin friction C_f^* can be approximated with the Karman–Schoenherr relation given in Eq. (B.4). Assume the Reynolds analogy factor is known ($R_{af} \approx 1$). Therefore, Eq. (B.6) can be used to determine the compressible Stanton number and Reynolds number or experimental compressible Stanton and Reynolds numbers can be transformed into incompressible Stanton and Reynolds numbers. The transformed compressible experimental data plotted as $F_c St$ versus $F_\theta Re_\theta$ should be near to the correlation curve given by Eq. (B.6) with C_f^* determined from Eq. (B.4) evaluated with Re_θ^*. Turbulent model predictions can be correlated in the same manner.

Two forms of the Stanton number are used with different locations for the evaluation of the enthalpy. The edge and adiabatic Stanton numbers for real and perfect gas models are

$$St_e = q_w/\rho_e u_e(H_e - h_w) = q_w/\rho_e u_e c_p(T_e - T_w),$$

$$St_{aw} = q_w/\rho_e u_e(h_{aw} - h_w) = q_w/\rho_e u_e c_p(T_{aw} - T_w),$$
$$c_p = \gamma R/(\gamma - 1). \tag{B.7}$$

The adiabatic wall enthalpy for a real gas is obtained from the following first equation and the second equation gives the adiabatic wall temperature for a perfect gas:

$$h_{aw} = h_e + \frac{r u_e^2}{2}, \quad T_{aw} = T_e(1 + rm),$$

$$m = \frac{u_e^2}{2c_p T_e} = \left(\frac{\gamma - 1}{2}\right) M_e^2.$$

The first form of the Stanton number St_e becomes infinite when $T_w = T_e$. The second form of the Stanton number St_{aw} becomes indeterminate when the heat flux is zero and $T_w = T_{aw}$. The Stanton numbers can use the free stream conditions for the density and velocity rather than boundary-layer edge conditions. Fernholz and Finley [29] use the second form in Eq. (B.7), but they recommend that the heat flux be written in the form suggested by Green (see in Fernholz and Finley [29, p. 50]), which is $CQ = N_{qw} = q_w/\rho_e u_e H_e$. This relation avoids the difficulties with having a indeterminate equation. Also the heat transfer coefficient h_c is used and is defined as $q_w = h_c(T_{aw} - T_w)$.

The *Reynolds analog factor* is used to predict the heat transfer and is defined in two forms

$$R_{afe} = St_e(C_{fe}/2) = \frac{u_e q_w}{\tau_w(H_e - h_w)}$$
$$= \frac{u_e q_w}{\tau_w c_p(T_e - T_w + m)},$$

$$R_{af} = St_{aw}(C_{fe}/2) = \frac{u_e q_w}{\tau_w(h_{aw} - h_w)}$$
$$= \frac{u_e q_w}{\tau_w c_p(T_{aw} - T_w)}. \tag{B.8}$$

The ratio of the Reynolds factors becomes

$$R_{afe}/R_{af} = (T_{aw} - T_w)/(T_e - T_w + m).$$

As the Mach number approaches zero, $m \to 0$, $T_{aw} \to T_e$, and the ratio of the Reynolds factors $R_{afe}/R_{af} \to 1$. For low-speed flows, authors usually use R_{afe}, while for compressible flow authors use R_{af}.

Many of the models for the Reynolds analogy factor for incompressible flow are of the form

$$R_{af} = [Pr_T(1 + g\sqrt{C_f/2})]^{-1}, \quad g = C_{sl}(1 - Pr). \tag{B.9}$$

The value of the constant C_{sl} depends on the model used for the velocity in the viscous sublayer. There are many models for the Reynolds analogy factor R_{af}, some are given below (note: unless otherwise stated, it is assumed that $Pr = 0.71$ in these models). The various models described below are evaluated with $Pr_T = 0.90$ and $Re_\theta = 10^4$ which gives $C_{f,i} = 2.6345 \times 10^{-3}$. The foregoing values of the parameters are used unless indicated otherwise. Some of the often referred to models or important models are briefly described next. In addition, results are included from an experimental investigation of the hypersonic Reynolds analogy factor.

Reynolds [194] assumed the laminar and turbulent Prandtl numbers are one, the flow is incompressible, and neglected the viscous sublayer, which gives $R_{af} = 1$.

Prandtl [195] and *Taylor* [196] were concerned with low-speed flows and used the Stanton number St_e and the Reynolds analogy factor as given in Eq. (B.9) with $Pr_T = 1$

Prandtl: $C_{sl} = 8.7$, $g = 2.523$, $R_{af} = 1.101$,

Taylor: $C_{sl} = 11.5$, $g = 3.335$, $R_{af} = 1.138$.

This model is described by von Karman [197] and by Schlichting [198] (p. 709). The authors assume the turbulent Prandtl number is one and the flow is incompressible. The velocity profile model includes the viscous sublayer which is neglected in the Reynolds model. Rubesin [199] gives $C_{sl} = 11.5$ for the Prandtl–Taylor model. von Karman indicates that Prandtl uses $C_{sl} = 8.7$ while Schlichting indicates Prandtl uses $C_{sl} = 5.0$.

Colburn [200] developed an empirical model for incompressible flow with $Pr_T = 1$ which gives $R_{af} = Pr^{-2/3} = 1.256$.

von Karman [197] considers low-speed flows and uses the Stanton number St_e and the Reynolds analogy factor is given in Eq. (B.9) with g defined as

$$g = 5\{(1 - Pr) - \ln[1 - 5(1 - Pr)/6]\} = 2.833,$$
$$Pr_T = 1, \quad R_{af} = 1.115.$$

The turbulent Prandtl numbers is assumed to have a value of one and the flow is incompressible. A three layer turbulent boundary-layer model is used with a viscous sublayer, a log layer, and a buffer layer,

which is approximated with a linear variation. The g function is more complex due to the three layer model.

van Driest [51,201] models compressible flow and uses the Stanton number St_{aw} and the Reynolds analogy factor is given in Eq. (B.9) with

$$g = C_{sl}\left\{ B - \ln\left(1 - \frac{5}{6}B\right) - 0.5A\left(\frac{\pi^2}{6} + 1.5A\right)\right\}$$
$$= 1.574, \quad C_{sl} = 5,$$

$$A = 1 - Pr_T = 0.1, \quad B = 1 - Pr/Pr_T = 0.21111,$$

$$R_{af} = 1.061.$$

The model assumes arbitrary constant turbulent Prandtl number. When $Pr_T = 1$, the above equation is the same as the von Karman model given above. The turbulent Prandtl number $Pr_T = 0.86$ and $Pr = 0.72$ in the paper of van Driest.

Chi and Spalding [138] use the transform relations in Eqs. (B.6) and (B.1). The van Driest transformation functions given in Eq. (B.3) are evaluated with the Spalding–Chi transformation theory [110]. Chi and Spalding developed the following skin friction relation which was then used in the compressible Reynolds analogy given in Eq. (B.6):

$$C_{f,i}/2 = [3.8 + 5.77\log(Re_{\theta i})]^{-2}. \tag{B.10}$$

The Stanton number correlation curve becomes

$$St_{e,i} = R_{af}[3.8 + 5.77\log(Re_{\theta,i})]^{-2},$$
$$C_f/2 = 1.60(\ln Re_x)^{0.772}.$$

When $Re_{x,i}$ is specified, the incompressible skin friction is obtained from the above Schultz–Grunow relation. The authors use $C_{f,i}$ and $St_{e,i}$ from the experimental data of Reynolds, Kays, and Kline [202] to determine the Reynolds analogy factor that matches the Stanton number database with the Stanton number correlation curve. The minimum error is obtained when $R_{af} = 1.16$. The relation used to correlate the compressible Stanton number data becomes

$$St_e^* \approx F_c St_e = 1.16[3.8 + 5.77\log(F_\theta Re_{\theta,i})]^{-2},$$
$$Re_\theta^* \approx F_\theta Re_\theta,$$

$$F_\theta = (T_w/T_e)^{-0.702}(T_{aw}/T_w)^{0.772}.$$

The transformation functions F_x and F_c are the same as van Driest II relations given Eq. (B.3) and F_θ is given above. The incompressible skin friction term $C_{fi}/2$ can also be obtained from Eq. (B.4). The

Chi–Spalding incompressible skin friction Eq. (B.10) gives values that are 5.5–4.5% higher as $Re_{\theta i}$ goes from 10^3 to 10^6 than obtained with the Karman–Schoenherr skin-friction relation. Therefore, if the Karman–Schoenherr relation is used for $C_{fi}/2$, then the Reynolds factor must be changed to $R_{af} = 1.22$ in order to obtain agreement with the database of Reynolds et al. [202]. The database used in testing the accuracy of the correlation of compressible Stanton numbers are from 11 experiments. With this database Chi and Spalding indicate that the Stanton number correlation function has been validated for Re_θ from 500 to 10^4, Mach numbers up to 10, T_{aw}/T_w from 0.5 to 2.7, and Re_x from 10^5 to 10^8.

Keener and Polek [140] made direct measurements of skin-friction and heat transfer on a smooth flat plate with a hypersonic turbulent boundary layer. The edge Mach number varied from 5.9 to 7.8 and T_w/T_{aw} was 0.32 and 0.50. The measured skin friction and heat transfer are estimated to be accurate within 5%. The authors are concerned with compressible flow and use the Stanton number St_{aw}. For these experimental conditions, the authors recommend that $R_{af} = 1.0$ with the maximum data scatter of 9% and with most of the data within 4%. This paper is further evaluation of the work of Cary [119] as seven of the data points in his database were preliminary measurements reported in Hopkins et al. [86].

Cebeci and Bradshaw [203] indicate that a number of investigators have developed the Reynolds analogy factor of the form of Eq. (B.9) with various values of the coefficients. Cebeci and Bradshaw suggest the following values:

$$Pr_T = 1/1.11 = 0.901, \quad g = 1.20, \quad R_{af} = 1.160.$$

Summary of Reynolds analogy: Experiments indicate that $0.9 < R_{af} < 1.3$, but may be close to unity for hypersonic flows. There is insufficient reliable experimental data to establish the Reynolds analogy factor for a wide range of flow conditions. Free stream turbulence has a significant impact on increasing the Reynolds analogy factor while surface roughness decreases the value. Also there is confusion on which Stanton number definition is being used when the Reynolds analogy factor R_{af} is being determined and compared with other results.

B.3. Mean temperature profiles

A review of the analysis used to obtain analytical solutions to the boundary-layer energy equation are

given in the report of Fernholz and Finley [29]. The initial relation developed by Crocco and Busemann assumes that the laminar and turbulent Prandtl numbers are one ($Pr = Pr_T = 1$). A solution to the total enthalpy energy equation is that the total enthalpy is constant across the boundary layer. Since $\tilde{u} = 0$ and $k = 0$ at the wall and $h = c_p T$, the following relations are obtained for the total enthalpy and the temperature:

$$H = h + \tilde{u}^2/2 + k = H_w = h_w,$$

$$T = T_w - \alpha \tilde{u} - \beta \tilde{u}^2 - \gamma_T k,$$

$$\alpha = 0, \quad \beta = 1/2c_p, \quad \gamma_T = 1/c_p. \tag{B.11}$$

The second relation developed by Crocco and Busemann assumes a zero-pressure gradient with an isothermal wall and that the laminar and turbulent Prandtl numbers are one. The momentum and energy equations are similar, which gives $H = C_1 + C_2 \tilde{u}$. With the wall and edge boundary conditions applied, the energy equation in terms of temperature becomes Eq. (B.11) with the coefficients

$$\alpha = [T_w - T_e - \beta \tilde{u}_e^2 - \gamma_T k_e]/\tilde{u}_e,$$

$$\beta = 1/2c_p, \quad \gamma_T = 1/c_p. \tag{B.12}$$

Van Driest extended the Crocco analysis for compressible laminar boundary flows to turbulent flows with a variable Prandtl number. The development of this Van Driest [133] temperature relation becomes very complex and not very useful. The mixed Prandtl number was initially introduced in this article by Van Driest and is defined as

$$Pr_m = c_p \left(\frac{\mu + \mu_T}{k + k_T}\right) = \frac{\mu + \mu_T}{(\mu/Pr) + (\mu_T/Pr_T)},$$

$$Pr = \frac{c_p \mu}{k}, \quad Pr_T = \frac{c_p \mu_T}{k_T}.$$

Fernholz and Finley [29] have presented the work of Walz where the temperature equation is developed for a constant Prandtl number which is restricted to $0.7 < Pr < 1$.

Huang et al. [54] (HBC) have developed the temperature equation by neglecting the convective terms in the momentum and energy equations. The reduced boundary-layer momentum equation with the pressure gradient neglected can be integrated once to obtain

$$(\mu + \mu_T)\frac{d\tilde{u}}{dy} = \tau_w. \tag{B.13}$$

The total enthalpy form of the reduced energy equation can be integrated once to obtain

$$-q + \tilde{u}\tau_w + (\mu + \mu_T)\frac{dk}{dy} = \text{constant}.$$

Since at the wall $\tilde{u} = 0$ and $k = c_k y^2 + \cdots$, the constant in the above equation is q_w and the energy equation becomes

$$q = q_w + \tilde{u}\tau_w + (\mu + \mu_T)\frac{dk}{dy}. \tag{B.14}$$

The heat flux normal and near to the wall becomes with the use of the momentum Eq. (B.13)

$$q = -\left(\frac{\mu + \mu_T}{Pr_m}\right)\frac{\partial h}{\partial y} = -\frac{c_p}{Pr_m}(\mu + \mu_T)\frac{\partial T}{\partial y}$$

$$= -\frac{c_p \tau_w}{Pr_m}\frac{\partial T}{\partial u}. \tag{B.15}$$

From Eq. (B.15) and the temperature relation in Eq. (B.11), the wall heat flux is $q_w = \alpha c_p \tau_w/Pr_m$ and when solved for q_w/τ_w gives

$$q_w/\tau_w = [T_w - T_e - \beta \tilde{u}_e^2 - \gamma_T k_e](c_p/\tilde{u}_e Pr_m),$$

$$\beta \tilde{u}_e^2 = \tilde{u}_e^2/2c_p = m T_e, \quad m = \tilde{u}_e^2/2c_p T_e = \left(\frac{\gamma - 1}{2}\right)M_e^2.$$

Using Eqs. (B.14) and (B.15), the differential form of the temperature equation becomes

$$dT = -\frac{Pr_m}{c_p}\left[\left(\frac{q_w}{\tau_w} + \tilde{u}\right)d\tilde{u} + dk\right]. \tag{B.16}$$

Integration of this equation with Pr_m constant gives the temperature Eq. (B.11) with the coefficients

$$\alpha = (Pr_m/c_p)(q_w/\tau_w),$$

$$\beta = Pr_m/2c_p, \quad \gamma_T = Pr_m/c_p. \tag{B.17}$$

Eqs. (B.13) and (B.14) have been used by HBC with μ and k neglected to obtain the energy Eq. (B.11) with coefficients given in Eq. (B.17) where $Pr_m = Pr_T$. The energy equation developed by Fernholz and Finley [29] is essentially the same as given above, except the turbulent Prandtl number in the coefficients α and β is replaced with the recovery factor r. The above coefficient α can also be written as

$$\alpha = [T_w - T_e - \beta \tilde{u}_e^2 - \gamma_T k_e]/\tilde{u}_e.$$

For an adiabatic wall $\alpha = 0$ and the above equation with Eq. (B.17) gives the adiabatic wall temperature $T_{aw} = T_e(1 + Pr_T m + \gamma_T k_e)$ where $Pr_m = Pr_T$. Since the adiabatic wall temperature is

defined as $T_{aw} = T_e(1 + rm)$, the recovery factor $r = Pr_T$ for this analysis. The total temperature $T_t = T + \tilde{u}^2/2c_p$ is written in non-dimensional form as $T^* = (T_t - T_w)/(T_{te} - T_w)$ and is plotted as function of $\tilde{u}/\tilde{u}_e$. At the wall $T^* = 0$ and at the edge of the boundary layer $T^* = 1$. When $Pr_T = 1$, the non-dimensional total temperature has a linear variation, $T^* = \tilde{u}/\tilde{u}_e$. When the wall is adiabatic $T_w = T_{aw}$ and the recovery factor equals the turbulent Prandtl number, the non-dimensional total temperature has quadratic variation, $T^* = (\tilde{u}/\tilde{u}_e)^2$.

The Van Driest form of the temperature or density equation with the turbulent kinetic energy neglected is

$$T/T_w = \overline{\rho}_w/\overline{\rho} = 1 + B(u/u_e) - A^2(u/u_e)^2, \quad (B.18)$$

where

$$A^2 = \beta u_e^2/T_w = Pr_T u_e^2/2c_p T_w,$$

$$B = -\frac{\alpha u_e}{T_w} = \left(\frac{T_e}{T_w}\right) - 1 + A^2 = -\frac{Pr_T u_e q_w}{c_p T_w \tau_w}.$$

In the 1951 paper of Van Driest [133], he assumed that $Pr_T = r = 1$. In a 1955 paper, Van Driest [134] considered a variable Prandtl number, and the analysis becomes more complex with the evaluation of a number of integral relations required.

Another form of the temperature or density equation with the turbulent kinetic energy neglected is

$$T/T_w = \overline{\rho}_w/\overline{\rho} = 1 - \overline{\alpha}u^+ - \overline{\beta}u^{+2}, \quad (B.19)$$

where

$$\overline{\alpha} = \alpha u_\tau/T_w = Pr_T q_w u_\tau/c_p T_w \tau_w = Pr_T B_q$$
$$= [(1 - T_e/T_w)/u_e^+] - \overline{\beta}u_e^+ = 2R^2 H,$$

$$\overline{\beta} = \beta u_\tau^2/T_w = Pr_T u_\tau^2/2c_p T_w$$
$$= Pr_T M_\tau^2(\gamma - 1)/2 = R^2,$$

$$B_q = q_w/\rho_w c_p T_w u_\tau,$$

$$M_\tau = u_\tau/a_w, \quad H = (q_w/\tau_w)/u_\tau.$$

B.4. Mean velocity profiles

In the *inner region of the turbulent boundary layer*, the total shear stress is approximately constant as given by Eq. (B.13). The Reynolds stress is written in terms of the eddy viscosity which is approximated

with the Prandtl mixing-length approach. The total shear stress equation, eddy viscosity μ_T, and mixing length l_m become

$$\overline{\rho}l_m^2\left(\frac{d\tilde{u}}{dy}\right)^2 + \mu\frac{d\tilde{u}}{du} - \tau_w = 0,$$

$$\mu_T = \overline{\rho}l_m^2\left|\frac{d\tilde{u}}{dy}\right|, \quad l_m = \kappa y D_f, \quad (B.20)$$

where Van Driest damping function is used in the viscous sublayer and is

$$D_f = 1 - e^{-y^+/A^+}, \quad A^+ = 25.53.$$

Introducing inner variables

$$u^+ = \tilde{u}/u_\tau, \quad y^+ = \overline{\rho}_w y u_\tau/\mu_w,$$

$$u_\tau = \sqrt{\tau_w/\overline{\rho}_w}, \quad l_m^+ = \kappa y^+ D_f,$$

the total shear stress Eq. (B.20) becomes

$$\left(a\frac{du^+}{dy^+}\right)^2 + b\frac{du^+}{dy^+} - 1 = 0,$$

$$a = l_m^+\sqrt{\overline{\rho}/\overline{\rho}_w}, \quad b = \mu/\mu_w. \quad (B.21)$$

This equation is solved for the first derivative and then can be integrated numerically to obtain the compressible velocity across the inner layer

$$\frac{du^+}{dy^+} = \frac{2/b}{1 + \sqrt{1 + (2a/b)^2}},$$

$$u^+ = \int_0^{y^+} \{(2/b)/[1 + \sqrt{1 + (2a/b)^2}]\}\,dy^+. \quad (B.22)$$

Also Eq. (B.21) can be solved with a velocity transformation by introducing the Van Driest transformed velocity u_c^+, which is defined as

$$\frac{du_c^+}{dy^+} = \sqrt{\overline{\rho}/\overline{\rho}_w}\frac{du^+}{dy^+},$$

$$\int du_c^+ = \int \sqrt{\overline{\rho}/\overline{\rho}_w}\,du^+ = \int du^+/\sqrt{T/T_w}, \quad (B.23)$$

Eq. (B.21) becomes

$$\left(\overline{a}\frac{du_c^+}{dy^+}\right) + \overline{b}\frac{du_c^+}{dy^+} - 1 = 0,$$

$$\overline{a} = l_m^+, \quad \overline{b} = (\mu/\mu_w)/\sqrt{\overline{\rho}/\overline{\rho}_w}. \quad (B.24)$$

This equation is solved for the first derivative and the transformed velocity becomes

$$\frac{\mathrm{d}u_{\mathrm{c}}^+}{\mathrm{d}y^+} = \frac{2/\overline{b}}{1 + \sqrt{1 + (2\overline{a}/\overline{b})^2}},$$

$$u_{\mathrm{c}}^+ = \int_0^{y^+} \{(2/\overline{b})/[1 + \sqrt{1 + (2\overline{a}/\overline{b})^2}]\}\,\mathrm{d}y^+. \quad (B.25)$$

The solution of this equation for u_{c}^+ as a function of y^+ requires a numerical solution since $\overline{b}$ varies across the inner region of the boundary layer.

In the *logarithmic region* $b \to 0$, $a = \kappa y^+$, and solving Eq. (B.21) for the first derivative gives

$$\frac{\mathrm{d}u^+}{\mathrm{d}y^+} = \sqrt{\overline{\rho}_{\mathrm{w}}/\overline{\rho}}/l_{\mathrm{m}}^+, \quad l_{\mathrm{m}}^+ = \kappa y^+. \quad (B.26)$$

For *incompressible flow* (constant density case $\overline{\rho}_{\mathrm{w}}/\overline{\rho} = 1$), the above becomes

$$\int_{u_0^+}^{u^+} \mathrm{d}u = \int_{y_0^+}^{y^+} \frac{\mathrm{d}y^+}{\kappa y^+}, \quad u^+ - u_0^+ = \frac{1}{\kappa}\ln y^+ - \frac{1}{\kappa}\ln y_0^+.$$

The incompressible solution becomes

$$u_{\mathrm{inc}}^+ = \frac{1}{\kappa}\ln(y^+) + C, \quad C = u_0^+ - \frac{1}{\kappa}\ln(y_0^+). \quad (B.27)$$

With the velocity $u_0^+ = 0$, the constant $C = -(1/\kappa)\ln(y_0^+)$, and the value of the coordinate $y_0^+ = \exp(-\kappa C)$. Bradshaw suggest that the von Karman constant $\kappa = 0.41$, and the constant $C = 5.20$, which gives $y_0^+ = 0.1186$. The value of the constants are based on a database of incompressible zero-pressure gradient boundary-layer experiments. The appropriate values of these constants are still being debated. Eq. (B.27) is only valid when y^+ is approximately 40 or larger and u_{inc}^+ is 14 or larger.

For *compressible flow in the logarithmic region* $\overline{b} \to 0$, $\overline{a} = \kappa y^+$, and the governing Eq. (B.25) and solution become

$$\frac{\mathrm{d}u_{\mathrm{c}}^+}{\mathrm{d}y^+} = \frac{1}{\kappa y^+}, \quad u_{\mathrm{c}}^+ = \frac{1}{\kappa}\ln y^+ + C,$$

$$C = u_{\mathrm{c0}}^+ - \frac{1}{\kappa}\ln(y_0^+), \quad y_0^+ = \exp[\kappa(u_{\mathrm{c0}}^+ - C)]. \quad (B.28)$$

With $u_{\mathrm{c0}}^+ = 0$, the coordinate $y_0^+ = \exp(-\kappa C)$, and $C = -(1/\kappa)\ln(y_0^+)$, which are the same as the incompressible values. In the logarithmic region, the transformed compressible velocity u_{c}^+ becomes the same as the incompressible velocity u_{inc}^+ as given in Eq. (B.27).

Also for the *compressible flow in the logarithmic region*, the density ratio is obtained from the temperature relation given by Eq. (B.19) with the turbulent kinetic energy neglected, then Eq. (B.26) is solved for the velocity u^+ as a function of y^+. The governing equation becomes

$$\int_{u_0^+}^{u^+} \frac{\mathrm{d}u^+}{\sqrt{1 - \overline{\alpha}u^+ - \overline{\beta}u^{+2}}} = \int_{y_0^+}^{y^+} \frac{\mathrm{d}y^+}{\kappa y^+}.$$

The evaluation of the integrals gives

$$\frac{1}{\sqrt{\overline{\beta}}}\mathrm{asin}\left(\frac{2\overline{\beta}u^+ + \overline{\alpha}}{\sqrt{\overline{\alpha}^2 + 4\overline{\beta}}}\right) - \frac{1}{\sqrt{\overline{\beta}}}\mathrm{asin}\left(\frac{2\overline{\beta}u_0^+ + \overline{\alpha}}{\sqrt{\overline{\alpha}^2 + 4\overline{\beta}}}\right)$$
$$= \frac{1}{\kappa}\ln(y^+) - \frac{1}{\kappa}\ln(y_0^+). \quad (B.29)$$

Eq. (B.29) can be written in the notation of Bradshaw with new variables R and H where $\overline{\alpha} = 2R^2H$, $\overline{\beta} = R^2$, and with the use of Eq. (B.28) the resulting equation is

$$\frac{1}{R}\mathrm{asin}\left(\frac{Ru^+ + RH}{D}\right) + C_1 = \frac{1}{\kappa}\ln(y^+) + C = u_{\mathrm{c}}^+,$$

$$C_1 = u_{\mathrm{c0}}^+ - \frac{1}{R}\mathrm{asin}\left(\frac{Ru_0^+ + RH}{D}\right),$$

$$R = u_\tau \sqrt{Pr_{\mathrm{T}}/2c_{\mathrm{p}}T_{\mathrm{w}}},$$

$$H = q_{\mathrm{w}}/\tau_{\mathrm{w}}u_\tau, \quad D = \sqrt{1 + (RH)^2}. \quad (B.30)$$

From Eqs. (B.27) and (B.28) at $y_0^+ = \exp(-\kappa C)$, $u_0^+ = u_{\mathrm{c0}}^+ = 0$. The compressible velocity transformation of Van Driest is obtained from Eq. (B.30) as

$$u_{\mathrm{c}}^+ = \frac{1}{R}\left[\mathrm{asin}\left(\frac{Ru^+ + RH}{D}\right) - \mathrm{asin}\left(\frac{RH}{D}\right)\right]. \quad (B.31)$$

The inverse of this equation has been given by Bradshaw as

$$u^+ = \frac{1}{R}\sin(Ru_{\mathrm{c}}^+) - H[1 - \cos(Ru_{\mathrm{c}}^+)]. \quad (B.32)$$

In the original notation, the *Van Driest velocity transformation* is obtained from Eq. (B.29) where the temperature is given by Eq. (B.18),

$\overline{\alpha} = -Bu_\tau/\tilde{u}_e$, and $\overline{\beta} = (Au_\tau/\tilde{u}_e)^2$, which gives

$$
\begin{aligned}
u_c^+ = \frac{\tilde{u}_c}{u_\tau} &= \frac{(\tilde{u}_e/u_\tau)}{A} \\
&\times \left\{ \text{asin}\left[\frac{2A^2(\tilde{u}/\tilde{u}_e) - B}{\sqrt{B^2 + 4A^2}} \right] \right. \\
&\quad \left. - \text{asin}\left(\frac{-B}{\sqrt{B^2 + 4A^2}} \right) \right\} \\
&= \frac{1}{\kappa}\ln(y^+) + C,
\end{aligned}
\tag{B.33}
$$

where A and B are defined after the Van Driest temperature Eq. (B.18). The velocity ratio is written as follows in the Van Driest article

$$
u_e^+ = \tilde{u}_e/u_\tau = 1/\sqrt{(C_f/2)(T_w/T_e)}.
$$

Also in the Van Driest transformation the turbulent Prandtl number is set equal to one. In the Bradshaw notation $A = R\tilde{u}_e/u_\tau$, $B = -2ARH$, and *Eq.* (B.33) *is the same as Eq.* (B.31) *when the turbulent Prandtl number is one*. A plot of $u_c^+ = \tilde{u}_c/u_\tau$ versus y^+ for experimental data or numerical solutions should match Eq. (B.27), which is the incompressible log-law. Also the above Eq. (B.33) should approach Eq. (B.27) as the Mach number at the edge of the boundary layer becomes very small and the temperature becomes uniform across the boundary layer.

The *Fernholz velocity transformation* uses the Prandtl mixing-length concept with a recovery factor of $r = 0.896$. The transformation evaluates the integration constant at the lower boundary where $(\tilde{u}/\tilde{u}_e) \approx 0.5$, $u_{c0}^+ \approx 14.5$, and $y_0^+ = \exp[\kappa(u_{c0}^+ - C)] \approx 43$. The von Karman constant $\kappa = 0.40$ and the constant $C = 5.10$ in the Fernholz analysis. With Fernholz notation the velocity transformation is

$$
\tilde{u}_c = \frac{\tilde{u}_e}{b}\,\text{asin}\left(\frac{2b^2(\tilde{u}/\tilde{u}_e) - a}{d} \right),
\tag{B.34}
$$

where the coefficients are

$$
a = (1 + rm)(T_e/T_w) - 1 = -Pr_T u_e q_w/c_p T_w \tau_w,
$$

$$
b^2 = rm(T_e/T_w) = r\tilde{u}_e^2/2c_p T_w, \quad d = \sqrt{a^2 + 4b^2}.
$$

Eq. (B.34) can be obtained in the Bradshaw notation by starting with Eq. (B.30) which is

$$
u_c^+ = \frac{1}{R}\,\text{asin}\left(\frac{Ru^+ + RH}{D} \right) + C_1 = \frac{1}{\kappa}\ln(y^+) + C,
\tag{B.35}
$$

where C_1 is defined in Eq. (B.30) and C is defined in Eq. (B.28). The coefficients in the Bradshaw form of the Fernholz velocity transformation are

$$
R = u_\tau b/\tilde{u}_e = u_\tau\sqrt{r/2c_p T_w}, \quad H = q_w/\tau_w u_\tau,
$$

$$
RH = -a/2b, \quad D = d/2b = \sqrt{1 + (RH)^2}.
$$

Fernholz has shown for an adiabatic wall ($H = 0$), that C_1 is small and can be neglected in Eq. (B.35). The Van Driest transformation given in Eq. (B.31) is the same as the Fernholz Eq. (B.35) if $r = Pr_T$ and asin (RH/D) is neglected in the Van Driest transformation.

In the *outer region of the turbulent boundary layer*, the similarity of the velocity profiles is obtained with the use of the velocity defect $(\tilde{u}_{ce} - \tilde{u}_c)/u_\tau$. The velocity defect outside the viscous sublayer is approximated as

$$
(\tilde{u}_{ce} - \tilde{u}_c)/u_\tau = -\frac{1}{\kappa}\ln(y/\delta) + \frac{\Pi}{\kappa}w(y/\delta).
\tag{B.36}
$$

Fernholz and Finley [29] has shown the above can be approximated as

$$
U_D = (\tilde{u}_{ce} - \tilde{u}_c)/u_\tau = -4.70\ln(y/\Delta^*) - 6.74,
$$

$$
\Delta^* = \delta \int_0^1 U_D \, \mathrm{d}(y/\delta).
\tag{B.37}
$$

Fernholz and Finley [29] use this relation to assess the accuracy of flat plate turbulent boundary layers in the outer region.

Huang et al. [54] have obtain the transformed velocity from the wall to the edge of the boundary by taking into account the viscous sublayer and by including a wake function. This procedure gives the skin friction, velocity, and temperature profiles as a function of the Reynolds number. It has been developed as a 7 step procedure with iteration of the solution until converged. The procedure is described for the case when the momentum thickness Reynolds number is used and the momentum thickness is specified. The following properties are specified:

$$
\theta, \overline{\rho}_e, c_p, Pr_T, p, T_w, \tilde{u}_e, \mu_w.
$$

Viscosity at the wall is determined from Sutherland or Keyes viscosity law with the specified wall temperature. From the above specified properties,

the following parameters are calculated:

$$\mu_w = \mu(T_w), \quad \overline{\rho}_w = p/RT_w, \quad T_e = p/R\overline{\rho}_e,$$
$$\mu_e = n(T_e).$$

The solution procedure is as follows:

1. Guess the *thickness ratio* θ/δ and the *wall friction velocity* $u_\tau = \sqrt{\tau_w/\rho_w}$; then determine the boundary-layer thickness $\delta = \theta/(\theta/\delta)$. The thickness ratio for incompressible flow is estimated as $\theta/\delta \approx 7/72$, while for compressible flow the relation developed by Smits and Dussauge [204] (see p. 194) can be used.
2. Calculate the momentum thickness Reynolds numbers $Re_\theta = \overline{\rho}_e \tilde{u}_e \theta/\mu_e$ and $Re_{\theta w} = \overline{\rho}_e \tilde{u}_e \theta/\mu_w = (\mu_e/\mu_w)Re_\theta$. Then determine the wall function $\Pi(Re_\theta)$ from Fig. 1a in the Huang et al. paper or use Cebeci–Smith correlation.
3. Calculate the non-dimensional boundary-layer thickness $\delta^+ = y_e^+ = \overline{\rho}_w u_\tau \delta/\mu_w$ and wall density $\rho_w = p/RT_w$. Then determine the law of the wall profile from the wall ($y^+ = 0$) to the edge of the boundary layer ($y^+ = \delta^+$) by numerical evaluation of the following relation:

$$u_{cb}^+ = \int_0^{y^+} \frac{2\mathrm{d}y^+}{1 + \sqrt{1 + 4(l^+)^2}},$$
$$l^+ = \kappa y^+(1 - \mathrm{e}^{-y^+/A^+}),$$
$$A^+ = 25.53, \quad \kappa = 0.41.$$

4. Obtain compressible velocity at the edge of the boundary layer, $\eta = y^+/\delta^+ = 1$.

$$u_e^+ = (1/R)\sin(Ru_{ce}^+) - H[1 - \cos(Ru_{ce}^+)]$$

$$u_{ce}^+ = u_{cb}^+(\eta) + (\Pi/\kappa)w(\eta), \quad \eta = 1 \quad w(1) = 2.$$

5. *Update shear velocity* $u_\tau = \tilde{u}_e/\tilde{u}_e^+$ and local skin friction $c_f = 2(T_e/T_w)(u_\tau/\tilde{u}_e)^2$.
6. Tabulate the transformed velocity, the compressible velocity, and the temperature across the boundary layer using the following relations:

$$u_c^+ = u_{cb}^+(\eta) + (\Pi/\kappa)w(\eta),$$
$$u^+ = (1/R)\sin(Ru_c^+) - H[1 - \cos(Ru_c^+)],$$

$$T = T_w(1 - \overline{\alpha}u^+ - R^2u^{+2}), \quad \overline{\alpha} = 2R^2H,$$

$$R = u_\tau\sqrt{Pr_T/2c_p T_w},$$
$$H = [(1 - T_e/T_w)/(R^2 u_e^+) - u^+]/2.$$

7. *Update the thickness ratio*

$$\theta/\delta = \int_0^1 \frac{\overline{\rho}u^+}{\overline{\rho}_e u_e^+}\left(1 - \frac{u^+}{u_e^+}\right)\mathrm{d}\eta, \quad \overline{\rho}/\overline{\rho}_e = T_e/T.$$

Steps 1–7 are repeated until the solution converges.

Appendix C. Turbulent sharp cone to flat plate transformations

Theories for cone to flat plate Mangler transformation are usually of the form

$$(C_f)_{Cone}/(C_f)_{FlatPlate} = (St)_{Cone}/(St)_{FlatPlate}$$
$$= G(Re, M_e, T_w/T_e).$$

The Mangler transformation parameter G for compressible flow could be a function of the boundary-layer edge Reynolds number based on x or θ, M_e, and T_w/T_e. Below is a brief indication of some of the contributions to this issue.

Van Driest [55] has developed a simple rule for transforming local flat plate skin friction and heat transfer to cones at zero angle of attack for fully turbulent boundary layers (no transition from laminar flow) in supersonic/hypersonic flows. His method is different than the standard approach. The flat plate compressible skin friction is determined from Van Driest II theory, which gives $(C_f)_{FlatPlate} = F(Re_x, M_e, T_w/T_e)$. Van Driest determined that the cone compressible skin friction may be calculated from $(C_f)_{Cone} = F(Re_x/2, M_e, T_w/T_e)$ where the flat plate skin friction relation is evaluated at one half the edge Reynolds number. The transformation parameter $G = F(Re_x/2, M_e, T_w/T_e)/(F(Re_x, M_e, T_w/T_e))$ with $G = 1.14$ at $Re_x = 10^5$ and $G = 1.08$ at $Re_x = 10^8$.

Seiff [205] has taken into account that the turbulent boundary layer begins down stream on the flat plate and has determined the effective or virtual origin of the turbulent boundary layer. It is assumed that the boundary layer is initially laminar and instantaneously transitions to turbulent flow at x_{tr}, which must be specified. The Blasius relation for incompressible skin friction is transformed to a compressible skin-friction relation which is used with the Karman momentum–integral relation for axisymmetric boundary-layer flow. The combined relation is a differential equation for the compressible skin friction which is integrated downstream from the transition location to obtain the local cone skin friction $(C_f)_{FlatPlate} = F_{Cone}(x_{tr}, M_e, T_w/T_e)$.

For the case of fully turbulent flow on the cone and flat plate, transformation parameter $G = 1.17$ where the edge Reynolds number, edge Mach number, and wall temperature ration are the same for the cone and flat plate.

Reshotko and Tucker [206] use the compressible turbulent boundary-layer integral equations for momentum thickness θ and form factor $H = \delta^*/\theta$, which are transformed into incompressible form with the Dorodnitsyn transformation. The compressible shear stress (skin friction) is required in these equations and is determined from the Ludwieg–Tillmann incompressible skin-friction relation which is transformed with the Eckert reference enthalpy method (variables with subscript r). The compressible skin friction is of the form $C_f = 2\tau_w/\rho_e u_e^2 = K_0(\rho_e u_e \theta/\mu_r)^m$ where $m = 0.268$ and K_0 is function of T_e/T_r and the form factor H. For the flat plate, the investigation gives the momentum thickness and skin friction as

$$\theta_{\text{FlatPlate}} = 0.0259 K_T x^{0.823},$$
$$(C_f)_{\text{FlatPlate}} = 0.086 K_f x^{-0.220}.$$

For the cone, the investigation gives the momentum thickness and skin friction as

$$\theta_{\text{Cone}} = 0.0135 K_T x^{0.823}, \quad (C_f)_{\text{Cone}} = 0.102 K_f x^{-0.220},$$

where K_T and K_f are functions of T_e/T_r, T_0/T_e, and $M_e \rho_0 a_0/\mu_0$. The authors obtain for the momentum thickness, skin friction, and heat transfer ratios

$$\theta_{\text{Cone}}/\theta_{\text{FlatPlate}} = 0.521,$$

$$G = (C_f)_{\text{Cone}}/(C_f)_{\text{FlatPlate}} = St_{\text{Cone}}/St_{\text{FlatPlate}} = 1.192,$$

where the boundary-layer edge properties and stagnation conditions on the cone and flat plate are the same.

Bertram and Neal [207] investigated the influence of the location of the virtual origin of the turbulent boundary layer and the relationship of the results obtained on cones to those obtained on flat plates. The theories usually assume the origin of the turbulent boundary layer is at the tip of the cone while most experiments have laminar flow near the tip with transition occurring at x_{tr} from the tip. The authors use the Mangler transformation to transform the cone boundary-layer equations into the flat plate boundary-layer equations. The details of the development of the theory are not presented; only the final results are given in an Appendix.

The authors assume the virtual origin is at the location where the peak shear stress or peak heating occurs. One transformation presented is applied to data obtained on cones to change the results to the values that would be obtained with the flow turbulent from the cone tip. The following Reynolds numbers are defined with the distance on the cone from the virtual origin $x_v = x - x_{\text{tr}}$, the distance on the flat plate from the virtual origin $\xi_v = \xi - \xi_{\text{tr}}$, and the parameter $Re_{ue} = \rho_e u_e/\mu_e$.

$$Re_{xv} = Re_{ue} x_v, \quad Re_{\xi v} = Re_{ue} \xi_v,$$
$$Re_x = Re_{ue} x, \quad R_x^* = Re_{x\text{tr}}/Re_{xv}.$$

The ratio of the local skin friction on a truncated cone (TC) to that on a pointed cone is

$$G^* = (C_f Re_{xv})_{\text{TC}}/(C_f Re_x)_{\text{Cone}}$$
$$= \{1 + R_x^* - R_x^*[R_x^*/(1 + R_x^*)]^{n/(n-1)}\}^{-1/n}.$$

The ratio of the local skin friction on a TC to that on a flat plate is

$$(C_f Re_{xv})_{\text{TC}}/(C_f Re_{\xi v})_{\text{FlatPlate}}$$
$$= [(2n - 1)/(n - 1)]^{1/n} G^*.$$

The authors suggest $n = 4$ for turbulent cone flow.

Tetervin [208] has extended the Mangler transformation to compressible boundary-layer flows. The flat plate incompressible skin friction is obtained from the Ludwieg–Tillmann relation which is modified to compressible flow with the Eckert reference enthalpy method. The compressible wall shear stress becomes

$$2\tau_w/\rho_r u_e^2 = k(Re_\theta)^{-m}, \quad Re_{\theta r} = \rho_r u_e \theta/\mu_r,$$
$$m = 0.268,$$

$$k = 0.246 e^{-1.561 H_i}(\rho_r/\rho_e)^{1-m}(\mu_r/\mu_e)^m.$$

The transformed flat plate compressible skin friction becomes

$$C_f = k(Re_{\theta e})^{-m}, \quad Re_{\theta e} = \rho_e u_e \theta/\mu_e.$$

The ratio of the axisymmetric to flat plate skin friction as given by Tetervin is

$$G = (C_f)_{\text{Cone}}/(C_f)_{\text{FlatPlate}}$$
$$= [(x/\xi)(r_w/L)^{m+1}(Re_\xi/Re_x)]^{m/(m+1)},$$

$$Re_\xi = \rho_e u_e \xi/\mu_e, \quad Re_x = \rho_e u_e x/\mu_e.$$

The Mangler transform of the turbulent boundary-layer equations gives the distance x along the axisymmetric body as a function of the distance ξ

along the flat plate as

$$\xi = \int_0^x (r_w/L)^{m+1}\, dx \quad L = \text{Reference length.}$$

For a cone $(r_w/L) = a(x/L)$ where $a = \sin\theta_c$ and

$$\xi/L = [a^{m+1}/(m+2)](x/L)^{m+2}.$$

The above equation for a cone with $\xi = x$ becomes

$$G = (C_f)_{\text{Cone}}/(C_f)_{\text{FlatPlate}} = (2+m)^{m/(m+1)} = 1.189.$$

If $(C_f)_{\text{Cone}} = (C_f)_{\text{FlatPlate}}$, then the above equation becomes

$$Re_\xi/Re_x = 1/(m+2) = 0.441.$$

White [56,209] has developed the Cone Rule with the Karman momentum–integral equation for axisymmetric, compressible flow $(j = 1)$ which is

$$\frac{d\theta}{dx} + j\frac{\theta}{r_w} = \frac{C_f}{2}.$$

The compressible skin friction is approximated as $C_f = K(Re_\theta)^{-m} = A\theta^{-m}$ where $A = K(\rho_e u_e/\mu_e)^{-m}$. For a flat plate $(j = 0)$ the solution of the integral equation gives the momentum thickness and skin friction as

$$\theta_{\text{FlatPlate}} = [(1+m)A\xi/2]^{1/(1+m)},$$
$$(C_f)_{\text{FlatPlate}} = A[(1+m)A\xi/2]^{-m/(1+m)}.$$

For a cone $(j = 1)$, the solution of the integral equation gives the momentum thickness and skin friction as

$$\theta_{\text{Cone}} = \left[\frac{(1+m)A\xi}{2(2+m)}\right]^{1/(1+m)},$$
$$(C_f)_{\text{Cone}} = A\left[\frac{(1+m)A\xi}{2(2+m)}\right]^{-m/(1+m)}.$$

The G transformation becomes with the cone and flat plate locations the same $(\xi = x)$

$$G = (C_f)_{\text{Cone}}/(C_f)_{\text{FlatPlate}} = (2+m)^{m/(1+m)}.$$

The skin-friction relation becomes, with $m = \frac{1}{4}$, $(C_f)_{\text{Cone}}/(C_f)_{\text{FlatPlate}} = 1.176$ and $(Re_\xi)_{\text{Cone}} = (Re_x)_{\text{FlatPlate}}$. If $(C_f)_{\text{Cone}} = (C_f)_{\text{FlatPlate}}$, then $\xi = (2+m)x$ and $(Re_\xi)_{\text{Cone}} = (2+m)(Re_x)_{\text{FlatPlate}}$. The constant K in the skin-friction relation has been determined by Young [210] for incompressible flow and is given on page 158 in his book. In the development of the above relation, it is assumed that the turbulent boundary layer begins at the tip of the cone and the leading edge of the flat plate.

Zoby et al. [211] have determined the power law velocity profile exponent as a function of the momentum thickness Reynolds number.

$$u/u_e = (y/\delta)^{1/n}, \quad n = 12.67 - 6.6\log(Re_\theta) + 1.21[\log(Re_\theta)]^2.$$

The skin-friction relation parameter is obtained from $m = 2/(n+1)$.

Seiler et al. [212] have used the Hantzsche and Wendt transformations to first transform the compressible boundary-layer equations on a cone (in spherical coordinates) to a new set of cone transformed governing equations. The compressible boundary-layer equations on a flat plate are transformed to a new set of flat plate transformed governing equations. The transformed governing equations for the cone and the flat plate are of the same form. This approach needs further development to determine the Mangler transformation parameter G.

Zoby et al. [57,58,211]: In a NASA Technical Note Zoby and Sullivan predicted the heating rate (Stanton number) on axisymmetric sharp cones at zero angle of attack and compared the results to six supersonic flight experiments. The flat plate heat rate is obtained from the Colburn form of Reynolds analogy, which is expressed as

$$St_e = \tfrac{1}{2}C_{fe}Pr^{-2/3}, \quad Pr = 0.71.$$

The incompressible skin-friction for a flat plate is obtained from the Blasius or Schultz–Grunow relations, which are of the form $(C_{fe})_{\text{FlatPlate}} = $ function of the surface distance Reynolds number $(Re_x)_{\text{FlatPlate}}$. The incompressible Reynolds number is modified for compressible flow with the Eckert reference-enthalpy method. The cone inviscid flow conditions at the edge of the boundary layer are obtained from the Sims tables. The cone Reynolds number $(Re_x)_{\text{Cone}}$ is related to the flat plate Reynolds number by the Van Driest relation $(Re_x)_{\text{Cone}} = 2(Re_x)_{\text{FlatPlate}}$. The calculated heat rates differ from the experimental heat rates by approximately 20% or less. In a synoptic journal article, Zoby and Graves [58] compared a larger experimental turbulent heating database including wind tunnel and flight experiments (no references for database) with prediction using the transformation to an incompressible plane approach as investigated by Peterson [105].

The compressible cone skin friction is transformed to compressible skin friction on a flat plate

with the relations

$$(C_{fC})_{\text{Cone}} = G(C_{fC})_{\text{FlatPlate}}, \quad (Re)_{\text{Cone}} = (Re)_{\text{FlatPlate}},$$

where the Reynolds number is held constant. The geometric parameter G has been given by White's cone rule (p. 561) to have a value between 1.087 and 1.176. Zoby et al. [211] have shown that G is a function of the momentum thickness Reynolds number, $G = 1.201$ at $Re_\theta = 10^4$ and $G = 1.123$ at $Re_\theta = 10^5$.

From the Colburn Reynolds analogy given above for the compressible flow, the geometric transformation for the Stanton number is $(St_{\text{ec}})_{\text{Cone}} = G(St_{\text{ec}})_{\text{FlatPlate}}$. Since no value of G is specified in this article, it is assumed that $G = 1$. The compressible flat plate Stanton number and Reynolds number are transformed to incompressible flat plate values with the relations

$$St_{\text{ei}} = F_c St_{\text{ec}}, \quad Re_{Li} = F_L Re_{Lc}, \quad L = x \text{ or } \theta.$$

The length scale in the Reynolds number is the distance along the surface x in this article. The prediction of the incompressible Stanton number as a function of incompressible Reynolds number is obtained from the Colburn Reynolds analogy given above where the incompressible skin friction is obtained from one of three relation investigated. With the Van Driest II transformation, Van Driest skin-friction relation, and with all of the experimental database used, the rms error of the transformed experimental data relative to the incompressible prediction is between 17.7% and 23%, depending on surface distance used in the Reynolds number.

In the paper by Zoby et al. [211], the skin friction is evaluated from $C_{\text{f}}/2 = C_1(Re_\theta)^{-m}$.

Hopkins et al. [86,139]: The investigation of Hopkins and coworkers on the correlation of skin friction and heat transfer for zero-pressure gradient flows at hypersonic Mach numbers uses mainly flat plate data but includes cones and hollow cylinder flows. This work has already been discussed in the flat plate case. The initial work was documented in a NASA technical note [86] and the complete investigation in a journal article [139]. The cone database is from the experiments of Mateer (see cone experimental database). The correlation of heat transfer as a function of wall temperature ratio for Mach 4.9–7.4 includes all three geometries and shows no influence of geometries on the correlation. There is no indication that the cone data has been transformed to flat plate data

(geometry transformation is discussed above in the Zoby et al. section). This investigation does not resolve the appropriate geometry transformation for cones and the Reynolds analogy factor for cones and flat plates.

Holden [48] has correlated his experimental heat transfer data into incompressible form where the experimental Stanton number St^* is plotted as a function of the transformed Reynolds number Re_x^*. The best documentation of this work is given in Holden [44]. Holden uses the Bertram and Neal cone to flat plate transformation to transform the experimental data to incompressible flat plate Stanton number. It appears that the Reynolds analogy factor has been set to one. In the Bertram and Neal transformation theory the virtual origin of the turbulent boundary layer must be specified and no information is given on this issue. The experimental data is correlated into reasonable agreement with the incompressible curve, but there is significant scatter of the data about the curve.

Appendix D. Perfect gas air model and molecular transport properties for hypersonic flows

Air is a multi-component gas mixture of nitrogen, oxygen and other components. The US Standard Atmosphere [213] has the following properties at sea level:

$$p_0 = 101325.0 \,\text{N/m}^2, \quad T_0 = 288.15 \,\text{K},$$
$$\rho_0 = 1.2250 \,\text{kg/m}^3. \tag{D.1}$$

The properties of a gas mixture can be written in terms of the mass fraction $c_s = \rho_s/\rho$ of the various species. The molecular weight of the mixture is then obtained from

$$M_{\text{w}} = 1 \bigg/ \left(\sum_{s=1}^{N_s} c_s/M_s \right) = 28.9644 \,\text{kg/(kg mol)}. \tag{D.2}$$

The gas constant is determined from the relation

$$R = R_{\text{u}}/M_{\text{w}} = 287.0583 \frac{\text{J}}{\text{kg K}},$$
$$R_{\text{u}} = 8314.472 \frac{\text{J}}{\text{kgmol K}}. \tag{D.3}$$

The molecular weight and gas constant of air at sea level are given in Eqs. (D.2) and (D.3)

In NACA Report 1135 [214], several terms are used to define types of perfect gases where there is *no chemically activity*. For a *thermally perfect gas*,

the equation of state is given as

$$p = \rho R T = (\gamma - 1)\rho e, \quad \gamma = c_p/c_v. \quad \text{(D.4)}$$

At sufficiently low gas temperatures, where there is *no significant vibrational excitation*, the internal energy of a mixture of diatomic molecules, which is *air without the trace species included*, becomes

$$e = \frac{5}{2}RT = c_v T, \quad c_v = \frac{5}{2}R. \quad \text{(D.5)}$$

The specific heat at constant pressure c_p and the specific heat at constant volume c_v are constant and become for air without the trace species

$$c_v = \frac{R}{(\gamma - 1)} = \frac{5}{2}R = 717.646\frac{J}{kg\,K},$$
$$c_p = \frac{\gamma R}{(\gamma - 1)} = \frac{7}{2}R = 1004.704\frac{J}{kg\,K}, \quad \text{(D.6)}$$

where

$$\gamma = \frac{7}{5}. \quad \text{(D.7)}$$

A *calorically perfect gas* is defined as a gas with constant specific heats. For a *perfect gas model* the specific heats of the gas are constant and the equation of state is given by Eq. (D.4). A *perfect gas model* is a thermally and calorically perfect gas.

At standard temperatures, Sutherland's law can be used for the absolute molecular viscosity of air, and is given by

$$\mu = 1.458 \times 10^{-6} T^{3/2}/(T + 110.4)$$
$$\text{units are kg/m/s}, \quad \text{(D.8)}$$

where T is given in Kelvin. For air at lower temperatures (say below $100\,K$) and for nitrogen, Keyes model [215] for viscosity should be used

$$\mu = a_0 \times 10^{-6}\sqrt{T}/(1 + a_1 T_1/T), \quad T_1 = 10^{-a_2/T}.$$

Air: $a_0 = 1.488, \quad a_1 = 122.1, \quad a_2 = 5.0.$

Nitrogen: $a_0 = 1.418, \quad a_1 = 116.4, \quad a_2 = 5.0. \quad \text{(D.9)}$

For a perfect gas, the thermal conductivity can then be determined from the Prandtl number and the specific heat at constant pressure from $c_p = \gamma R/(\gamma - 1)$ where for air

$$R = 287.0583\frac{J}{kg\,K} \quad \text{(D.10)}$$

and $\gamma = 1.4$. For diatomic nitrogen with molecular weight 28.01344 and $\gamma = 1.4$, the specific gas constant R and the specific heats can be determined from the preceding equations.

References

[1] Settles GS, Dodson LJ. Hypersonic shock/boundary-layer interaction database. NASA CR 177577; 1991.

[2] Settles GS, Dodson LJ. Hypersonic turbulent boundary-layer and free-shear layer database. NASA CR177610; 1993.

[3] Settles GS, Dodson LJ. Hypersonic shock/boundary-layer interaction database: new and corrected data. NASA CR 177638; 1994.

[4] Settles GS, Dodson LJ. Supersonic and hypersonic shock/boundary-layer interaction data-base. AIAA J 1994;32(7):1377–83.

[5] Marvin JG, Huang GP. Turbulence modeling—progress and future outlook. In: Hafez M, Oshima K, editors. Computational fluid dynamics review 1998, vol. II. Singapore: World Scientific; 1998. p. 891–906, see also keynote lecture, 15th international conference on numerical methods in fluid dynamics, Monterey, CA, June 1996.

[6] Wilcox DC. Turbulence modeling for CFD, 2nd ed. La Canada, CA: DCW Industries, Inc.; 1998.

[7] Coakley TJ, Horstman CC, Marvin JG, Viegas JR, Bardina JE, Huang PG, Kussoy MI. Turbulence compressibility corrections. NASA Technical Memorandum 108827; May 1994.

[8] Aupoix B, Viala S. Compressible turbulent boundary layer modeling. In: FED-vol. 224, Transitional and turbulent compressible flows. ASME; 1995.

[9] Horstman CC. Prediction of hypersonic shock-wave/turbulent-boundary-layer interaction flows. AIAA paper 87-1367; 1987.

[10] Horstman CC. Hypersonic shock-wave/turbulent-boundary-layer interaction flows. AIAA J 1992;30(6):1480–1.

[11] Coakley TJ, Huang PG. Turbulence modeling for high speed flows. AIAA paper 92-0436; 1992.

[12] Huang PG, Coakley TJ. Turbulence modeling for complex hypersonic flows. AIAA paper 93-0200; 1993.

[13] Bardina JE, Huang PG, Coakley TJ. Turbulence modeling validation, testing, and development. NASA TM-110446; April 1997.

[14] Bardina JE, Huang PG, Coakley TJ. Turbulence modeling validation. AIAA paper 97-2121; 1997.

[15] Marvin JG. Perspective on computational fluid dynamics validation. AIAA J 1995;33(10):1778–87.

[16] Roy CJ, Blottner FG. Methodology for turbulence model validation: application to hypersonic flows. J Spacecr Rockets 2003;40(3):313–25.

[17] Moore JG, Moore J. Realizeability in two-equation turbulence models. AIAA paper 99-3779; 1999.

[18] Roache PJ. Verification and validation in computational science and engineering. New Mexico: Hermosa Publishers; 1998.

[19] Knupp P, Salari K. In: Rosen KG, editor. Verification of computer codes in computational science and engineering. Boca Raton, FL: Chapman & Hall/CRC; 2003.

[20] Roy CJ, Nelson CC, Smith TM, Ober CC. Verification of Euler/Navier–Stokes codes using the method of manufactured solutions. Int J Num Meth Fluids 2004;44(6):599–620.

[21] Roy CJ. Review of code and solution verification procedures for computational simulation. J Comp Phys 2005;205(1):131–56.

[22] Roache PJ. Perspective: a method for uniform reporting of grid refinement studies. ASME J Fluids Eng 1994;116(3): 405–13.

[23] Carpenter MH, Casper JH. Accuracy of shock capturing in two spatial dimensions. AIAA J 1999;37(9):1072–9.

[24] Roy CJ. Grid convergence error analysis for mixed-order numerical schemes. AIAA J 2003;41(4):595–604.

[25] Cebeci T, Bradshaw P. Uncoupled turbulent boundary layers. In: Physical and computational aspects of convective heat transfer. New York: Springer; 1984, p. 173 [chapter 6].

[26] Craft TJ, Launder BE, Suga K. Prediction of turbulent transitional phenomena with a non-linear eddy-viscosity model. Int J Heat Fluid Flow 1997;18(1):15–28.

[27] Oberkampf WL, Aeschliman DP. Joint computational/experimental aerodynamics research on a hypersonic vehicle, part 1: experimental results. AIAA J 1995;9(3): 432–7.

[28] Fernholz HH, Finley PJ. A critical compilation of compressible turbulent boundary layer data. AGARDograph no. 223; 1977.

[29] Fernholz HH, Finley PJ. A critical commentary on mean flow data for two-dimensional compressible turbulent boundary layers. AGARDograph no. 253; May 1980.

[30] Fernholz HH, Finley PJ. A further compilation of compressible boundary layer data with a survey of turbulence data. AGARDograph no. 263; November 1981.

[31] Coleman GT, Stollery JL. Heat transfer from hypersonic turbulent flow at a wedge compression corner. J Fluid Mech 1972;56:741–52.

[32] Kussoy MI, Horstman CC. Documentation of two- and three dimensional hypersonic shock wave/turbulent boundary layer interaction flows. NASA TM 101075; January 1989.

[33] Holden MS, Havener AG, Lee CH. Shock wave/turbulent boundary layer interaction in high-Reynolds number hypersonic flows. Calspan-University of Buffalo Research Center, CU-BRC-86681, Buffalo, NY; 1986.

[34] Holden MS. Experimental studies of quasi-two-dimensional and three-dimensional viscous interaction regions induced by skewed-shock and swept-shock boundary layer interactions, AIAA paper 1984-1677; 1984.

[35] Kussoy MI, Horstman CC. An experimental documentation of a hypersonic shock-wave turbulent boundary layer interaction flow—with and without separation. NASA TM X-62412; February 1975.

[36] Kussoy MI, Horstman CC. Intersecting shock-wave/turbulent boundary-layer interactions at Mach 8.3. NASA TM 103909; February 1992.

[37] Law CH. 3D shock wave-turbulent boundary layer interactions at Mach 6. Aeronautical Research Laboratory, ARL TR 75-0191; 1975.

[38] Kussoy MI, Horstman CC. Documentation of two- and three dimensional shock wave/turbulent boundary layer interaction flows at Mach 8.2. NASA TM 103838; May 1991.

[39] Kussoy MI, Horstman CC. Three-dimensional shock-wave/turbulent boundary-layer interaction. AIAA J 1993; 31(1):8–9.

[40] Rodi PE, Dolling DS. An experimental/computational study of sharp fin induced shock wave/turbulent boundary layer interactions at Mach 5. AIAA paper 92-0749; 1992.

[41] ERCOFTAC Online Database: 〈http://ercoftac.mech.surrey.ac.uk/〉, last accessed 26 November 2006.

[42] Holden MS, Moselle JR. A database of aerothermal measurements in hypersonic flow for CFD validation. AIAA paper 1992-4023; 1992.

[43] Holden MS. Experimental studies of the effects of asymmetric transition on the aerothermal characteristics of hypersonic blunted slender cones. AIAA paper 1985-0325; 1985.

[44] Holden MS. Studies of the mean and unsteady structure of turbulent boundary layer separation in hypersonic flow. AIAA paper 1991-1778; 1991.

[45] Holden MS. An experimental investigation of turbulent boundary layers at high Mach number a Reynolds numbers. Calspan Report no. AB-5072-A-1, see also NASA CR-112147; 1972.

[46] Holden MS. A database of aerothermal measurements in hypersonic flows in "building block" experiments for CFD validation. AIAA paper 2003-1137; 2003.

[47] Holden MS. Shock wave-turbulent boundary layer interaction in hypersonic flow. AIAA paper 1972-0074; 1972.

[48] Holden MS. Shock wave-turbulent boundary layer interaction in hypersonic flow. AIAA paper 1977-0045; 1977.

[49] Hornung HG. 28th Lanchester memorial lecture- experimental real-gas hypersonics. Aeronaut J 1988;12(5–6): 379–89.

[50] Groenig H, Olivier H. Experimental hypersonic flow research in Europe. JSME Int J Ser B 1998;41(2):397–407.

[51] Van Driest ER. Problem of aerodynamic heating. Aeronaut Eng Rev 1956;15:26–41.

[52] Squire LC. The accuracy of flat plate, turbulent skin friction at supersonic speeds. Aeronaut J 2000;104(1036): 257–63.

[53] Cary AM, Bertram MH. Engineering prediction of turbulence skin friction and heat transfer in high-speed flow. NASA TN D-7507; July 1974.

[54] Huang PG, Bradshaw P, Coakley TJ. Skin friction and velocity profile family for compressible turbulent boundary layers. AIAA J 1993;31(9):1600–4.

[55] Van Driest ER. Turbulent boundary layer on a cone in a supersonic flow at zero angle of attack. J Aeronaut Sci 1952;19:55–7.

[56] White FM. Viscous fluid flow. New York: McGraw-Hill; 1974.

[57] Zoby EV, Sullivan EM. Correlation of free-flight turbulent heat-transfer data from axisymmetric bodies with compressible flat-plate relations. NASA TN D-3802; 1967.

[58] Zoby EV, Graves RA. Comparison of turbulent prediction methods with ground and flight test heating data. AIAA J 1977;15:901–2.

[59] Roy CJ, Blottner FG. Further assessment of one- and two-equation turbulence models for hypersonic transitional flows. AIAA paper 2001-0210; 2001.

[60] Martin MP. Preliminary DNS database of hypersonic turbulent boundary layers. AIAA paper 2003-3726; 2003.

[61] Yan H, Knight D, Zheltovodov AA. Large eddy simulation of supersonic flat plate boundary layer using MILES technique. J Fluids Eng 2002;124(4):868–75;
see also Yan H, Knight D, Zheltovodov AA. Large eddy simulation of supersonic flat plate boundary layer part I. AIAA paper 2002-0132; 2002.

[62] Pruett CD, Chang C-L. Spatial direct numerical simulation of high-speed boundary-layer flows part II: transition on a cone in Mach 8 flow. Theor Comput Fluid Dyn 1995;7: 397–424.

[63] Stetson KF, Thompson ER, Donaldson JC, Siler LG. Laminar boundary layer stability experiments on a cone at Mach 8, part 1: sharp cone. AIAA paper 83-1761; 1983.

[64] Pruett CD. Direct numerical simulation of hypersonic boundary-layer flow on a flared cone. Theor Comput Fluid Dyn 1998;11:49–67.

[65] Lachowicz JT, Chokani N, Wilkinson SP. Hypersonic boundary-layer stability over a flared cone in a quiet tunnel. AIAA paper 96-0782; 1996.

[66] Coleman GT. Hypersonic turbulent boundary layer studies. PhD thesis. Department of Aeronautics, University of London, London; 1973.

[67] Elfstrom GM. Turbulent hypersonic flow at a wedge-compression corner. J Fluid Mech 1972;53(1):113–27.

[68] Babinsky H, Edwards JA. On the incipient separation of a turbulent hypersonic boundary layer. Aeronaut J 1996; 100(996):209–14.

[69] Babinsky H. A study of roughness in turbulent hypersonic boundary-layers, PhD thesis. Cranfield University, College of Aeronautics; December 1993.

[70] Marvin JG, Horstman CC, Rubesin MW, Coakley TJ, Kussoy MI. An experimental and numerical investigation of shock-wave induced turbulent boundary-layer separational hypersonic speeds. AGARDograph-CPP-168; May 1975.

[71] Mikulla V, Horstman CC. Turbulence measurements in hypersonic shock-wave boundary-layer interaction flows. AIAA J 1976;14(5):568–75.

[72] Hillier R, Kirk D, Soltani S. Navier–Stokes computations of hypersonic flows. Int J Numer Meth Heat Fluid Flow 1995;5(3):195–211.

[73] Hillier R, Boyce RR, Creighton SA, Fiala A, Jackson AP, Mallinson SG, et al. Development of some hypersonic benchmark flows using CFD and experiment. Shock Waves 2003;13:375–84.

[74] Murray N, Hillier R. Hypersonic shock wave/turbulent boundary layer interactions in a three-dimensional flow. AIAA Paper 2006-0121; 2006.

[75] Murray N, Hillier R. Separated shock wave/turbulent boundary layer interactions at hypersonic speeds. AIAA Paper 2006-3038; 2006.

[76] Schulein E, Krogmann P, Stanewsky E. Documentation of two-dimensional impinging shock/turbulent boundary layer interaction flow. DLR Report IB 223-96 A 49, Gottingen, Germany; October 1996.

[77] Schulein E. Skin-friction and heat flux measurements in shock/boundary-layer interaction flows. AIAA J 2006; 44(8):1732–41 [See also AIAA Paper 2004–2115; 2004].

[78] Schulein E. Personal communications; May 23, 2006 and October 30; 2006.

[79] Hopkins JE, Keener ER. Studies of surface pitots for measuring turbulent skin friction at supersonic Mach numbers. NASA TN D-3478; 1966.

[80] Hopkins EJ, Keener ER. Pressure-gradient effects on hypersonic turbulent skin-friction and boundary-layer profiles. AIAA J 1972;10:1141–2.

[81] Keener ER, Hopkins EJ. Turbulent boundary layer velocity profiles on a non-adiabatic flat plate at Mach 6.5. NASA TN D-6907; 1972.

[82] Owen FK, Horstman CC. On the structure of hypersonic turbulent boundary layers. J Fluid Mech 1972;53:611–36.

[83] Horstman CC, Owen FK. Turbulent properties of a compressible boundary layer. AIAA J 1972;10:1418–24.

[84] Owen FK, Horstman CC, Kussoy MI. Mean and fluctuating flow measurements on a fully-developed non-adiabatic hypersonic boundary layer. J Fluid Mech 1975;70(2): 393–413.

[85] Coleman GT, Elfstrom GM, Stollery SL. Turbulent boundary layers at supersonic and hypersonic speeds. AGARD-CP-93, January 1972.

[86] Hopkins JE, Rubesin MW, Inouye M, Keener ER, Mateer GG, Polek TE. Summary and correlation of skin-friction and heat-transfer data for a hypersonic turbulent boundary layer on simple shapes. NASA TN D-5089; 1969 [See also hypersonic turbulent skin-friction and boundary-layer profiles on nonadiabatic flat plates. AIAA J 1972;10:40–8].

[87] Hopkins JE, Keener ER, Louie PT. Direct measurements of turbulent skin friction on a non-adiabatic flat plate at Mach number 6.5 and comparisons with eight theories. NASA TN D-5675; 1969.

[88] Holden MS. Turbulent boundary-layer development on curved compression surfaces. Calspan report no. 7724-1, 1992.

[89] Kimmel RL. Experimental transition zone lengths in pressure gradient in hypersonic flow. In: Kral LD, Zang TA, editors. Transitional and turbulent compressible flows 1993, FED-vol. 151. New York: ASME; 1993. p. 117–27.

[90] Kimmel RL. The effects of pressure gradients on transition zone length in hypersonic boundary layers. J Fluids Eng 1997;119(1):36–41.

[91] Rumsey CB, Lee DB. Measurements of aerodynamic heat transfer and boundary-layer transition on a 15 degree cone in free flight at supersonic Mach numbers up to 5.2. NASA Technical Note D-888; August 1961.

[92] Merlet CF, Rumsey CB. Supersonic free-flight measurement of heat transfer and transition on a 10 degree cone having a low temperature ratio. NASA Technical Note D-951; August 1961.

[93] Chien K-Y. Hypersonic, turbulent skin-friction and heat-transfer measurements on a sharp cone. AIAA J 1974; 12(11):1522–6.

[94] Desideri J-A, Glowinski R, Periaux J, editors. Hypersonic flows for reentry problems, vols. I and II. Berlin: Springer; 1991.

[95] Deman PA, Harvey JK, Hillier R. Hypersonic boundary layer base and flow workshop test problem 1 and 2. In: Desideri J-A, Glowinski R, Periaux J, editors. Hypersonic flows for reentry problems, vols. I and II. Berlin: Springer; 1991. p. 43–56.

[96] Mallinson SG, Hillier R, Jackson AP, Kirk DC, Soltani S, Zanchetta M. Gun tunnel flow calibration: defining input conditions for hypersonic flow computations. Shock Waves 2000;10:313–22.

[97] Dinavahi SPG. Comparison of two transition models. In: Hussaini MY, Voigt RG, editors. Instability and transition, vol. II. Berlin: Springer; 1989. p. 453–62.

[98] Holden MS, Bower D, Chadwick K. Measurements of boundary-layer transition on cones at angle of attack for Mach numbers from 11 to 13. AIAA Paper 95-2294; 1995.

[99] Van Driest ER. On turbulent flow near a wall. J Aeronaut Sci 1956;23(1036):1007–11.

[100] Holden MS, Bergman RC, Harvey J, Duryea GR, Moselle JR. Studies of the structure of attached and separated regions of viscous/inviscid interaction and the effects of combined surface roughness and blowing in high Reynolds number hypersonic flows. AFOSR-89-0033TR; 1988.

[101] Holden MS. Experimental database from CUBRC studies in hypersonic laminar and turbulent interacting flows including flowfield chemistry, Prepared for RTO code validation of DSMC and Navier–Stokes code validation studies, Calspan-University at Buffalo Research Center, Buffalo, NY; June 2000. p. 105–14.

[102] Holden M. Personal communication; April 11, 2006.

[103] Murray N. Personal communication; December 4, 2006.

[104] Sommer SC, Short BJ. Free-flight measurements of turbulent boundary-layer skin friction in the presence of severe aerodynamic heating at Mach numbers from 2.8 to 7.0. NACA TN 3391; 1955, see also J Aeronaut Sci 1956;23(6):536–42.

[105] Peterson JB. A comparison of experimental and theoretical results for the compressible turbulent-boundary-layer skin friction with zero pressure gradient. NASA Technical Note D-1795; March 1963.

[106] Korkegi RH. Transition studies and skin-friction measurements on an insulated flat plate at a Mach number of 5.8. J Aeronaut Sci 1956;23(2):97–107.

[107] Hill FK. Boundary-layer measurements in hypersonic flow. J Aeronaut Sci 1956;23:35–42.

[108] Hill FK. Turbulent boundary layer measurements at Mach number 8 to 10. Phys Fluids 1959;2:668–80.

[109] Tendeland T. Effects of Mach number and wall-temperature ratio on turbulent heat transfer at Mach numbers from 3 to 5. NACA TN 4236; April 1958, also NACA TR R-16, 1959.

[110] Spalding DB, Chi SW. The drag of compressible turbulent boundary layer on a smooth flat plate with and without heat transfer. J Fluid Mech 1964;18:117–43.

[111] Brevoort MJ, Arabian DB. Summary of experimental heat-transfer measurements in turbulent flow for a Mach number range 0.87 to 5.05. NACA TN 4248; May 1958.

[112] Winkler EM, Cha MH. Investigation of flat plate hypersonic turbulent boundary layers with heat transfer at a Mach number of 5.2. NOL NAVORD Report 6631; 1959, see also Trans ASME, Ser E 1961;83:323–9.

[113] Matting FW, Chapman DR, Nyholm JR, Thomas AG. Turbulent skin friction at high Mach numbers and Reynolds numbers in air and helium. NACA TN-4236; April 1958, also NASA TR R-82, 1961.

[114] Moore DR. Velocity similarity in the compressible turbulent boundary layer with heat transfer. DRL 1962;480.

[115] Young FL. Experimental investigation of the effects of surface roughness on compressible turbulent boundary layer skin friction and heat transfer. Defense Research Lab., University of Texas, Austin, Texas, Report DRL-480; 1962.

[116] Wallace JE, McLaughlin EJ. Experimental investigation of hypersonic turbulent flow and laminar leeward-side flow on flat plates. Cornell Aeronautical Lab., Buffalo, NY, Technical Report AFFDL-TR-66-63, vol. 1; July 1966.

[117] Wallace JE. Hypersonic turbulent boundary layer studies at cold wall conditions. In: Libby PA, Olfe DB, Van Atta CW, editors. Proceedings of the 1967 Heat Transfer and Fluid Mechanics Institute. Stanford University Press; 1967. p. 427–51.

[118] Heronimus GA. Hypersonic shock tunnel experiments on the W7 flat plate model—expansion side, turbulent flow and leading edge transpiration data. CAL Report no. AA-1952-Y-2 (Contract no. AF 33 (615)-1847), Cornell Aeronautical Lab; February 1966.

[119] Cary AM. Summary of available information on Reynolds analogy for zero-pressure-gradient, compressible, turbulent-boundary-layer flow. NASA TN D-5560; January 1970.

[120] Neal L. A study of the pressure, heat transfer, and skin friction on sharp and blunt flat plates at Mach number 6.8. NASA TN D-3312; 1966.

[121] Cary AM, Morrisette EL. Effect of two-dimensional multiple sine-wave protrusions on the pressure and heat-transfer distribution for a flat plate at Mach 6. NASA TN D-4437; 1968.

[122] Hopkins EJ, Keener ER, Polek TE, Dwyer HA. Hypersonic turbulent skin-friction and boundary-layer profiles on nonadiabatic flat plates. AIAA J 1972;10(1):40–8.

[123] Cary AM. Turbulent boundary layer heat-transfer and transition measurements with surface cooling at Mach 6. NASA TN D-5863; June 1970.

[124] Weinstein LM. Effects of two-dimensional sinusoidal waves on heat transfer and pressure over a plate at Mach 8.0. NASA TN D-5937; August 1970.

[125] Watson RD, Harris JE, Andeps JB. Measurements in a transitional/turbulent Mach 10 boundary layer at high Reynolds numbers. AIAA paper 73-165; 1973.

[126] Watson RD. Characteristics of Mach 10 transitional and turbulent boundary layers. NASA TP-1243; November 1, 1978, see also Wall cooling effects on hypersonic transitional/turbulent boundary layers at high Reynolds numbers. AIAA J 1977;15(10):1455–61.

[127] Laderman AJ, Demetriades A. Mean and fluctuating flow measurements in the hypersonic boundary layer over a cooled wall. J Fluid Mech 1974;63:121–44, see also Investigation of the structure of a cooled wall turbulent supersonic boundary layer. Aeronautics Publication no. U-6370.

[128] Equations, tables, and charts for compressible flow. NACA Report 1135; 1953.

[129] Stainback PC, Fischer MC, Wagner RD. Effects of wind-tunnel disturbances on hypersonic boundary transition. AIAA paper 72-181; 1972.

[130] Lawrence SL. Hypersonic cone flow predictions using an implicit upwind space-marching code, In: Desideri et al., editors [94] pp. 75–91.

[131] Hillier R, Kirk DC, Sell M, Soltani S. Studies of hypersonic viscous flows. In: AGARD Conference Proceedings, vol. 514, Theoretical and experimental methods in hypersonic flows. May 4–8; 1992.

[132] Abgrall R, Desideri JA, Mallet M, Periaux J, Perrier P, Stoufflet B. The European hyper- sonic data base: a new CFD validation tool for the design of space vehicles. AIAA paper 93-3045, July 1993.

[133] Van Driest ER. Turbulent boundary layer in compressible fluids. J Aeronaut Sci 1951;18:145–60.

[134] Van Driest ER. The turbulent boundary layer with variable Prandtl number. In: Gortler H, Tollmien W, editors. 50 jahre grenzschichtforschung. Braunschweig: Friedr. Vieweg & Sohn; 1955.

[135] Coles D. Measurements in the boundary layer on a smooth flat plate boundary-layer at jet propulsion laboratory. Jet Propulsion Lab., California Institute of Technology, Pasadena, CA, Report 20-71; 1953, see also J Aeronaut Sci 1955;21(7):433–48.

[136] Chapman DR, Kester RH. Measurements of turbulent skin friction on cylinders in axial flow at subsonic and supersonic velocities. J Aeronaut Sci 1953;20:441–8.

[137] Wilson RE. Turbulent boundary-layer characteristics at supersonic speeds—theory and experiments. J Aeronaut Sci 1950;17:585–94.

[138] Chi SW, Spalding DB. Influence of temperature ratio on heat transfer to a flat plate through a turbulent boundary layer in air. Proceedings of the third heat transfer conference. Chicago, IL, August 1966.

[139] Hopkins EJ, Inouye M. An evaluation of theories for predicting turbulent skin friction and heat transfer on flat plates at supersonic and hypersonic Mach numbers. AIAA J 1971;9(6):993–1003.

[140] Keener ER, Polek TE. Measurements of Reynolds analogy for a hypersonic turbulent boundary layer on a nonadiabatic flat plate. AIAA J 1972;10(6):845–6.

[141] Holden MS. An experimental investigation of turbulent boundary layer at high Mach number and Reynolds numbers. NASA CR-112147; November 1972.

[142] Sims JL. Tables for supersonic flow around right circular cones. NASA SP-3004; January 1964.

[143] Mateer GG, Larson HK. Unusual boundary-layer transition results on cones in hypersonic flow. AIAA J 1969;7(4):660–6.

[144] Mateer GG. Effects of wall cooling and angle of attack on boundary-layer transition on sharp cones at Mach = 7.4. NASA Technical Note D-6908; August 1972.

[145] Mateer GG. The effect of angle of attack on boundary-layer transition on cones. AIAA J 1972;10(8):1127–8.

[146] McKeel SA, Walters RW, Chadwick KM. Investigation into transition modeling. AIAA paper 95-1746; June 1995.

[147] Spalart PR, Allmaras SR. A one-equation turbulence model for aerodynamic flows. AIAA Paper 92-0439; 1992.

[148] Spalart PR, Allmaras SR. A one-equation turbulence model for aerodynamic flows. La Rech Aerosp 1994;1:5–21.

[149] Goldberg U. Hypersonic flow heat transfer prediction using single equation turbulence models. ASME J Heat Transfer 2001;123:65–9.

[150] Goldberg U, Batten P, Palaniswamy S, Chakravarthy S, Peroomian O. Hypersonic flow predictions using linear and nonlinear turbulence closures. J Aircr 2000;37(4):671–5.

[151] Menter FR. Eddy viscosity transport equations and their relation to the $k-\varepsilon$ model. J Fluids Eng 1997;119(4):876–84.

[152] Jones WL, Launder BE. The prediction of laminarization with a two-equation model of turbulence. Int J Heat Mass Transfer 1972;15:301–14.

[153] Launder BE, Sharma BI. Application of the energy dissipation model of turbulence to the calculation of flow near a spinning disk. Lett Heat Mass Transfer 1974;1(2):131–8.

[154] Chien JY. Predictions of channel boundary-layer flows with a low-Reynolds-number turbulence model. AIAA J 1982;20(1):33–8.

[155] Nagano Y, Hishida M. Improved form of the $k-\varepsilon$ model for wall turbulent shear flows. J Fluids Eng 1987;109:156–60.

[156] Rodi W. Experience with two-layer models combining the $k-\varepsilon$ model with a one-equation model near the wall. AIAA paper 1991-0216; 1991.

[157] So RM, Zhang HS, Speziale CG. Near-wall modeling of the dissipation rate equation. AIAA J 1991;29(12):2069–76.

[158] Zhang HS, So RMC, Speziale CG, Lai YG. Near wall two-equation model for compressible turbulent flows. AIAA J 1993;31:196–9.

[159] Wilcox DC. Turbulence modeling for CFD, 1st ed. La Canada, CA: DCW Industries Inc.; 1988.

[160] Menter FR. Two-equation eddy-viscosity turbulence models for engineering applications. AIAA J 1994;32(8):1598–605.

[161] Smith BR. Prediction of hypersonic shock-wave/turbulent boundary-layer interactions. J Spacecr Rockets 1996;33(5):614–9 (see also AIAA Paper 95-0232; 1995).

[162] Smith BR. A near wall model for the $k-l$ two equation turbulence model. AIAA paper 1994-2386; 1994.

[163] Robinson DF, Harris JE, Hassan HA. Unified turbulence closure model for axisymmetric and planar free shear flows. AIAA J 1995;33(12):2324–31.

[164] Robinson DF, Hassan HA. Further development of the $k-\zeta$ (enstrophy) turbulence closure model. AIAA J 1998;36(10):1825–33.

[165] Coakley TJ. Turbulence modeling methods for the compressible Navier–Stokes equations. AIAA paper 1983-1693; 1983.

[166] Roy CJ, Blottner FG. Further assessment of one- and two-equation turbulence models for hypersonic transitional flows. AIAA paper 2001-0210; 2001.

[167] Smith BR. The $k-kl$ turbulence model and wall layer model for compressible flows. AIAA paper 90-1483; 1990.

[168] McDaniel RD, Hassan HA. Study of transition in a high disturbance environment. J Aircr 2001;38(6):1051–5.

[169] Craft TJ, Launder BE, Suga K. Prediction of turbulent transitional phenomena with a non-linear eddy-viscosity model. Int J Heat Fluid Flow 1997;18(1):15–28.

[170] Horstman CC. Hypersonic shock-wave/turbulent-boundary-layer interaction flows. AIAA paper 1991-1760; 1991.

[171] Coratekin T, van Keuk J, Ballmann J. Performance of upwind schemes and turbulence models in hypersonic flows. AIAA J 2004;42(5):945–57.

[172] Nance RP, Hassan HA. Turbulence modeling of shock-dominated flows with a $k-\zeta$ formulation. AIAA paper 99-0153; 1999.

[173] Xiao X, Edwards JR, Hassan HA, Gaffney RL. Role of turbulent Prandtl number on heat flux at hypersonic Mach numbers. AIAA Paper 2005-1098; 2005.

[174] Bedarev IA, Borisov AV, Fedorova NN. Modeling of supersonic turbulent flows in the vicinity of axisymmetric configurations. J Appl Mech Tech Phys 2002;43(6):861–6.

[175] Olsen ME, Lillard RP, Coakley TJ. The lag model applied to high speed flows. AIAA paper 2005-0101; 2005.

[176] Marvin JG, Coakley TJ. Turbulence modeling for hypersonic flows. NASA TM-101079; 1989.

[177] Fedorova NN, Fedorchenko IA, Schulein E. Experimental and numerical study of oblique shock wave/turbulent boundary layer interaction at $M = 5$. Comput Fluid Dyn J 2001;10(3):376–81.

[178] Bradshaw P, Launder BE, Lumley JL. Collaborative testing of turbulence models. J Fluids Eng 1996;118:243–7.

[179] Huang PG, Bradshaw P, Coakley TJ. Turbulence models for compressible boundary layers. AIAA J 1994; 32:735–40.

[180] Catris S., Aupoix B. Improved turbulence models for compressible boundary layers. AIAA paper 98-2696; 1998.

[181] Catris S, Aupoix B. Density corrections for turbulence models. Aerosp Sci Technol 2000;4:1–11.

[182] Warren ES, Harris JE, Hassan HA. Transition model for high-speed flow. AIAA J 1995;33:1391–7.

[183] McDaniel RD, Nance RP, Hassan HA. Transition onset prediction for high-speed flow. J Spacecr Rockets 2000; 37(3):304–9.

[184] A.L. Kistler, Fluctuation measurements in supersonic turbulent boundary layers. Ballistic Research Laboratories, Report 1052; 1958, see also Physics Fluids 1959;2.

[185] Hasting RC, Sawyer WG. Turbulent boundary layers on a large flat plate at $M = 4$. R.A.C. Technical Report 70040 and R&M 3678; 1970.

[186] Mabey DG, Meier HU, Sawyer WG. Experimental and theoretical studies of the boundary layer on a flat plate at Mach numbers from 2.5 to 4.5. RAE TR 74127; 1974.

[187] Mabey DG. Some observations on the wake component of the velocity profiles of turbulent boundary layers at subsonic and supersonic speeds. RAE TR 77-004; 1977.

[188] Richmond RL. Experimental investigation of thick, axially symmetric boundary layers on cylinders at subsonic and hypersonic speeds. Guggenheim Aeronautics Lab., Cal Tech, Pasadena, CA, Hypersonic Research Project Memo 39; 1957.

[189] Fedorova NN, Fedorchenko IA. Computations of interaction of an incident oblique shock wave with a turbulent boundary layer on a flat plate. J Appl Mech Tech Phys 2004;45(3):358–66.

[190] Sinha K. Shock unsteadiness model applied to hypersonic shock-wave/turbulent boundary layer interactions. AIAA Paper 2006-126; 2006.

[191] Brinckman KW, Kenzakowski DC, Dash SM. Progress in practical scalar fluctuation modeling for high-speed aero-propulsive flows. AIAA Paper 2005-508; 2005.

[192] Spalart PR. Trends in turbulence treatments. AIAA 2000-2306; June 2000.

[193] Fluent 6.1 User's guide, vols. 1–3; 2003.

[194] Reynolds O. On the extent and action of the heating surface for steam boilers. Manch Lit Philos Soc 1874;14:7–12.

[195] Prandtl L. Eine Beziehung zwischen warmeaustausch und stromungswiderstand der flussigkeiten. Phys Z 1910;11: 1072–8.

[196] Taylor GI. The transport of vorticity and heat through fluids in turbulent motion. Appendix by Fage A and Falkner VM. Proc R Soc 1932;135:685–706.

[197] Von Karman T. The analogy between fluid friction and heat transfer. Trans ASME 1939;61:705–10.

[198] Schlichting H. Boundary-layer theory, 7th ed. Kestin J Trans. New York: McGraw-Hill; 1979.

[199] Rubesin MW. A modified Reynolds analogy for the compressible turbulent boundary layer on a flat plate. NACA Technical Note 2917; March 1953.

[200] Colburn AP. A method of correlating forced convection heat-transfer data and a comparison with fluid friction. Trans Am Inst Chem Eng 1933;29:174–210.

[201] van Driest ER. Convective heat transfer in gases. In: Lin CC, editor. Turbulent flows and heat transfer. Princeton, NJ: Princeton University Press; 1959. p. 339–427.

[202] Reynolds WC, Kays WM, Kline JS. Heat transfer in turbulent incompressible boundary layers—I constant wall temperature. NASA Memo. 12-1-58W; 1958.

[203] Cebeci T, Bradshaw P. Physical and computational aspects of convective heat transfer. New York: Springer; 1988.

[204] Smits AJ, Dussauge J-P. Turbulent shear layers in supersonic flow. Woodbury, NY: American Institute of Physics; 1996.

[205] Seiff A. Examination of the existing data on the heat transfer of turbulent boundary layers at supersonic speeds from the point of view of Reynolds analogy. NACA Technical Note 3284; August 1954.

[206] Reshotko E, Tucker M. Approximation calculation of the compressible turbulent boundary layer with heat transfer and arbitrary pressure gradient. NACA TN 4154; December 1957.

[207] Bertram MH, Neal L. Recent experiments in hypersonic turbulent boundary layers. NASA Technical Memorandum X-56335; 1965.

[208] Tetervin N. A transformation between axisymmetric and two-dimensional turbulent boundary layers. AIAA J 1970;8(5):985–7.

[209] White FM, Lessmann RC, Christoph GH. Analysis of turbulent skin friction in thick axisymmetric boundary layers. AIAA J 1973;11(6):821–5.

[210] Young AD. Boundary layers. AIAA Education Series. Washington D.C.: AIAA; 1989.

[211] Zoby EV, Moss JN, Sutton K. Approximate convective-heating equations for hypersonic flows. J Spacecraft 1981; 18(1):64–70.

[212] Seiler F, Werner U, Patz G. Ground testing facility for modeling real projectile flight heating in earth atmosphere. J Thermophys Heat Transfer 2002;16(1):101–8.

[213] US Standard Atmosphere. National Oceanic and Atmospheric Administration, NASA, and U.S. Air Force. Washington, DC; October 1976.

[214] Ames Research Staff. Equations, tables, and charts for compressible flow. NACA Report 1135; 1953.

[215] Keyes FG. A summary of viscosity and heat-conduction data for He, A, H_2, O_2, CO, CO_2, H_2O, and air. Trans ASME July 1951: 589–96.